Addis Ababa University
School of Graduate Studies
Faculty of Technology
Department of Civil Engineering

Remote sensing based assessment of water resource potential for Lake Tana basin

Yohannes Daniel

2007

Remote sensing based assessment of water resource potential for Lake Tana basin

Yohannes Daniel

A thesis submitted to School of Graduate Studies, Addis Ababa University in partial fulfillment of the requirements for the Degree of Masters of Science in Civil Engineering

April 2007

ACKNOWLEDGMENTS

First and foremost, I would like to express my deepest gratitude to my supervisor Dr.Ing Abdulkerim Hussien Seid, whose expertise, understanding, and advice, added greatly to my knowledge. He devoted his time to guide and assist me in the process of the research work. Without him, this research work wouldn't have been possible.

A very special thanks goes out to Ato Melakamu Amare and Ato Shimelis Behailu for their continuous assistance, advice and encouragement through out this work. I would like to thank Dr.Ing Zelalem Hailu and Dr.Ing Yonas Michael, they have provided me with materials and softwares need for the research work, which greatly contributed to the outputs of this thesis work.

I must also thank all staffs of Addis Ababa University Civil engineering Department and the Ministry of Water Resources Hydrology department for their cooperation in providing me with the necessary data for this research work.

Finally, I would like to owe many thanks to my family and all my friends for their endless support.

Table of Content

List of Tables

List of figures

Abstract

1. Remote sensing techniques have been applied to augment estimation of hydrologic variables. Thus rainfall, evaporation, flooded zone delineation and runoff estimation has been carried out. TRMM monthly rainfall products were employed in rainfall gap filling techniques, the satellite estimates were first validated against observed ground station records and results indicated good correlation, average of 81%. Combination equation (Energy balance-mass transfer) is used to determine gridded potential evapotranspiration from the sub-basin by making use of MODIS 16 days Albedo products. Spatial extent and amount of water on flood plains during wet seasons of the year has also been determined by making use of spot NDVI temporal images through calibrating with high resolution SAR and optical images. Furthermore, land use/land cover information is extracted from Landsat imagery and existing data of land cover has been updated. Using the update land cover information spatial Curve Number (CN) map was developed. Runoff estimation, using SCS method and a soil water balance simulation using WatBal model, was then carried out in order to determine the runoff from un-gauged catchments and the results from the two models were compared. Results indicated that the soil water balance simulation model gave better correlation with the observed than the SCS method. Therefore, runoff estimation from un-gauged catchments was carried out using the soil water balance simulation techniques. Lake water balance simulation was finally carried out using continuity equation within simulation time span of 1998 to 2003 considering the variables, i.e. inflow estimation form the contributing catchments, the improved evaporation estimation; the rainfall data obtained incorporating TRMM images and water lost in the flood plains due to evaporation. Simulation results were compared with the Lake Tana Storage computed using the recorded Lake water surface elevation. The six year average results indicated that out of the total of 7,688 MCM estimated runoff from the catchments 3.59% is lost in the flood plains due to evaporation. Similarly, out of the 10,574 MCM inflow to the lake (net runoff plus rainfall over lake area) 5,110 MCM is lost through evaporation from the lake surface, 5,012 MCM is outflow from the lake to the head of main Abbay river. Average reduction in reservoir storage was computed to be 330 MCM. Therefore, the remaining 1414 MCM is assumed to be seepage loss and other un-accounted losses from the system.

2. Introduction

2.1. Problem Statement

Before any planning activity for water resources development works in a certain river basin it is essential first to identify and evaluate the total available water resource of that basin. One of the main problems for water resource development planning in Lake Tana basin was the uncertainty in the information available regarding the water resource potential of the basin.

Previous studies [13][14][30][4] have attempted to quantify the total available water for development in the basin using different approach. However, the results show significant variations. One of the specific problems was to identify the total inflow to Lake Tana. Out of the major rivers flowing into the lake, the gauged part accounts for only less than half of the total catchment area of the basin. As reported from previous studies [14], the Long term mean annual lake outflow is 121 m^3/s which is equivalent to 3820 MCM, while inflow coming from only the gauged catchments is about 111 m^3/s, which is equivalent to 3556MCM. However, more than half part of the sub-basin is un-gauged, indicating the need for estimating the runoff coming from this un-gauged portion of the basin. Different studies carried out previously have attempted to estimate the total amount of water flowing in to the lake.

Mean annual net inflow (i.e. Streamflow from the catchments and direct rainfall over the lake surface), as computed by different investigators, is summarized in Table 1.1. The difference of estimates can clearly be noted.

Table 2-1 Comparison of net Inflow estimated to Lake Tana as Computed by Different Investigators

Investigator	Study works	Net Inflow (BCM)
Studio Pietrangeli (1990),[13]	Tana-Beles project studies	9.380
Humphrey & Associates(1996),[4]	Tis Abbay II Hydropower Studies	9.530
Melkamu Amre (2005),[14]	Reservoir operation & establishment of operation rule for Lake Tana	12.052
Waterwatch (2005),[30]	Remote Sensing Studies of Tana-Beles Sub Basins	11.560

Moreover, the surrounding flood plains are mostly inundated during wet periods, which would result in a substantial amount of water loss through evaporation. A rough estimate of the water that remains in the flood plains is about 2-2.5 BMC (Based on estimates from preliminary Study work prior to this thesis). However, none of the studies carried out previously have tried to account the loss from these flood plains. One of the gaps in previous carried out studies is that lack to address this phenomenon and thus the total water yield of the basin has not yet been properly investigated. This, therefore, implies the need for in depth assessment of water resource potential in the basin.

2.2. Objective and scope of the study

With all these previous studies carried out the Lake Tana basin water resource potential question still persists while the need for a better description of hydro-system raises on the other hand. Therefore, this thesis work bases at answering the core question, that asks “How much water resource is available for development in Lake Tana basin”, with in acceptable accuracy. Accordingly, the development work in the hydro system could be made lying on sound engineering bases providing with more confidence in decision to the implemented developments and ‘no regret development decisions’ can be carried out in the basin. In its way, this research work is hoped to contribute to the already existing hydrologic description of the basin but to obtain it using a more rigorous and different approach of solving the problem.

Therefore, this thesis has a general objectives to improve the hydrological description of Lake Tana basin and thus to contribute towards an improved Integrated Water Resource Management (IWRM) works in the Tana Basin. Aiming the following specific objectives

- To enhance the past estimation of hydrological variables, specifically water balance components, i.e. rainfall, evaporation, runoff from un-gauged catchments and ground water seepage. Thus, to improve hydrological description of the basin incorporating analysis from remotely sensed data.
- Devise an operational flow estimation mechanism for un-gauged catchments.

2.3. Methodology

This research work makes use of remote sensing techniques in the estimation of hydrologic components of the water balance specifically,

- In the estimation of evaporation satellite derived parameters have been applied to come up with data that are not obtained from ground measuring stations. Five years of time span analysis has been carried out in modeling 1998 -2003.This span was selected based on the available public domain satellite data that can be obtained free of charge.
- Satellite based Rainfall estimates have been validated against ground measured rainfall data and were used to fill missing records.
- Furthermore, Analysis of time series images has also been applied to estimate historical flooded water that remains in Lake Tana neighboring flood plains. The analysis mainly employed hybrid (combination of supervised and unsupervised) classification techniques to distinguish historical inundated area during wet season of the year and determine the area. These time series maps combined with elevation information assisted to estimate volume of water.
- Similarly land cover information has been updated through the use moderate resolution optical images. Again classification techniques have applied here to derive land cover classes from satellite imagery.

Using this improved estimates of hydrological components two runoff estimation mathematical models have been tested to estimate the water yield from un-gauged catchments within the above mentioned simulation time span. Namely, SCS curve number on monthly level and soil water balance model have been tested and verified .The results were applied to estimate the contribution from these un-gauged catchments and to fill missing data in flow from the gauged catchments.

After the inflow to the lake is determined, water balance of the Lake was carried out to validate the results and to illustrate the hydro-interaction of the lake with the abutting catchments. Details of the methodology followed to estimate the hydrological components are discussed in depth in chapter 5 under each relevant section.

2.4. Thesis Outline

The presentation of this report has been organized as follows.

Chapter 2: Presents General description of the study area. Mainly, hydrology, climate, topography and water resource are summarized and discussed briefly.

Chapter 3: Literature review part is compiled and presented in three main topics hydrology, remote sensing and previous related studies in the study sub-basin. The first two topics cover basic concept and technical parameters which are adopted in this thesis work

Chapter 4: Data availability and collected data from different sources is presented.

Chapter 5: Explains data analysis on the basic inputs parameters along with the results obtained, accompanied with brief description of the methodology followed in each analysis.

Chapter 6: Covers, rainfall runoff modeling together with the procedures followed. Runoff contribution estimates from the un-gauged catchment is well dealt in depth.

Chapter 7: water balance simulation for the lake is discussed and output results are interpreted.

Finally, conclusion and recommendations for future work are presented in chapter 8

3. The Study area

3.1. General

Lake Tana sub-basin is part of the Blue Nile basin in Ethiopia. It comprises of Lake Tana and the surrounding sub-basins abutting the lake. Total drainage area of the sub-basin is about 15,046 km^2. Of which about 20% of the area is Lake Tana. (Based on estimates in this research work). The lake is fed by over 60 rivers and streams flowing from the Simen Mountains to the north, the large central plateau to the east and the gentler sloping land to the west.

Lake Tana sub-basin is characterized by enormous potential for development of irrigated agriculture, hydropower, tourism, bio-diversity and recreations. For this reason, it is one of the richest sub-basin concerning water resource

Two major Cities are located in this sub-basin, Gondar and Bahirdar. The total population in the basin is estimated to be a bit more than 3 million out of which the female constituted 47% of the population as of 2001/2002 CSA Estimates.

3.2. Location and accessibility

Lake Tana basin is found in north west part of Ethiopia in Amhara administrative region covering eight Woreda regions (smaller administrative units) .Dembia and Gondar Zuria in the northern part of the sub-basin; Libo Kemkem ,Fogera,Farta and Dera in the eastern part of the basin, Achefer and Alefa-Bechigne on the western part and with Bahirdar Zuria on the southern part of the basin. Geographically it extends between 10.95^{o}N to 12.78^{o}N latitude and from 36.89^{o}E to 38.25^{o}E longitude.

One major road originating from Addis Ababa passes across the basin connecting the major cities/towns namely Merowi,Wetet Abbay ,Bahir-dar ,Addis Zemen and Gonder. This Sub-basin can also be accessed by another secondary road that originates from Weldiya passing through the towns Debretabor and Nefas Mewcha and joins the main road in Jiggna. Two International airports are located inside this basin found in Bahir dar and Gondar Cities.

Figure 3-1 Location map of Tana Basin

3.3. Topographic Characteristics and Land feature

Topography

The topography of the sub-basin is generally flat where 60% of the area has average slope less than 5%. However, terrain slope within the basin ranges from 0% to 120%. Elevations generally vary from 4,620m at peaks of mount Ras Dashen down to 1,780 m at the out let of the lake in Bahir dar. The mean elevation of the sub basin is found to be 2025m above sea level. Lake Tana water surface has its natural mean sea level of 1786.

Land

About 52% of all the available land in Lake Tana basin is used for agricultural farms while 21% and 5.77% is used for agro-pastoral purpose and for pastoral only respectively. Only about 0.1 % constitutes urban lands.

The Dominant Soil grounps in the basin are Haplic Luvisols,Chromic Luvisols,Eutric Leptosols and Eutric Fluvisols constituting 21%,16%,12% and 11% of the total area respectively. The remaining 20% is composed of different soil groups. Landforms in the area mainly constitute Alluvial, residual structural and volcanic landforms. Majority of the area is of residual landform.

Geology

Basalt lavas of the tertiary volcanic, fresh and massive in structure and of the Miocene age are found in the highlands surrounding the Lake. In the west and south west of Gondar the Chilga beds dominated with shale’s and sand stones are observed.

Quaternary Volcanics mostly represented by olivin alkali basalts, often inter-bedded with clayey palaeosoils are observed. The latitude of the Quaternary volcanic is not always perfectly horizontal. Besides congenital dips of some lava flows, also gentle tectonic deformations can be noted, like the anticline fold found between Chara-Chara and Kamforo along the Blue Nile. Other edifices, mostly lavic, rise over the plain covered by basalt flows, extending from Bahir Dar to beyond the Gilgel Abbay.

Alluvium deposits cover the banks of the lower reaches of the main Lake Tana tributaries. They are composed of fine sediments, partly of marsh environment, which usually are represented by clays.

3.4. Climate

Rainfall

Based on the rainfall pattern, the year is divided into two seasons: a rainy season mainly centered on the months of June to September, and a dry season from October to March. In the southern parts of the basin the months of April and May are an intermediate season where minor rains often occur. Of the total annual rainfall, 70% to 90% occurs in the June to September rainy season

There is a significant the spatial variation of rainfall within the basin. The mean annual rainfall at Bahir Dar (south portion of the basin) is 1450mm, 1200mm at Addis Zemen (eastern portion) and 1050 mm at Gondar Air Port meteorological station (northern portion). Rainfall distribution, both in time and space, decreases northwards in the basin. The weighted mean annual rainfall depth over the basin is estimated to be 1341.6 mm.

Temperature

The spatial variation of temperature is fairly constant in the middle and upper part of the catchment which ranges within the limits of 19^{o}C to 20^{o}C.On the other hand, a small portion with about 10% by area at the lowest most part of the basin is observed to have a higher temperature record with average value of 23^{o}C.Total weighted basin average temperature is estimated to 20^{o}C. The average temporal variation ranges from 7.5^{o}C down to 3^{o}C within a year as we go to the southern portion of the sub-basin.

Relative Humidity

The average relative humidity is about 65% (as computed from Satellite products) therefore the sub-basin is characterized as humid climate. Temporal variation of humidity is relatively stable within the basin. However, the spatial variation decreases as we go to the northern part of the sub-basin measured annual average relative humidity is observed to be 61% and 54.7% in Bahirdar and Gonder ground stations respectively.

3.5. Hydro-System

The hydro-system configuration is a radial system in which Lake Tana is found at the center of the basin and it is surrounded by sub-basins of total 12,005 Km2 by area. The surrounding sub-basins are drained with several small rivers and 11 major streams that flow into the lake.

The eastern portion is drained by Ribb and Gumara that accounts 28% of the basin. These two rives are major rivers flowing through out the year. Starting from the Guna Mountain having an altitude of above 4000masl .Ribb and Gumara rivers approximately travel 93 and 86 kms respectively and find their way to the lake passing through Farta plateau and the flat fields of Fogera flood plain. In wet seasons, July to September, when majority of the runoff occurs, the flow in these rivers overflows the banks and inundates the adjoining flood plains. As more flood comes in, the inundated area grow wider and some seasons with heavy rainfall these impoundments even get combined forming a wider flooded area.

The northern part of the basin is drained by four rivers namely, Ambagenen, Megech, Gumaro and Arno-Garno, which account 14.7% of the basin by area. The Megech River is the major tributary contributing large proportion of Lake Inflows coming from north directions of the lake and it constitutes 5.1% of the total basin area. This river joins the lake passing through the Dembia flood plains. Similar flood plain inundation incident occurs on the Dembia plain due to this river as in the case of Ribb and Gumara.

Koga and Gilgel Abbay are the two major rivers draining the southern portion of the basin constituted to be 30% of the basin. The western part of the basin is mainly drained by small streams. The total area drained by these small streams account 7.2% of Lake Tana sub-basin by area.

The outflow from the lake joins the head of the Blue Nile. In previous studies [13][14] Long term annual average outflow from the lake has been reported to be 3.556 BMC. However, the five year (1998 to 2003) mean annual runoff is estimated to be 5.012 BMC in this research work.

Figure 3-2 Lake Tana sub-basin drainage pattern and gauging stations

3.6. Current Development activity and existing structures

Irrigation

So far no large scale irrigated agriculture has been implemented in the basin. Only few hectares of recession cropping along the shore of the lake and some small scale irrigation activities are being practiced in the eastern portion of the basin. These small-scale development works are estimated to be in the order of not more than 500ha [13].

Hydropower

In the Tana basin the existing Tis Abbay I & II hydropower plants with installed capacity of 84MW, are considered as the only medium scale hydropower scheme available so far.

Chara-Chara weir

Currently the only existing structure is The Chara-Chara weir which is located at the mouth of the lake 1km upstream of the Gondar-Bahir Dar Bridge .The purpose of Chara-Chara weir is to improve the existing natural shape of the water course by raising the water level and to regulate the reservoir water available between the minimum and maximum operating levels. The minimum operating level of Tana reaches 1784masl. The Maximum operating level is fixed to be at 1787.5masl [14].

4. Literature review

In order to properly state the available water resource potential of a certain river basin it is first essential to determine the amount of water available in that system. Accordingly, that requires understanding of the hydro-system and its interaction with the environment and to be able to properly describe the water flow, ‘in and out’, of the basin. Information and data regarding the basin such as runoff, evaporation and rainfall, for example, are some of the components that would be necessary in describing the water movement or circulation. A scientific approach to that is to carry out a hydrologic analysis of the basin. Remote sensing is a tool [7] that can be useful to a hydrologist in terms of providing advanced ways of retrieving data and information and enabling spatial, ‘grid based’, analysis techniques.

This chapter, therefore, presents a general review of literatures relevant to the research work. Thus, describes some of the theoretical backgrounds of the computational methodologies employed and review of previous study in the basin. Hydrology, remote sensing and review of previous related studies in Lake Tana basin are the major topics that are focused on.

4.1. Hydrology

3.1.1. General

Hydrology is a science which is concerned with the circulation of water and its constituents through the hydrologic cycle. It deals with precipitation, evaporation, infiltration, groundwater flow, runoff stream flow and the transport of substance dissolved or suspended in the flowing water [7].

Hydrologic Analysis is a set technique for simulating components of the hydrologic cycle in which the components are analyses and processed to provide an understanding of the basin hydrology [16].In water resource analysis that targets to determine available water, hydrologic analysis can be very helpful in terms of providing mechanisms of flow estimation from un-gauged watersheds.

In most hydrologic analysis procedures the following steps are commonly included

- Delineation of catchment morphology from topographies or elevation information
- Analysis of available hydrologic components like evaporation, rainfall etc
- Estimation of missing hydrologic variables using watershed modeling

3.1.2. Watershed hydrology model

A watershed hydrology model is an assemblage of mathematical descriptions of components of the hydrologic cycle [17].It is away of abstracting the real system in terms of simpler mathematical equations.

Watershed models are fundamental to water resources assessment, development, and management. They are, for example, used to analyze the quantity and quality of stream flow, reservoir system operations, groundwater development and protection, surface water and groundwater conjunctive use management, water distribution systems, water use, and a range of water resources management activities [18].Here in this framework, mathematical models are used in this thesis work to analyze quantity of water from un-gauged catchments.

ASCE [19] reviewed and categorized flood analysis models into

1) Simple, Single event, rainfall runoff models;
2) Continuous-stream-flow simulation models;
3) Steady flow routing models;
4) unsteady-flow flood routing models;
5) Reservoir regulation models; and
6) Flood frequency analysis models.

The fist two sets of modeling approach are used in this thesis and are discussed below.

Simple, Single event, rainfall runoff models:

Single event models are designed to simulate individual rainfall-runoff events. Their emphasis is primarily placed on infiltration and surface runoff their purpose is the evaluation of direct runoff. Examples to such kind of models are infiltration models such as Green-Ampt and standard rainfall-runoff relation, such as the U.S. Soil Conservation Service relation (SCS-CN model)[8].In this thesis work SCS-CN method has been employed to determine the runoff from un-gauged catchments. The theoretical explanation is discussed below in this section.

Continuous-stream-flow simulation models

A second major class of hydrological models is one that continuously accounts in time for all precipitation that falls on the watershed and movement of water through the catchments into the outlet[7].Continuous accounting of water movement involves the consideration of precipitation, snow melt, surface loss, infiltration, and surface transport processes. Other processes that need to be considered are evapotranspiration, soil moisture redistribution, and groundwater transport. The integration of all these processes in a watershed model is usually termed as continuous soil moisture accounting [16]. The complexity of the soil moisture accounting model varies greatly depending on the degree of conceptualization employed in integrating the subsurface processes. An example to such kind of model is the simple 'one-dimensional bucket soil water balance model' which is discussed in depth below.

3.1.3. The SCS-CN (Soil Conservation Service curve number) Model

The US Soil Conservation Service model is widely used for estimating floods on small to medium-sized un-gauged drainage basins [7]. Together with the SCS triangular unit hydrograph, the method can be used to estimate peak floods from a known rainfall hyetograph. According to this method, the volume of direct runoff resulting from a rainfall is given by

$$Q = \frac{(P - I_a)^2}{P - I_a + S} \qquad (3.\ 1)$$

Where Q = direct flow volume expressed as a depth (mm)

Ia= is the initial abstraction,

S= potential maximum retention after runoff begins(mm)

P = rainfall.(mm)

The basic assumption of the SCS curve number method is that, for a single storm, the ratio of actual soil retention after runoff begins to potential maximum retention is equal to the ratio of direct runoff to available rainfall [8].

No runoff occurs until rainfall equals an initial abstraction I_a is satisfied. After allowing for I_a the depth of runoff Q is the residual after subtracting F.

Commonly it is taken that the initial abstraction is about 20 % of the potential retention in any storm, i.e. the emperical relationship suggested by Nation Engineering Handbook [8].

$$I_a = 0.2S \qquad (3.2)$$

and thus ,

$$Q = \frac{(P - 0.2S)^2}{P + 0.8S} \qquad (3.3)$$

The potential retention is expressed in terms of a dimensionless curve number CN, which depends on soil type and land use/cover in the drainage basin. In English units, where S is in inches,

$$CN = \frac{25400}{254 + S} \qquad (3.4)$$

The value of CN depends on the soil, cover, and hydrologic conditions of the land surface. A detail computation of CN is well documented in National Engineering hand book [8]. Computation of Gridded-CN for each sub-basin in Lake Tana basin is discussed in chapter 5 of this report.

3.1.4. Soil water balance Model (one-dimensional bucket model)

The common link in most soil water balance approaches is the computation of a mass balance within the soil moisture zone [9]. The soil-water budget that is discussed here is a simple accounting scheme used to predict soil-water storage, evaporation, and water surplus. Surplus is the fraction of precipitation that exceeds potential evapotranspiration and is not stored in the soil.

Water enters the soil moisture store through precipitation and is removed either by evapotranspiration or direct runoff, surface runoff, subsurface runoff or baseflow. Figure 3-1 shows schematic representation of the system.

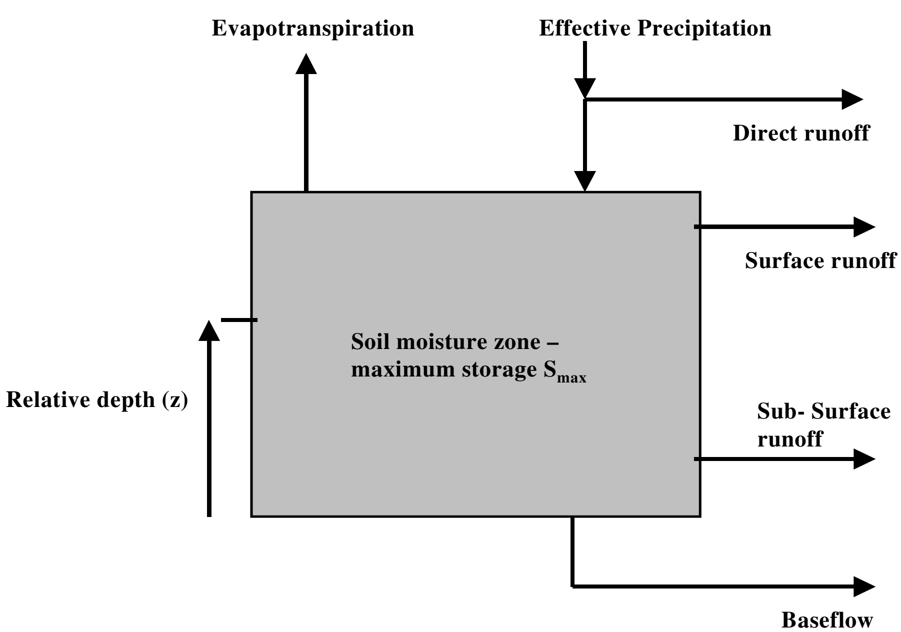

Figure 4-1 Conceptualization of the water balance for the WatBal model. (adopted from [8])

The change of stored water in the soil can be expressed as the difference of input and output parameters. Therefore, mathematically it can be expressed as

Surplus = precipitation - evaporation - (change in storage)

Yates [9], has rewritten this equation in a more discritized form as a function of each parameters shown in figure 3-1,

$$S_{\max}\frac{dz}{dt} = P_{eff}(t)(1-\beta) - R_s(z,t) - R_{ss}(z,t) - E_v(Pet,z,t) - R_b \tag{3.5}$$

where:	Peff	=	effective precipitation (length/time)
	Rs	=	surface runoff (length/time)
	Rss	=	sub-surface runoff (length/time)
	Ev	=	evapotranspiration (length/time)
	Pet	=	potential evapotranspiration (length/time)
	Rb	=	baseflow (length/time)
	Smax	=	maximum storage capacity (length)
	z	=	relative storage (length) ($0 \leq z \geq 1$)

S_{max}, the maximum water holding capacity of a catchment reflects the relative importance of water storage on the hydrological regime of a catchment. It is dependent primarily on the nature of catchment geology and soils. The storage variable, z, is given as the relative storage state and is a value between 0 and 1. Consequently, when S_{max} is multiplied by z, it gives the volume of water stored in the catchment at any given time.

Effective precipitation:is the amount of water entering the storage zone after losses or contributions from snowmelt accumulation.

Evapotranspiration: is a function of potential evapotranspiration (PET) and the relative catchment storage state. A non-linear relationship has been used to descibe evapotranspiration [10] as equation 3-6 below.

$$E_v(z,Pet,t) = Pet\left(\frac{5z-2z^2}{3}\right) \tag{3.6}$$

Surface runoff Rs, is described in terms of the storage state, z, and the effective precipitation, Peff.. ε, a calibration parameter, allows for surface runoff to vary both linearly and non-linearly with storage [9].

$$R_s(z,P,t)=\begin{cases} z^{\varepsilon}(P_{eff}-R_b) & \text{for } P_{eff}>R_b \\ 0 & \text{for } P_{eff}\le R_b \end{cases} \tag{3.7}$$

Sub-Surface runoff Rss, is a function of the relative storage state, multiplied by a coefficient α. In most cases the value of γ is 2 [9].but can be different depending on catchment property

$$R_{ss}=\alpha\ z^{\gamma} \tag{3.8}$$

Direct runoff (Rd), equation 3.9, is from impervious surface. Direct runoff coefficient, β, is proportional to area of water bodies and urban territories in the sun-basin. It is the proportion of effective precipitation that becomes direct runoff.

$$R_d=\beta P_{eff} \tag{3.9}$$

The baseflow (R_b): must be entered into the model as a constant value

Therefore if the parameters γ, β, ε and S_{max} are estimated, it is possible to simulate the stored water in soil, runoff, and evapotranspiration at any give time step within simulation time span. Here, in this thesis work an excel based application, developed by the Stockholm Environment Institute (SEI) in the USA, that implements the above discussed theoretical frame work has been used. The software model is called WATBAL.

In WATBAL, hydrological processes are simulated, as described above, on the basis of a conceptual approximation. Consequently it is necessary to adjust or optimize parameters until the model output is an acceptable estimate of the observed runoff regime. In order to do this it is necessary to have observed runoff data against which to calibrate parameter values.

3.1.5. Computer models

Computer models are software products that implement the mathematical models, such as the once discussed above, and automate the simulation. Most of These models have graphical user interface that interact with user to provide inputs and display output. In this thesis work, the following computer models were utilized each to a certain extent.

i) HEC-HMS : The HEC-HMS is designated to simulate the precipitation-runoff processes of dendritic watershed systems. In addition to unit hydrograph and hydrologic routing options, capabilities include linear quasi-distributed runoff transform (ModClark) for use with gridded precipitation, continuous simulation with either a one-layer or more complex five-layer soil moisture method, girded and sub-basin average Priestly-Taylor evapotranspiration, a gridded and elevation-band temperature-index snowmelt method, multiple outlets and spillways for reservoirs, and an automatic depth-area reduction analysis tool frequency storms.

ii) WATBAL: It is a model that simulates changes in soil moisture and runoff. It is essentially an accounting scheme based on a conceptualized, one-dimensional bucket that lumps both the root and upper soil layer. The model comprises two elements. The first is a water balance component that describes water movement into and out of a conceptualized basin (Figure 1). The second is the calculation of potential evapotranspiration, for which there are three possible alternatives, depending on data availability

iii) SWAT base flow filter model : The baseflow filter estimates baseflow and groundwater recharge from streamflow records using the methodology outlined in Automated methods for estimating baseflow and groundwater recharge from streamflow records by J.G. Arnold and P.M Allen [20] and Automated base flow separation and recession analysis techniques by J.G. Arnold, P.M. Allen, R. Muttiah, and G. Bernhardt [15].

4.2. Remote Sensing

3.2.1 Concept of Remote Sensing

The United Nations, Conference on the Exploration and Peaceful uses of Outer Space, defined the term Remote Sensing as "The sensing of the Earth's surface from space by making use of the properties of electromagnetic waves emitted, reflected or diffracted by the sensed objects, for the purpose of improving natural resources management, land use and the protection of the environment" [22].

Remote Sensing can be defined as the science and technology by which the characteristics of objects of interest can be identified, measured or analyzed through the information obtained by a device that records reflected, emitted, or diffracted electromagnetic energy without direct contact [21].

Remote-sensing systems, mainly the once deployed on satellites, provide a continuous and consistent view of Earth transmitting the information to ground station facilitating the ability to monitor Land surface and the atmosphere surrounding the earth.

In much of remote sensing, the process involves an interaction between incident radiation and the targets of interest. This is exemplified by the use of imaging systems where the following seven elements are involved. Note, however that remote sensing also involves the sensing of emitted energy and the use of non-imaging sensors.[36] Figure 3.3 illustrates the process.

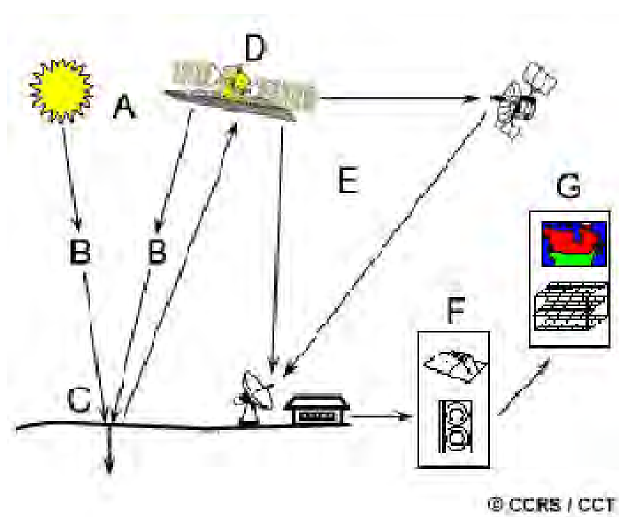

Figure 4-2 Process of Remote sensing systems (Adopted from [36])

i) Energy Source or Illumination (A) – the first requirement for remote sensing is to have an energy source which illuminates or provides electromagnetic energy to the target of interest.

ii) Radiation and the Atmosphere (B) – as the energy travels from its source to the target, it will come in contact with and interact with the atmosphere it passes through. This interaction may take place a second time as the energy travels from the target to the sensor.

iii) Interaction with the Target (C) - once the energy makes its way to the target through the atmosphere, it interacts with the target depending on the properties of both the target and the radiation.

iv) Recording of Energy by the Sensor (D) - after the energy has been scattered by, or emitted from the target, we require a sensor (remote - not in contact with the target) to collect and record the electromagnetic radiation.

v) Transmission, Reception, and Processing (E) - the energy recorded by the sensor has to be transmitted, often in electronic form, to a receiving and processing station where the data are processed into an image (hardcopy and/or digital).

vi) Interpretation and Analysis (F) - the processed image is interpreted, visually and/or digitally or electronically, to extract information about the target that was illuminated.

vii) Application (G) - the final element of the remote sensing process is achieved when we apply the information we have been able to extract from the imagery about the target in order to better understand it, reveal some new information, or assist in solving a particular problem.

3.2.2 Definition of Technical terms

This section introduces 1) Definition of some important remote sensing terms that have been adopted and were relevant to the study and 2) Remote sensing techniques of data analysis and interpretation methodologies applied while carrying out this thesis work.

a) Passive Satellites sensors:

The sun provides a very convenient source of energy for remote sensing. The sun's energy is either reflected, as it is for visible wavelengths, or absorbed and then reemitted, as it is for thermal infrared wavelengths. Remote sensing systems which measure energy that is naturally available are called passive sensors. Passive sensors can only be used to detect energy when the naturally occurring energy is available. This can only take place during the time when the sun is illuminating the Earth. Energy that is naturally emitted (such as thermal infrared) can be detected day or night, as long as the amount of energy is large enough to be recorded[36].

b) Active satellite sensors:

Active sensors, on the other hand, provide their own energy source for illumination. The sensor emits radiation that is directed toward the target to be investigated. The radiation reflected from that target is detected and measured by the sensor. Advantages for active sensors include the ability to obtain measurements anytime, regardless of the time of day or season. Active sensors can be used for examining wavelengths that are not sufficiently provided by the sun, such as microwaves, or to better control the way a target is illuminated. However, active systems require the generation of a fairly large amount of energy to adequately illuminate targets. One example of active sensors is the Synthetic Aperture Radar (SAR)[36].

Radar is an acronym for Radio Detection and Ranging. It operates in part of the microwave region of the electromagnetic spectrum, specifically in the frequency interval from 40,000 to 300 megahertz (MHz). Unlike Optical sensors that passively sense radiation from targets illuminated by the Sun or thermal sources, radar generates its own illumination by sending bursts or pulses of EM energy that reflect off of a target. A fraction of the reflected energy then returns to the radar's receiving antenna, which collects it and passes it to the electronic system. Thus, a radar system is a ranging device that measures distances as a function of round trip travel times (at light speed) of a directed beam of pulses (the signal, whose strength is measured in decibels, dB) spread out over specific distances. In this way radar determines the direction and distance from the instrument (fixed or moving) to an energy-scattering object.

Although, radar images are relatively more difficult to interpret than optical images [7], they have several other advantages over optical satellite

- Radar microwaves can penetrate the atmosphere day or night under virtually all weather conditions, providing data even in the presence of haze, light rain, snow, clouds or smoke.
- Under certain circumstances, radar can partially penetrate arid and hyper-arid surfaces, revealing subsurface features of the earth.
- Although radar does not penetrate standing water, it can reflect the surface action of oceans, lakes , and other bodies of water .surface eddies, swells, and waves are greatly affected by the bottom features of the water body , and a careful study of surface action can provide accurate details about the bottom features.

Due to the first mentioned reason above, radar images are found to be specifically useful in application on wet season where cloud cover dominantly covers the atmosphere. Hence, in application such as flood monitoring SAR images have shown to provide more effective result than optical images [23].

c) Resolution

Resolution is a term that is stated in this report in a number of places. In broad terms, if it is not mentioned otherwise, resolution refers to the area on the ground a pixel represents on an image dataset. Following are some of the terms which are related to resolution

Spectral resolution: refers to the specific wavelength interval in the electromagnetic spectrum that a sensor can record [24].

Spatial resolution: is a measure of the smallest object that can be resolved by the sensor, or the area on the ground represented by each pixel [24].

Temporal resolution: this refers to how often a sensor obtains imagery of a particular area. Temporal resolution is an important factor to consider in change detection studies

d) The Normalized Difference Vegetation Index (NDVI):

The Normalized Difference Vegetation index, NDVI, is an index that is obtained by combining Channels of visible and near infrared of a satellite image. NDVI Provides a standardized method of comparing vegetation and it can be used as an indicator of relative biomass and greenness [25].

The formula to calculate NDVI is given as

$$NDVI = \frac{(Near\_IR\_band - \mathrm{Re}d\_Band)}{(Near\_IR\_band + \mathrm{Re}d\_Band)}$$

Where

Near_IR_band is band corresponding to the amount of near-infrared light reflected

Red_band is band corresponding to the amount of red light reflected.

Index values range from -1.0 to 1.0 and are unit-less. Vegetation values typically range between 0.1 and 0.7. Higher index values are associated with higher levels of healthy vegetation cover, whereas values between 0 and 0.1 are commonly characteristic of rocks and bare soil, and values less than 0 sometimes indicate ice-clouds, water-clouds, water body and snow. [24][26].

Although NDVI is principally used for vegetation monitoring it can also serve the purpose of indirect identification and monitoring of water body and flooded area extent. By applying a certain threshold value in which cell values less than that can be identified as water body or flooded area. Generally, NDVI value for inundated surface features remains negative while the value for non inundated surface is commonly greater than 0.

In some studies however, NDVI values of flood water were found to be significantly positive [25].Thus, it is worth noting that a straight forward approach of using setting threshold value of zero might not be universally effective in delineation of inundated area [23].

3.2.3 Remote sensing techniques

In the pending sections some of Image processing and interpretation techniques that have been used in this thesis work as are discussed briefly

Pre-processing: Preprocessing functions involve those operations that are normally required prior to the main data analysis and extraction of information .This process mainly involves two procedures radiometric corrections and Geometric corrections.
Radiometric corrections include correcting the data for sensor irregularities and unwanted sensor or atmospheric noise, and converting the data so they accurately represent the reflected or emitted radiation measured by the sensor. Geometric corrections include correcting for geometric distortions due to sensor-Earth geometry variations, and conversion of the data to real world coordinates (e.g. latitude and longitude) on the Earth's surface.

Image classification and analysis: Image classification is a means to convert spectral raster data into a finite set of classifications that represent the surface types observed in the imagery. These may be used to identify vegetation types, anthropogenic structures, mineral resources, or transient changes in any of these properties

Image classification is one of the important components of image interpretation. Image acquired through satellite mostly contains cells of values in which further classification will only result in meaningful information. In some activities the classification of image is the goal of the interpretation such as like land use mapping [37].The image classification therefore forms an important tool for examination of the digital images. There are many methods of image classification out of which unsupervised, supervised and a hybrid of these two classifications are used in this thesis work.

i) Supervised Classification

This is a classification technique is supported on prior information of the scene the image represents and is closely controlled by the analyst. In this process, pixels that represent patterns or land cover features that can be recognized, or that can be identified with the help from another sources, such as aerial photos, ground truth data, or maps are overlaid and with the raw image and pixels with similar characteristics are classified to the corresponding classes.

ii) Unsupervised Classification

In unsupervised classification any individual pixel is compared to each discrete cluster to see which one it is closest to. A map of all pixels in the image, classified as to which cluster each pixel is most likely to belong, is produced in black and white or more commonly in colors assigned to each cluster. This then must be interpreted visually as to what the color patterns may mean in terms of classes, etc. that are actually present in the real world scene; this requires some knowledge of the scene's feature/class/material content from general experience or familiarity with the specific area. However, the process of classification is mostly more computer automated.

3.2.4 Remote sensing systems and Hydrologic analysis

The use of remote sensing techniques and satellite derived data has grown a wide popularity in hydrologic analysis. Remote sensing techniques provide a means of monitoring and measuring hydrological state variables over large areas. And it has become a powerful tool in its advantage of capturing spatial as well as temporal distribution of the variables within practical accuracy.

Even though remote sensing techniques have quite diverse application, this section attempts to discuss some of the methods employed with regard to the application in hydrologic analysis and water resource assessment.

I. Application of Remotely acquired DEM for Determining watershed Geometry

Remote sensing data can be used to obtain almost any information that is typically obtained from maps or aerial photography. The availability of relatively high resolution digital elevation data has replaced the classical method of watershed delineation. Making use of GIS system with the help remotely acquired DEM (Digital elevation Model) data, it has become simple to obtain physical characteristic of a watershed such as catchments boundaries, drainage lines and slope.

GIS based Modules and utilities are being developed to automate these processes of deriving catchments boundary and drainage line processing [27].The level of accuracy has been validated with manual delineation of catchment and the results have provided high accuracy.

In this study also satellite derived products of The Shuttle Radar Topography Mission (SRTM) obtained elevation data have been utilized to derive the catchment geometry and drainage pattern of Lake Tana basin and the sub catchments within the basin.

II. Application of Satellite imaginary for land cover /land use classification

Land use is an important characteristic of the rainfall/runoff process that affects infiltration, erosion, and evaporation. Remotely sensed images along with image classifying technique are often utilized to produce information regarding land-use. Such information is usually extracted from the images in terms of statistical measures or in terms of classified and labeled images with land-cover categories like water, forest, agricultural, mire and urban areas.

Optical LandSat images, for example have been used in several cases to derive landuse information [28][29].The different channels available corresponding to classes of wave length from Landsat imagery have made it possible to identify land forms from images based on the values of reflectance that different material respond to different wavelength of radiation. Similarly, Ledwith [6] has demonstrated the use of Spot images to produce a classified land cover map

III. Application of Satellite imaginary for Hydrologic Component Estimation

Hydrologic variables such as rainfall, evaporation etc. which are used as major input components of hydrological analysis for water assessment can be estimated or measured directly or indirectly by the use of remote sensing systems and techniques, supplementing the already existing familiar method of component estimation and measuring [7].

Rainfall

Direct measurement of rainfall from satellite has not been generally feasible because the presence of cloud prevents observation of the precipitation directly with visible, near-infrared and thermal-infrared sensors[7].However, it has been possible to make estimation of precipitation based on other primary image products such as temperature, cloud cover, DEM etc... . Thus, for decades, different algorithms have been employed to provide estimates of spatial rainfall. Most of the algorithms deal within the visible, near infrared and thermal infrared wavelengths to utilize information on cloud height and coldness which are both related to the amount of precipitation that is expected from the cloud. Likewise, improved analysis of rainfall has been achieved by combining satellite and conventional ground station rainfall data [7].

Remotely sensed estimates of precipitation have been successfully used in hydrological modeling when conducting monthly water balance [30][2]. They have also been used operationally as input in hydrological models in the Sudan, Egypt, Senegal and other places in Africa.

Precipitation products are currently available through or sponsored by a variety of agencies including the NOAA, NASA, WMO and NCDC. One of the widely used precipitation satellite based products is the Tropical Rainfall Measuring Mission (TRMM) datasets that are provided through NASA[38].

In this thesis work monthly image products from TRMM satellite have been used to fill gaps in ground rainfall records and to extend short records of stations. It is demonstrated in the chapter 5 of this report. A good correlation of estimates from this Satellite product and ground measurement has been obtained.

Evaporation

Many tasks in hydrology require an accurate representation of how incoming radiant energy is partitioned at the land surface into sensible and latent heat. However evaporative fluxes are inherently difficult to measure, especially at regional scales and beyond. Evapotranspiration remains the variable with the greatest uncertainty in hydrological analysis because of its significant spatial and temporal variability.

Remote sensing based estimates, therefore, have become powerful means to compute evaporation due to their advantage of describing spatial as well as temporal distribution in a practical accuracy. The methods used in estimating evaporation can differ mainly based on theoretical frameworks they follow and requirement of data, ground station as well as satellite image data, to quantify the evaporation.

Some of the algorithms are independent of ground observations [3] while some still make partial use of ground observations[39].On the other hand, some use the classical theories of evaporation estimation while making use of the input from satellite images while others use indirect techniques such as by making use of relationships between NDVI and ET [5].

Soil moisture

Passive microwave remote sensing techniques are used to measure near surface soil moisture because at microwave frequencies the most striking feature of the emission from the earth's surface is large contrast between water and land. Microwave remote sensing offers four unique advantages over other spectral remote sensing techniques:

Runoff

Runoff cannot be directly measured by remote sensing techniques. However, there are two general areas where remote sensing can be used in hydrologic and runoff modeling: (1) determining watershed geometry, drainage network, and other map-type information for distributed hydrologic models and for empirical flood peak, annual runoff or low flow equations; and (2) providing input data such as soil moisture or delineated land use classes that are used to define runoff coefficients

IV. Application of Satellite image for Flood Plain delineation

Information obtain through remote sensing systems have appreciably been applied in determining area extent of flooded zone. Many researcher have made use of different remote sensing products for flood plain delineation

NDVI products area used for flood delineation with the assumption that water has very low reflectance in the near infrared portion of the spectra. SPOT multi spectral imageries NDVI maps were used along with a DEM for delineation of monsoon flood in Bangladesh[23].Landsat derived NDVI images have also been incorporated in flooded area analysis as demonstrated by Zehtabian,Panah and Rahin[41]. Three input satellite image products NDVI, NDWI and the original SWIR band has been applied to distinguish water bodies. Delineation of flooded areas and flood hazard mapping using remote sensing and GIS were also been demonstrated by making use of AVHRR images [23].SAR images have also found wide application in flood delineation[1].

Shamseddin [40] has made estimation of flooded area in Bahir-el Jebel basin using MODIS Terra derived images by employing unsupervised classification techniques.

3.2.5 Other application of remote sensing techniques

Remotely sensed data and techniques have also been applied in many field of investigation. Images obtained from satellite have been used to detect active fires and extract the extent of the burned area during the fire [29].
Remote sensing techniques can be used in all three aspects of disaster management viz: forecasting, monitoring and damage assessment Monitoring and near-real time assessment of affected by forest fires and floods areas has been demonstrated by the use of NDVI from NOAA/AVHRR.

Other applications involve natural hazards includes: asteroid, avalanche, drought prediction, earthquake, flood, hurricane, insect infestation, landslide, volcanism, forest fire, tornado, and tsunami.

4.3. Previous related studies in the study area

Water resource potential of Lake Tana has been studied previously by different investigators. In the documents reviewed, evaporation computation, runoff estimation for the un-gauged catchments and computation methodology to determine total inflow to the lake was focused on mainly.

A) Melkamu Amare [14].tried to estimate the total water resource of Tana basin mainly employing conventional methods of rainfall-runoff simulation techniques,

Rainfall-runoff simulations involved running four methods namely the regression model, the monthly water balance simulation techniques, the Area-Ratio methods and the SCS-CN methods. Additionally, he also carried out late Tana water balance simulation on monthly time step to verify the results obtained. After running modeling of the simulated and observed runoff, Melkamu stated that the water balance simulation technique best fits for the southern and eastern sub basins and area ratio method is used in the northern sub basins.

Moreover, he also made a computation of the mean annual lake evaporation of Lake Tana water surface using the combination of the Mass Transfer method and the Energy Budget method and he computed evaporation at Bahir dar station to be 161.8m3/s which is equivalent to 5102.3MCM per annum.

In his study he made use of regressional techniques to fill missing records from stations. Final result of his analysis showed that annual inflow estimated of 12051.5MCM is generated from the entire Lake Tana basin including the lake area with total drainage area of 15340km2. From simulation of the lake water balance he reported that 69.2% of the inflow is lost through reservoir losses and 31% lost as an outflow.

B) Henk Pelgrum and Wim Bastiaanssen [30]

Carried out a Remote Sensing Studies of Tana-Beles Sub Basins .The study mainly made use of remote sensing techniques and satellite derived image products for input to their analysis

The actual evaporation has been calculated using the SEBAL algorithm[39]. SEBAL converts the satellite measured spectral radiances into surface energy fluxes including evaporation. And carried out water balance computation for the year 2001.

Data from the Moderate Resolution Imaging Spectrometer (MODIS) satellite for the year of 2001 have been used in combination with SPOT-Vegetation to compute the spatial distribution of actual evaporation and soil moisture across the Tana-Beles basin. The (MODIS) data is used to derive Normalized Difference Vegetation Index (NDVI), albedo and surface temperature. SPOT data is used for NDVI only. Distributed rainfall data are based on the Tropical Rainfall Measuring Mission (TRMM) sensor .

The report stated, for the year 2001, annual lake evaporation with 95% accuracy was estimated to be 4,735 MCM. Report of the analysis has also indicated that the total inflow and outflow of the lake is about 5,118 MCM and 5,041 BMC respectively.

C) Tana-Beles project [13]

This study was conducted by Studio Peterngeli (Studio Pietrangeli, 1990) for the Ministry of Construction between late 1986 and mid 1990.

Evaporation computation was carried out in this study and Studio Pietrangeli has assumed that the pitch reading to be directly proportional to Lake Evaporation. And according to this study the mean annual Lake evaporation is estimated to be 190.3m3/s, which is equivalent to 6000MCM per annum.

Furthermore, backward simulation of the lake water balance to was carried out to estimate total inflows to Lake Tana .The mean annual inflow to Lake Tana is computed to be 297.4m3/s, which is equivalent to 9380 MCM.

5. Data source and availability

5.1. Climate data

There are about 41 climate stations within the extent of Lake Tana basin and the neighboring area monitored by the Ethiopian meteorological agency. Out of which 33 of them are still operational and contain records of climate data with in the time analysis of this study work. These 33 stations are then selected and have been used in the data analysis and mean area rainfall computation process of the sub-basins, figure 2-2. Temperature records are available from three stations. However, only two stations namely, Gondar and Bahirdar Stations, is where measurements of pitche evaporation, wind speed, humidity and sunshine hours data are available on daily level. The remaining stations contain either rainfall or rainfall and temperature information only.

Pitche evaporation, wind speed, humidity and sunshine hours data for Gondar and Bahirdar stations were collected from the National Meteorological Agency and were used in this study work.

5.2. Lake Levels and Streamflow

Out of the 11 major steams that flow into the lake stream flow records are available for only 8 stations monitored and collected by the Ministry of Water Resources. Daily Stream flow records for the years 1998 to 2003 from this flow measuring stations were collected for this research work.One of the flow measuring stations available is located at the out let of the lake in Bahirdar. Therefore Lake out flow records are taken from this station, Figure 2-2.

Furthermore, Lake Levels are recoded at Bahir Dar, Gorgora and Kunzila stations. The data recorded at Bahir Dar is observed to have both long recording life (since 1964) and quality so that the record at Bahir Dar has been used for the analysis. The records at other two stations are observed to have appreciable discontinuity.

5.3. Land feature

GIS Dataset of Soil, Land use and Landover information are available at the ministry of water resource. The data was compiled during master plan study of the Abbay river basin study 1996.

The soil data basically contains information of general soil group as per FAO classification. Land use and Landover datasets contain information such as general description of land cover classification, bare area coverage, percentage of impervious area, land use classification.

GIS maps of global soil data is also available from FAO.The FAO-Unesco Soil Map of the World was published between 1974 and 1978 at 1:5.000.000 scale. GIS layers were derived based on this Soil Map of the World. The legend of the soil map of the World contains information regarding, major soil units , Phases, Textural classes and Slope classes at different layer of soil depth [34].This data set was acquired from the internet and was used in this research work.

5.4. Lake Tana feature

Bathymetry

The Bathymetry survey conducted during the Tana-Beles project study was performed in 22 bathymetry profiles for a total of about 900km of measurements. The survey of the Lake profile was made based on 22 bathymetric profiles, 15 in the east-west directions at 5km interval and numbered from south to north for an estimated total distance of 550km. The remaining 7 bathymetric profiles were conducted in the north-south directions at 10km intervals and numbered from east to west for a total distance of about 330km. So far it is only this bathymetry survey that has been conducted for the lake. This study work has also used the data from this bathymetric survey for the purpose of water balance simulations

Volume-Area-Elevation Curves

On the basis of the bathymetric profiles some bathymetric maps at a scale of 1:50,000 and 1:100,000 were prepared (Studio Pietrangeli, 1990). Using these maps the Volume-Area-Elevation relationships of the lake reservoir were estimated and associated curves were established. The reservoir volume versus area and area versus elevation curves are directly taken from the reports of the Tana-Beles Project [13].and are presentred in figure 4-1 and figure 4-2 for reference purpose.

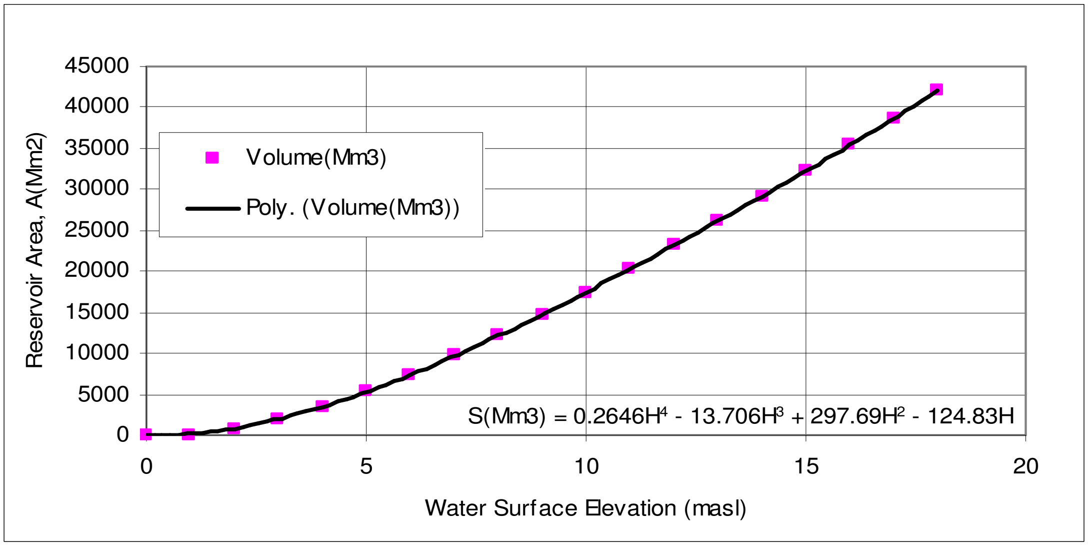

Figure 5-1 Water Surface Elevation Vs Reservoir Volume Curve

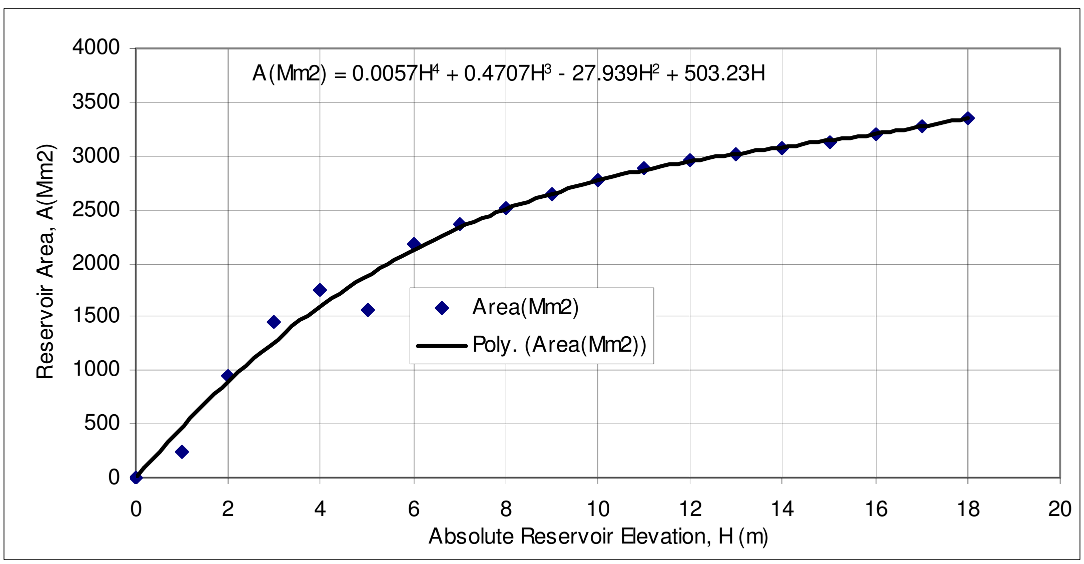

Figure 5-2 Lake Tana Elevation Vs Reservoir Area Curve

5.5. Satellite images

Digital Elevation Model (DEM)

The Shuttle Radar Topography Mission (SRTM) provided a near-global digital elevation model (DEM) of the Earth using a measurement method called radar interferometry. The SRTM was the main payload on the Space Shuttle Endeavour. During the month of February, 2000 it flew for 11 days to conduct a global mapping exercise. During that time the SRTM mapped the continents between 60 degrees North and 56 degrees South latitude, which comprises almost exactly 80% of the total landmass of Earth.

The SRTM data for the world were processed into geographic "tiles," each of which represents one by one degree of latitude and longitude. It is part of the world's first high-resolution, near-global elevation model. The resolution of the publicly released data is three arc-seconds (1/1,200 of a degree of latitude and longitude), which is about 90 meters (295 feet).

Tiles covering the Lake Tana basin were downloaded from the official site[web-10]. These tiles were merged and clipped in the extent of lake Tana basin boundary and were used to derive catchment morphology and for the purpose of sub-basins delineation.

Rainfall

Tropical Rainfall Measuring Mission (TRMM) provides global precipitation data on monthly level [web-8]. The Tropical Rainfall Measuring Mission (TRMM) satellite was launched November 27, 1997 into a near circular orbit of approximately 350 km in altitude with an inclination of 35 degrees to the equator and a period of 91.5 minutes. The TRMM Science Data and Information System (TSDIS) processes TRMM data from the Precipitation Radar (PR), TRMM Microwave Imagery (TMI), and Visible and Infrared Scanner (VIRS) instruments into data products oriented toward measuring rainfall in the tropics [38].

Monthly rainfall products of this satellite have been acquired and used for rainfall analysis and gap filling.

NDVI

Different NDVI data sets are available with different spatial and temporal resolutions, and different temporal coverage. Three distinguished satellite products available as a public domain datasets are, Advanced Very High Resolution Radiometer (NOAA–AVHRR) time-series extending from 1981 to the present with the coarse scale (8–16 km resolution)[web-4][web-1] , Moderate Resolution Imaging Spectroradiometer (MODIS–TERRA) data set with 250–1000 m resolution extending from 2000 to the present [web-1], and Satellite Pour l'Observation de la Terre–Vegetation (SPOT–VGT) data 1000 m resolution extending from 1998 to the present [web-3].

In this thesis work 10 days temporal resolution products from the SPOT-Vegetation satellite sensor were acquired and used because of the longer time span than the MODIS products and better spatial resolution than AVHRR products.

LandUse/ Land Cover

The U.S. Geological Survey's (USGS) National Center for Earth Resources Observation and Science (EROS), the University of Nebraska-Lincoln (UNL) and the Joint Research Centre of the European Commission have generated a 1-km resolution global land cover characteristics data base for use in a wide range of environmental research and modeling applications[web-1].

The data set is derived from 1-km Advanced Very High Resolution Radiometer (AVHRR) data spanning a 12-month period (April 1992-March 1993) and is based on a flexible data base structure and seasonal land cover regions concepts.

This data can be downloaded from the official website site free of charge. Thus, dataset for Africa was downloaded and was used in this research work.

SAR Imagery

SAR Imageries from RADARSAT and ASAR satellites have been collected and employed in this research work[web-11]. RADARSAT is Canada's first series of sophisticated Earth observation satellites. RADARSAT-1 was launched in 1995 and RADARSAT-2, is planned for launch in 2006/ 2007. Both are equipped with advanced radar sensors called a Synthetic Aperture Radar (SAR). The SAR is a powerful microwave instrument that transmits and receives signals to "see" through clouds, haze, smoke, and darkness, and obtains high quality images of the Earth in all weather, day or night. Three images were obtained from this satellite product showing Lake Tana surrounding flood plains taken on March-14 -2005 , July- 20- 2005 and July- 27 -2005.These images are in resolution of 30 meters.

LandSat

The American LANDSAT satellite program dates back to 1972, when Landsat-1, then called ERTS-1 (Earth Resources Technology Satellite), was launched. The most recent satellite in the series, Landsat 7, was launched in 1999 featuring an upgraded Enhanced Thematic Mapper (ETM+) sensor. A program of evolving sensor technology and almost continuous data collection has made LANDSAT the most successful civilian Earth observation program to-date. The spatial resolutions of image products from this satellite are 15 m and 30m. Both images were acquired and used in this thesis work.

Albedo

Global land surface Albedo datasets derived from the Terra Moderate-Resolution Imaging Spectroradiometer (MODIS) from March 2000 to present have been completed for ready use and are distributed by NASA. These data sets can be obtained in 1000m spatial resolution and in 9 different spectral resolutions. These dataset was downloaded for the years 2000 to 2003 from the internet and was employed in this research activity.

5.6. Ground data through study site tour

Through study visit conducted August 14 2006 to August 19 2006 .it was able to collect true ground information on fogera and dembia flood plains regarding the inundation that occurs in wet season of the year. The collected information includes height of flood marks, spatial extent of flood and general information on the mechanism and locations on the reaches where the flood brakes into the flood plains. This was carried out through visual observation, measurement and consultation with the inhabitant in the flood plains

6. Data Analysis and estimation of hydrological variables

This chapter describes the methods applied and results obtained to estimate the major hydrological variables that served as inputs to the runoff estimation process which is discussed in pending chapter 6 and Lake Water balance simulation dealt later in chapter 7 of this report.

Mainly,

1) Watershed Geometry delineation from Digital Elevation Model and preparation of catchment division for semi-distributed modeling.
2) Climate data analysis and gap filling. This includes statistical analysis of rainfall, temperature, wind speed and relative humidity time series data.
3) Hydrometric data analysis
4) Estimation of Potential evapotranspiration, discussion of procedure followed to compute the spatial potential evapotranspiration using combined equation,
5) Assessment of flood plains. Delineation of historical flood inundation and determination of their temporal extent using NDVI images,
6) Enhancement of existing Land use/Land cover database with the help of optical images,
7) Soil data analysis and deriving of modeling parameters, SCS-CN and water holding capacity.

are dealt in depth below.

6.1. Catchment Morphology

Shuttle Radar Topography Mission (SRTM) Digital Elevation Model (DEM)[12] with spatial resolution of approximately 90 meter were obtained and pre-processed to fill missing void pixels and to geometrically correct into the required projection. This data was then used to identify the watershed geometry and the drainage pattern of Lake Tana sub-basin.

ArcHydro utility was used to delineate the catchments in to selected spatial resolution and based on specified catchments division points. ArcHydro is a GIS based geospatial and temporal data model for water resources. It is a Geodatabase design and a set of accompanying tools geared for support of water resources applications in GIS environment [27].These tools can be used to process DEM data to produce catchments and drainage pattern networks.

Delineation of sub-catchments of Lake Tana basin was carried out in three levels. Initially, a course resolution image was used to generally distinguish boundary of the Lake Tana basin. Then two consecutive delineations were carried out in order to identify the major sub-basins and smaller catchment divisions within these sub-basins.

A total of 11 major sub-basins were first identified corresponding to the main rivers that drain the area. Afterwards, sub-basins were further divided into smaller sub-catchments. As shown in Figure 5.1. Selection of number catchment is carried out considering the following criteria's.

1. Grouping based on common land use / land cover and soil and property
2. Maximum/minimum catchments size requirement for the selected hydrological models.
3. Maximum/minimum size of catchments supported by modeling software
4. Additional divisions were also introduced in order to separate gauged and un-gauged part of each major sub-basin.

Finally, areas of gauged and un-gauged were determined from the sub-basin map derived. Table 5.1 summarizes the identified sub-basins within Lake Tana basin along with the corresponding area.

Table 6-1 Gauged and Un-gauged area estimate in Lake Tana Basin

Sub-basin Name	Gauged Area (sqr.km)	Un-Gauged Area (sqr.km)	Total (sqr.km)
Ambagenen	-	512.01	512.01
Arno-Garno	100.14	229.62	329.76
Gelda	-	436.37	436.37
Gumara	1354.20	250.12	1604.32
Gumaro-Sizele	158.71	442.17	600.88
Koga	300.70	-	300.70
Lower Gilgel Abbay	-	2558.57	2558.57
Megech	512.56	254.50	767.06
Ribb -Shine	1522.56	633.34	2155.91
Upper Gilgel Abbay	1657.89	-	1657.89
West Tana	-	1081.29	1081.29
Total Lake Tana Basin	**5606.76**	**6397.99**	**12004.76**
Average area of Lake Tana	-	-	3041.56
Total Including Lake area			**15046.32**

Total catchment area of Lake Tana basin excluding area of the lake is about 12,004 sqr.km, in which about 5,606.8 sqr.km (46.7%) of the total area is gauged and the remaining 6,398 sqr.km (53.3 %) is un-gauged. This total area of Lake Tana Basin has been estimated to be 12260 km^2 and 12230 km^2 during the study of the Tana-Beles Project[13] and study work conducted by Melkamu[14] respectively.

Figure 6-1 Sub-Basin Divisions of Lake Tana Basin

6.2. Stream Flow

Stream flow measurements are collected from the mentioned stations in chapter 4 and annual runoff from the catchments is calculated and presented in table 5.2 below.

Table 6-2 Mean Annual Runoff (1998-2003) recorded at stations

Location of Gauging Station	Mean Annual Recorded flow (1998-2003), MCM
Upper Gilgel Abbay near Marawi	1,711.28
Garno at station near Enfranz	28.12
Gummaro near Maksegnit	21.43
Gumera near Bahir dar	1,062.58
Koga near Merawi	182.13
Megech Near Azezo	239.75
Ribb Near Addis Zemen	483.18
Total gauged	**3,728.47**

As can be seen from table 5.2 the total runoff captured at station corresponding to 5,606.8 sqr.km, which is 46.7 % of the entire area, is about 3,728 MCM. This value is calculated from daily 5 years of stream flow record, 1998 up to 2003.

It was observed during study site tour that the gauging stations some times during high flood events could get submerged and the stream flow record could be disrupted .One observation worth noting is daily hydrograph plot of Ribb gauging station near Addis Zemen for the year 1998 , figure 5.2. It can be observed that starting july-29 up to September-5 the recorded flow shows a constant graph which is unlikely to happen referring to records from other year. One of the possible reason for this could be the over flowing of the river out of the banks and to the flood plains during high flood even .River steam flow could be hydraulically connected with the flooded area on the surround flood plains adjacent to Ribb river. Therefore in such events the measured stream level does not represent the flow in the rivers. The same event is also observed in the 1985.

These records were considered as missing records. Flow estimation for these records was carried out during un-gauged catchment analysis which is discussed in chapter 6 of this report.

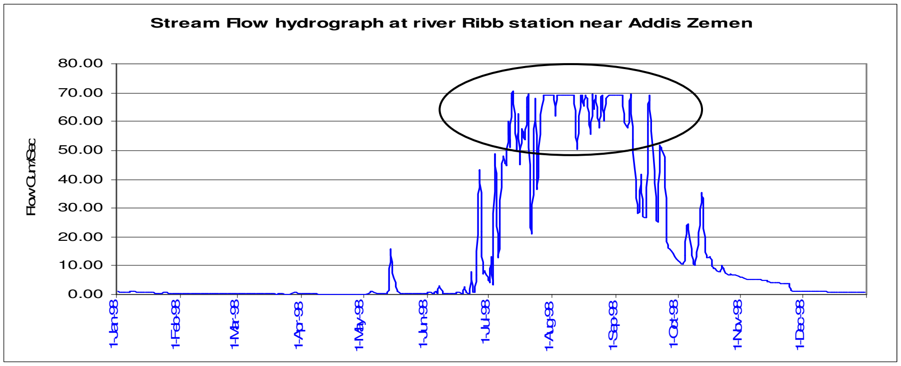

Figure 6-2 Stream flow hydrograph at river Ribb station near addis zemen

Figure 6-3 River flow Gauging station at Ribb river (August 17 2005)

Base flow separation: The foremost step in hydrograph analysis involves separation of the measured flow in to two components surface runoff and baseflow. Especially for SCS model of runoff estimation it is essential first to separate the baseflow from the surface runoff component. Baseflow separation for all the rivers was carried out using SWAT Baseflow filter program. SWAT baseflow filter program estimates baseflow and groundwater recharge from stream flow records using the methodology outlined by Arnold and Allen[15].It mainly implements automated recursive digital filter and recession analysis techniques.

The method first uses automated recursive digital filter technique employing the analogy of filtering high frequency from low frequency in signal analysis. The following equation is used to perform the filtering .

$$q_t = \beta q_{t-1} + (1+\beta)/2 * (Q_t - Q_{t-q}) \tag{5.2.1}$$

Where q_t is the filtered surface runoff(quick response) at time step t, Q_t is the original stream flow, and β is the filter parameter. Base flow b_t is calculated with the equation (5.2.2).

$$b_t = Q_t - q_t \tag{5.2.2}$$

The filter can be passed over the stream flow data three times, depending on user's selected estimates of base flow. The next step in the analysis is to quantify the characteristics of the base flow diminishes in the absence of recharge and the recession characteristics are estimated using an exponential decaying curve function.

As indicated by Arnold and Allen [15], this computational technique has been validated with the traditional graphical technique. The results were comparable in accuracy in predicting the manually separated base flow [15].

This baseflow filter program was selected in its advantage of being easy to operate and has the ability to be adjusted based on users choice. Output parameters of this software are the time series of base flow and surface runoff, baseflow recession constant (alpha factor) and Baseflow Days i.e. number of days for the baseflow recession to decline through one log cycle.

Parameters and mean values of base flow estimation are outlined in table 5-3.

Table 6-3 Output parameters and mean values of base flow as computed by SWAT base flow filter

River	Mean stream flow (m^3/s)		Base Flow	alpha factor	Baseflow Days
	Wet seasons	Dry Seasons	Mean(m^3/s)		
Upper Gilgel bbay	121.490	5.480	11.860	0.029	80
Gumaro	4.070	0.150	0.360	0.030	77
Gummera	75.250	3.460	7.690	0.014	160
Koga	11.380	1.690	3.550	0.017	136
Megech	15.120	2.120	4.650	0.016	88
Ribb	33.960	1.740	7.410	0.035	66

Separated base flow for Ribb river from 2000- 2001 is presented below in figure 5.3 for demonstration purpose.

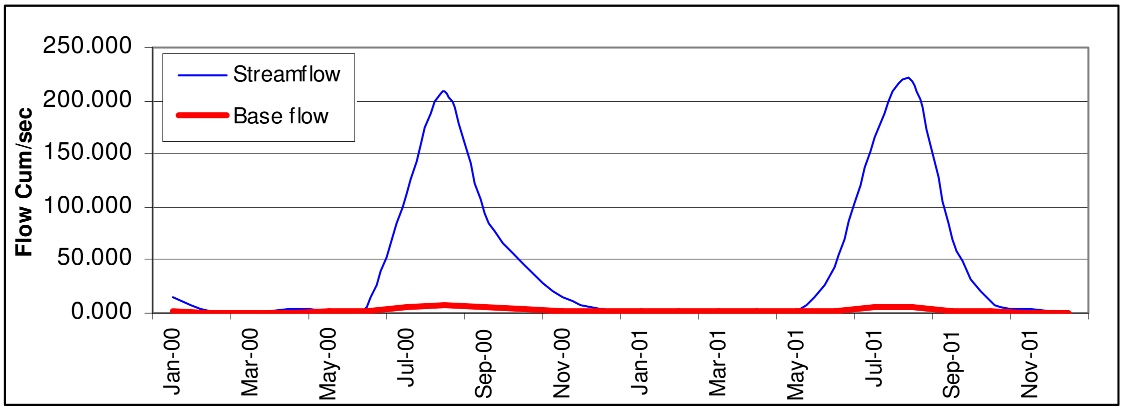

Figure 6-4 stream flow and base flow plot for Ribb river (2000-2001)

Estimated base flow has been validated against graphically separated base flow and the result is quite consistent.

6.3. Climate data analysis

Rainfall

Most of the rainfall recorded from the stations have missing data ranging from 10 to 50 % and some cases the readings contains corrupted values. Therefore before using the data to runoff modeling it was first essential to apply a gap filling techniques and statistical analysis to filter out-liars from the rainfall record data.

One of the options considered to fill the missing data gaps was through the use of multiple regression techniques from nearby stations. The other option considered was through the use of data from satellite estimate of rainfall. This second option, with satellite based estimate, however, provided closer estimate when compared to existing observation. Results of Statistical analysis using multiple regression techniques is presented in Annex V.

Two datasets were obtained from daily FEWS satellite product with spatial resolution of 1000 meter and monthly TRMM product with spatial resolution of 0.25^0. However, statistical test result have showed that the rainfall satellite estimated from FEWs satellite and the ground measured rainfall data show very little correlation and the satellite measured rainfall highly underestimates the rainfall. Statistical results are annexed in this report, ANNEX I.

On the other hand, rainfall estimate products from TRMM satellite have shown good correlation with the ground stations. Average correlation coefficient of 81.2% is obtained. Result for each station is shown in Table 5-4.

Table 6-4 Correlation of TRMM satellite and ground Station Statistical Test results

West Stations	R2	South Stations		North Stations	R2	East Stations	R2
Aykel	87.6	Enjibar	83.1	Amba Giorgis	77.1	Debre Tabor	80.4
Chandiba	85.4	Feresbet	86.8	chauit	76.6	Ebnet	82.4
Shaura	82.1	Meshnti	72.4	Dabat	84.7	Hamusit	78.2
		Tis ababy	72.3	Enfraz	74.8	Korata	88.3
		Bahirdar	84.3	Gondar	73.8	Wenziye	83.0
				Shembekit	78.6	Werota	85.4
						Yifag	80.4
mean	**85.0**	**mean**	**79.8**	**mean**	**77.6**	**mean**	**82.6**

Linear regression techniques, therefore, were applied to fill the missing gaps Using TRMM products. Minitab statistical software was used to assist in the mathematical modeling of the equations for regression model and Arcview was used for spatial interpolation of IDW techniques to converts the point data into gridded rainfall.

After the missing gaps are filled and the short records are extended, with the procedure mentioned above, the point rainfall was then converted to spatial rainfall grid using IDW method of interpolation and the interpolated spatial rainfall was later summarized into a single value for the smallest unit of sub-basin division on monthly level.

Temperature, Humidity, Wind speed ,sunshine hours

Other available and collected meteorological data records in lake Tana basin include air Temperature records available from the three stations as mentioned in chapter 3 of this report i.e Bahirdar,Addis Zemen,Gondar; humidity ,wind speed and sunshine hour records from Bahirdar and Gonder stations . These monthly Climate record values were converted to Spatial maps and were later aggregated into the smallest unit of sub-basin division.

Melkamu[14] has marked the shift in wind speed records at Bahirdar meteorological station and has indicated both the negative trend as well as the downward shift. Same pattern were also observed, trend in the wind speed is observed since in the early seventies until in the mid eighties and afterwards the trend becomes steady and regular in pattern. Shifts are observed at mid seventies and latter at mid eighties. In this research work it is assumed that the cause of the shift is attributed to the change of local environment around the gauging stations, possibly as the result of development of Bahirdar City. However, evaporation record from this station is used to represent a wider range of area around Bahirdar .Therefore it was necessary to remove this shifts so that it can represent the majority of area in the basin. It was done accordingly using the method outlined by Maidment[7]. Figure 5-5 shows raw data as obtained and corrected time series plot.

The assumption stated above regarding the shift in wind speed is base on observation during study tour however there could also be other reasons for the shift in wind speed. Therefore, the author recommends further research work be carried out to investigate the cause of the shift .

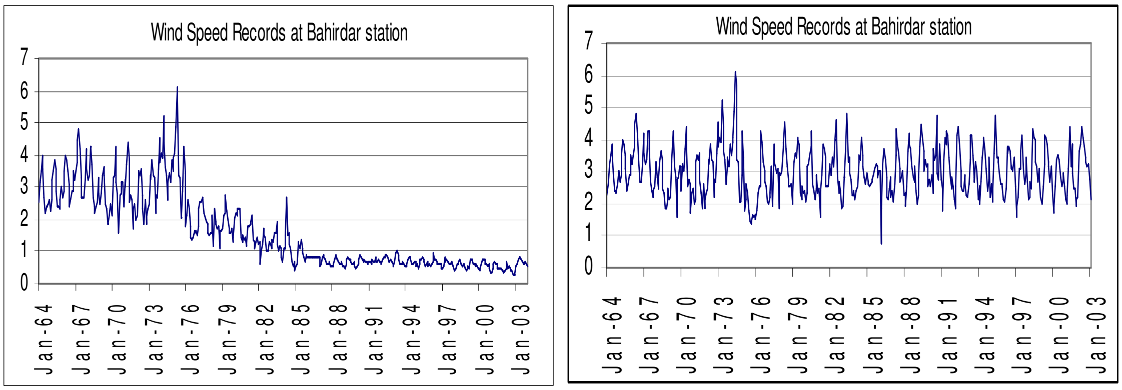

Figure 6-5 Wind Speed time series plots before and after Shit is removed

6.4. Evaporation estimation

Evaporation is one of the major components of hydrological variables in water balance simulation models. Accurate estimation of evaporation has the major impact on the result of the model. As a result some studies carried out previously have tried to give estimation of evaporation in Lake Tana basin using different techniques. It was necessary to model the potential evapotranspiration in this research work for two reasons. One, because this research work mainly implements remotely sensed spatial data it was hoped to capture the spatial variation of evaporation across the sub-basin. Two, the pitch evaporation measurement from the two stations, Bahirdar and Gondar, may not represent the evaporation that takes place in the sub-basin as location of the station might have its own impact. For example Bahir Dar meteo station is located in the middle of the town.

Wim Bastiaanssen and Henk Pelgrum[30] have made an estimation of actual evaporation using remotely sensed information and it was estimated to be 1588 mm/year for year 2001 mainly using the SEBAL algorithm (Surface Energy Balance Algorithm for Land). SEBAL converts the at-satellite measured spectral radiances directly into surface energy balance fluxes, including evaporation, without the need to solve the water balance first [30]. Melkamu has obtained annual mean Lake evaporation value of 1655 mm/year [14].

In this thesis work remotely sensed data from MODIS satellites along with simulation by combined equation[7] below has been used to compute the spatially distributed potential evapotranspiration for the entire Lake Tana basin within the time range of 1998-2003.

Methodology

The potential evapotranspiration can be modeled using equation 5.1 [7].

$$E_p = \frac{\Delta}{\Delta+\gamma}(R_n + A_h) + \frac{\gamma}{\Delta+\gamma} * \frac{6.43(1+0.536U_2)D}{\lambda} \tag{5.1}$$

Where

R_n =net radiation exchange for the free water surface ,mm/day

A_h =energy advected to the water body, mm/day

U_2 =wind speed measured at 2m, m/ s

D = vapor pressure deficit

Net radiation is the net input of radiation at the surface the difference between the incoming and reflected solar radiation. It is given as summation of the difference between the incoming and reflected solar radiation (net solar radiation) and the difference of incoming and outgoing long wave radiation(net long wave radiation)[7].

$$R_n = S_n + L_N \qquad (5.2)$$

Because net radiation data are often scarce, for general purpose when only sunshine, temperature, and humidity data are available as in the case for lake Tana basin net radiation can be computed with the following empirical equation 5.3[7].

$$R_n = f(n, N, R_a, \alpha, e_d, \sigma, T) = \left[\left(0.25 + 0.5\frac{n}{N}\right)R_a(1-\alpha)\right] - \left[\left(0.9\frac{n}{N} + 0.1\right)(0.34 - 0.14\sqrt{e_d})\sigma T^4\right]$$

(5.3)

Where R_a is the extraterrestrial radiation and total day length the following equations were used.

$$R_a = 15.392 d_r (w_s \sin f \sin d + \cos f \cos d \sin w_s \qquad (5.4)$$

The amount of radiant energy captured at the earth surface is the dominant control on the regional evaporation rate in the case where evaporation rate is not limited by the availability of water and hence the computed evaporation rate is sensitive to accurate estimation of radiation spatially as well as temporally.

In equation 5.3 above the sensitive and relatively uncertain parameter is the surface albedo α. Surface Albedo is defined as the fraction of incident radiation that is reflected by a surface. It can be estimated using remote sensing techniques detail computation is discussed below.

Surface Albedo

A simplified non-remote-sensing approach has often been applied previously for many evaporation models. In this approach, land cover map is mainly used to make a distinction between the major surface types, and a single average albedo value is assigned to each of these surfaces. Madment[7], for example suggests a value of 0.08 for open water,0.20-0.26 for grass and pasture and the values of snow and ice ranges from 0.2 up to 0.8. However, this technique aggregates the albedo both spatially and temporally. Now a days advanced remote-sensing based methods are being developed and employed to compute surface albedo estimates from satellite remote sensing data, by using different algorithms through the available sensors and the results have shown to provide better estimates of albedo.

MODIS instrument aboard NASA's Earth Observing System (EOS) spacecraft is one of the available popular active sensor producing white-sky and black-sky albedo products in different wavelength.In this thesis work, images of 1km grid spatial resolution and 16 days temporal resolution images were acquired and were used for estimation of actual albedo from white-sky , black-sky albedo and aerosol optical depth products. For surface energy balance studies typically require broadband shortwave (0.3–3.0 um)[7].Hence, MODIS bands in this range were used to represent the radiation.

The MODIS albedo product generates operationally a set of two albedo measurements for a spatial resolution of 1km grid point on the ground. The two measurements represent components of the actual surface albedo. The first component is the directional hemispherical reflectance, or "black-sky albedo," The second component is the diffuse bihemispherical reflectance, or "white-sky albedo,"

Exhaustive explanation of the algorithm followed by MODIS to produce these image products is well discussed in the MODIS user guide, Shunlin [31] and W. Lucht; Crystal B. Schaaf; Alan H. Strahler[32].

The actual albedo (blue-sky) value however, is computed in thesis by using A liner combination of black and white sky albedo algorithm on monthly time step for the years 2000-2003.using equation 5.5 [33].

$$\alpha_A = (\alpha_W * skyl) + \alpha_B(1 - skyl) \tag{5.5}$$

Where α_A , Actual or blue Sky Albedo.

α_W , α_B white sky and Black sky albedo respectively.

Skyl, Fraction of diffuse skylight (a function of aerosol optical depth at 550nm and solar zenith angle [0..89])

As a result spatial and temporal mapping of surface albedo was obtained in monthly time step. These were later aggregated in sub basin level for the computation of soil water balance and validation of evaporation estimates. A typical albedo map is shown below, figure 5-5, for year 2002.Monthly distribution of Albedo for the year 2002 has been tabulated in table 5.5 for Bahirdar and Gondar cities.

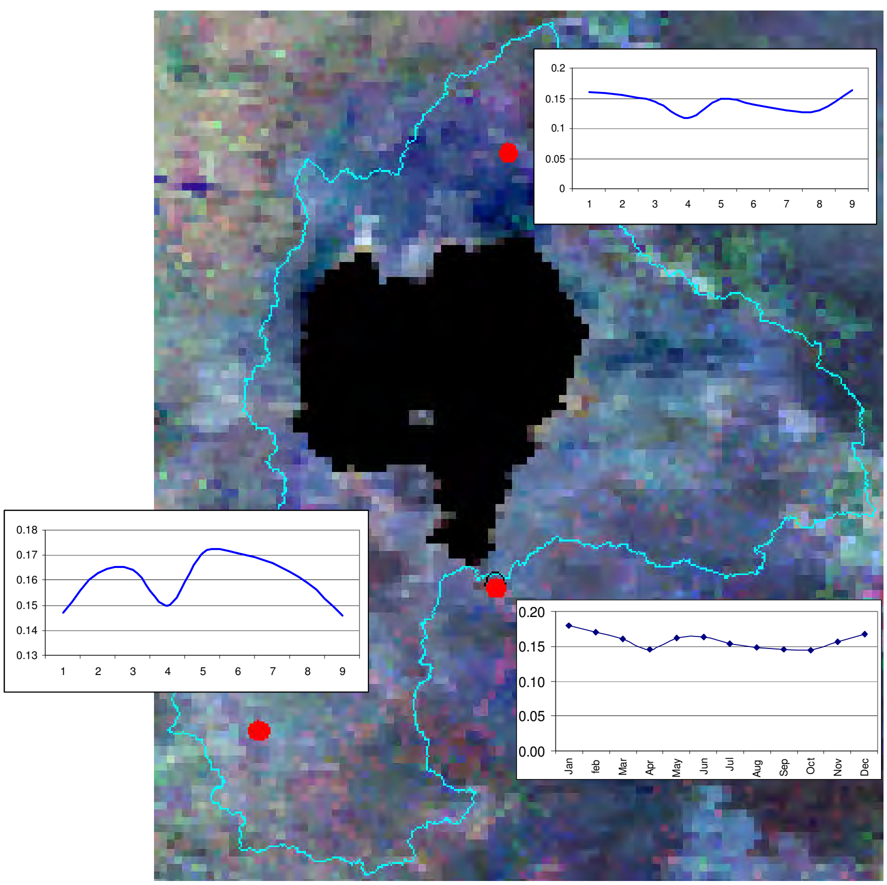

Figure 6-6 Blue Sky Surface Albedo Map For year 2002

	Albedo Values	
Month	Bahirdar	Gondar
Jan-02	0.172	0.180
Feb-02	0.177	0.170
Mar-02	0.153	0.160
Apr-02	0.141	0.145
May-02	0.151	0.161
Jun-02	0.165	0.163
Jul-02	0.175	0.153
Aug-02	0.174	0.149
Sep-02	0.166	0.145
Oct-02	0.160	0.144
Nov-02	0.168	0.156
Dec-02	0.178	0.167

Table 6-5 Albedo result for Bahirdar and Gondar cities

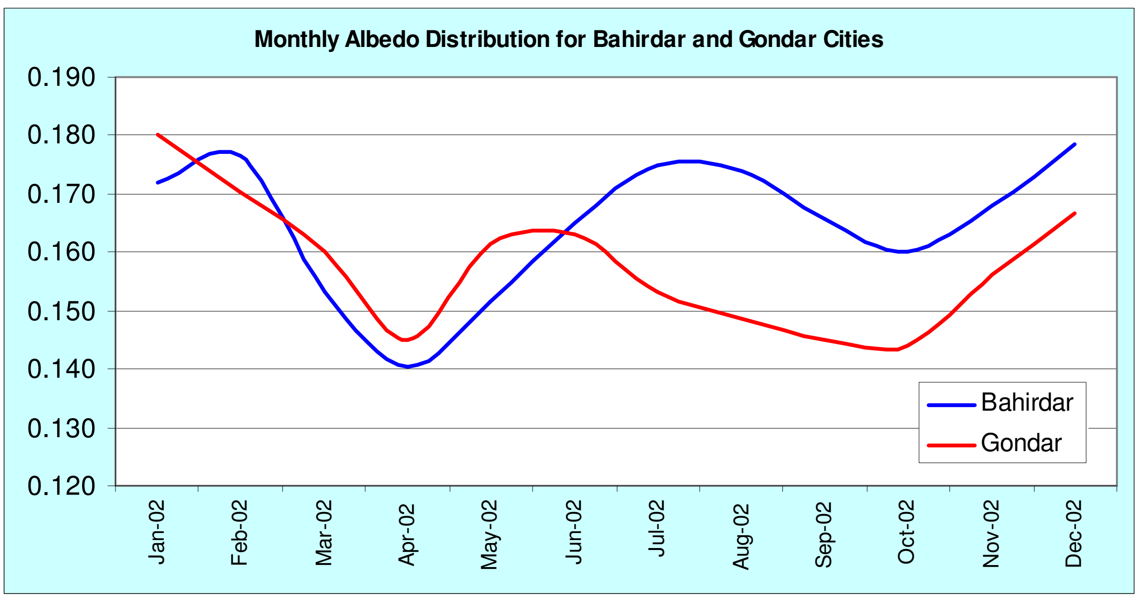

Monthly Albedo distribution for Bahirdar and Gondar cities for the year 2002

Result

The spatially mapped albedo results were aggregated in sub basin level and computation of potential evapotranspiration was carried out using the equations discussed in the methodology section above. Point evapotranspiration was also computed with the parameters at Bahirdar and Gondar station. The computed potential evaporation was then compared with the measured evaporation at the two stations. Correlation coefficients of 70% and 63 % were obtained for Bahirdar and Gondar stations respectively. However, percentage of error in annual mean estimates is found to be 2% for Bahirdar and 4% Gondar. Annual mean evaporation 1666mm and 1485mm was obtained at Bahirdar and Gonder Stations respectively.

A) Mean Monthly Plots

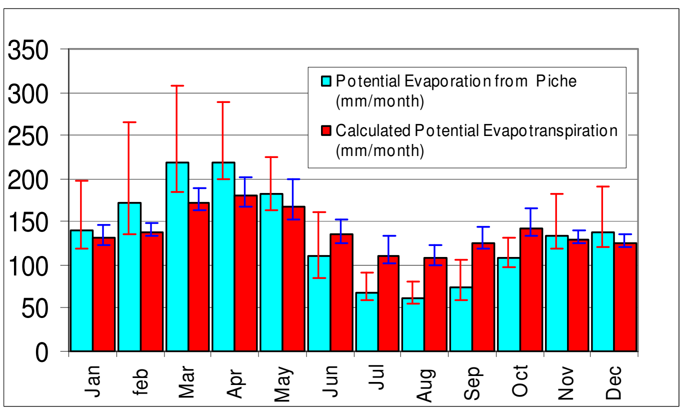

B) Correlation plot

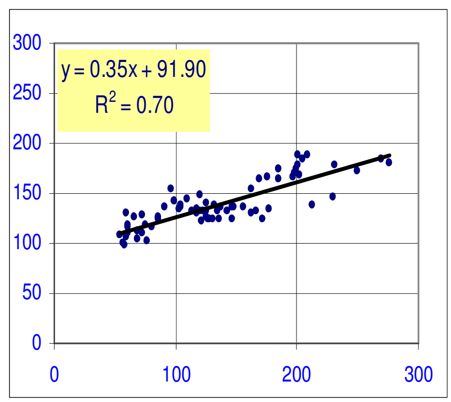

C) Time Series plots of measured and computed

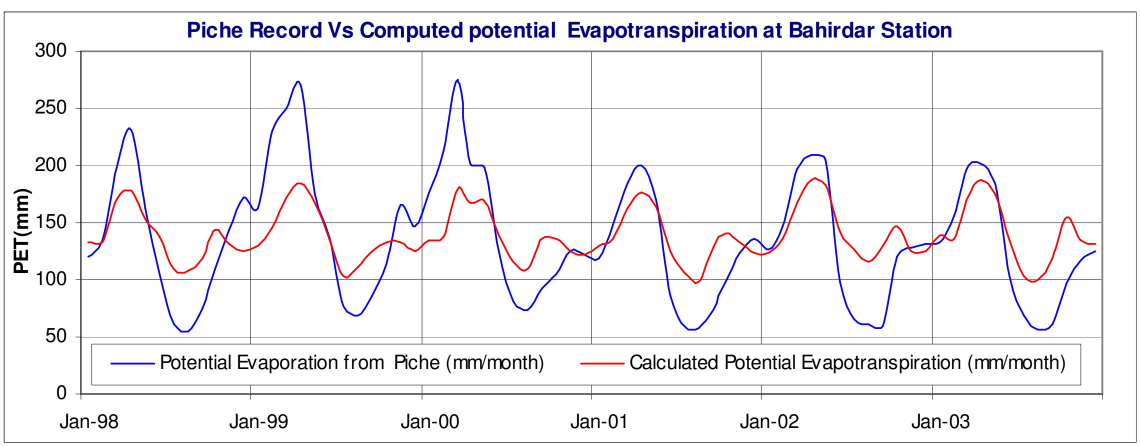

Figure 6-7 Computed Vs Measured Potential Evapotranspiration at Bahirdar Station

6.5. Flood plain inundation analysis

As described in literature review part of this document, quite significant methods have been previously used to identify and mark flood extent zones by making used of satellite acquired image. In this thesis also satellite imagery were used to identify the flooded zone in the surrounding flood plains i.e. Fogera, Dembia, West Tana and Gilgel Abbay plains.

These flooded zones were preliminarily identified by simple visual interpretation of false color images from Landsat Thematic Mapper (TM) imageries with approximately 15 meter resolution images. Moreover, visit to the Lake Tana neighboring flood plains further asserted the hypothesis and these flood plains were further investigated to carry out detailed mapping of historical flooded extent area and quantify the time series values of water surface area and total water volume.

As it was been able to observe from the visit to the flood plains the floods primarily occur as a result of

1) Back water flow from the lake
2) River line flooding .Outflow from the banks as a result of heavy flood.
3) Due to the very flat topographic character of the plains direct precipitation on the plains does not get drained rapidly therefore this creates small impoundments which later grow into a wider inundation.

Methodology

Delineation of historical flooded extent was basically carried out by threshoilding techniques of NDVI images of SPOT multi spectral imageries. The threshold values were first set to 0 and areas of negative values were kept as “water bodies”. Due to the fact that the NDVI value for inundated surface features remains negative. It was further improved iteratively by contrasting with surrounding dryland and using four levels of verification by means of data available from RADAR SAT high resolution SAR images, LandSat, ASAR satellite images (ANNEX II) and information gathered from study area visit during Aug-12-2005 upto Aug-19-2005.

Following establishing of the spatial extent of historical flooded area, the results was superimposed over a DEM to be able to determine the time series of volume that stays on the flood plains during wet season of the year.

10 days temporal images were collected from SPOT multi spectral imageries website with spatial resolution of 1000 m by 1000 m starting apr-1998 up to dec-2003. These images were first geometrically corrected on basis of UTM projection and WGS-84 datum projection and clipped to the extent of Lake Tana basin. Since SPOT images are optical images cloud cover can significantly tarnish the results hence, with a consideration of avoiding cloud contamination, statistical methods were employed to filter out cloud free images in the extent of the study flood plains. The results were further refined with MOIDS daily images of 250 m resolution false color images. The statistical method mainly is carried out using comparison of frequency curve plots of NDVI values with the preceding time image frequency plot and average values accordingly images deviating much from the normal plot were discarded. This was further improved and validated by visual comparison of the images taken from MODIS satellite.

Ground collected information was initially converted to points on a map and overplayed with RADARSAT SAR image taken 27-jul, 20-jul and march-14. and using supervised classification method four classed were identified Lake Tana boundary , completely flooded and submerged zone, partially flooded marshes and dry lands the classification. Apart from its all weather capability the most important advantage of using SAR imagery lies in its ability to sharply distinguish between land and water[23]. And for this reason these images provided dependability to be used for calibration. Similarly, two SAR images from ASAR satellite and other two images from LandSat were also processed using the same approach and provided additional 4 sets of images to be used for calibration (ANNEX II).

Using these reference images, the initially assumed threshold value on the NDVI map was improved and decadal images of spot were classified and temporal mapping of flooded zone was carried out from 1998 to 2003. These maps were overplayed with the corrected DEM grid to determine floodplain storage and their changes in time. In this procedure ground information regarding submerged height was also incorporated to produce the water levels. Decadal series of volumes on the flood plains were calculated using the equation 5-6.

$$V = \sum_{i=1}^{n} (DEM - h_W) * res \tag{5.6}$$

where hw is water level Grid data

DEM digital elevation model

Res: the spatial resolution of the images

N number of cells identified within the flooded zone.

In above equation 5.6 is water level Grid data, h_w, was determined from information gathered during study site tour lake level and relative NDVI values of cells identified as flooded area.

Since the flood plains surrounding Lake Tana are very flat ,average slope of less than 3%, a vertical error of 1 m in the DEM may lead to an error of 100s of square kilometers in flood estimation, and hence the DEM data was further corrected and validated with digitized 1:50,000 topographic map and from ground collected information.

Result

Time series plots of NDVI values at selected known flooded areas and dry lands is shown below we can observe that in dry land areas the monthly NDIV distribution is almost similar to the rainfall patter Figure 5-7. However, in flooded area a different distribution is obtained. The distribution indicated that, in wet season, lower values are observed this corresponds to the water inundations in the area and in dry seasons higher values are observed and this corresponds to the vegetation cover that soon takes over after the flooding season is over.

Results also showed that flooding has occurred in all of the years. Often, it starts at beginning of June and it disappears end of September. As it was able to observe from the temporal pattern, the way the area of the flooded water diminishes indicated that most of the water does seem to either infiltrate(to join the lake or the river through subsurface flow) or evaporates to the atmosphere.

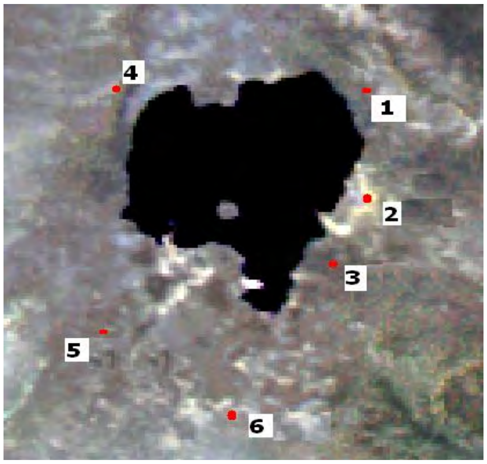

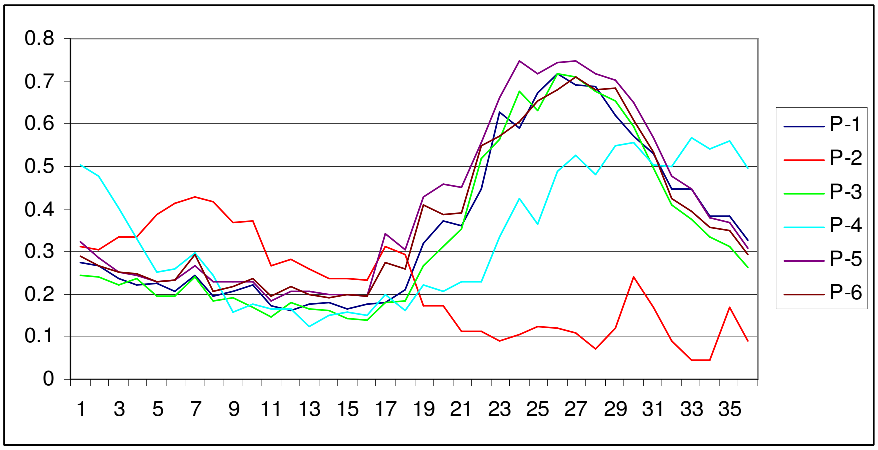

Figure 6-8 Selected Temporal plot of NDVI values

Table 5-5 shows the resulted monthly series of area of water on the flood plains for the year 2003. Average amount of water for July alone on Fogera, Dembia and Gilgel Abbay was found to be 86 MCM,70 MCM and 30 MCM respectively . Detailed tabular values are attached in ANNEX II of this report.

Table 6-6 Flood inundation area sqr.km for 2003

Month	Ribb	megech	WestTana	Gumara	Gabbay
june	19.50	18.00	15.00	7.50	20.50
july	101.33	98.00	45.33	13.33	24.07
august	196.67	138.67	75.67	33.47	39.90
september	191.67	141.33	91.67	39.67	44.13
october	100.67	30.33	76.67	32.33	43.70
november	45.67	21.33	34.67	21.80	36.60
december	43.67	21.33	40.33	17.00	31.50

The values indicate considerable amount of water is delayed in the flood plains which seeps to the ground and joins the lake or evaporated back to the atmosphere. Total Evaporation loss of 276.3 MCM/year from the flood plains were estimated this was later accounted in the Lake water balance computation illustrated in chapter 7 of this report. Monthly five years average area in sqr.km monthly maximum area within the five years is tabulated in Table 5-6 and Table 5-7 below respectively.

Table showing the monthly result is attached in ANNEX II.

Table 6-7 Monthly five years average area(1998-2003) in sqr.km

	Ribb	Megech	West Tana	Gumara	Gilgel abbay	Total
January	0.00	0.00	0.00	0.00	0.00	0.00
February	0.00	0.00	0.00	0.00	0.00	0.00
March	0.00	0.00	0.00	0.00	0.00	0.00
April	0.00	0.00	0.00	0.00	0.00	0.00
May	0.00	0.00	0.00	0.00	0.00	0.00
June	25.44	14.36	25.06	8.14	39.47	112.47
July	107.22	122.01	79.40	12.96	27.43	349.01
August	204.29	150.42	128.95	31.19	47.72	562.58
September	145.35	146.88	86.80	20.60	32.06	431.69
October	222.10	43.83	136.68	27.00	106.70	410.66
November	59.31	25.00	44.64	25.69	54.38	209.02
December	51.36	23.62	51.73	20.58	45.40	192.69

Table 6-8 Monthly five years maximum area(1998-2003) in sqr.km

	Ribb	Megech	West Tana	Gumara	Gilgel abbay
January	0.00	0.00	0.00	0.00	0.00
February	0.00	0.00	0.00	0.00	0.00
March	0.00	0.00	0.00	0.00	0.00
April	0.00	0.00	0.00	0.00	0.00
May	0.00	0.00	0.00	0.00	0.00
June	50.96	19.50	38.85	13.62	48.57
July	133.08	161.51	123.77	15.37	34.56
August	235.56	221.65	177.48	37.77	53.35
September	191.67	190.65	93.57	39.67	44.13
October	646.62	78.48	243.71	48.18	184.19
November	145.28	44.60	63.68	36.82	93.32
December	182.82	41.38	79.64	30.71	63.95

Typical Flooded area map for 21-aug-2003 is displayed in figure below

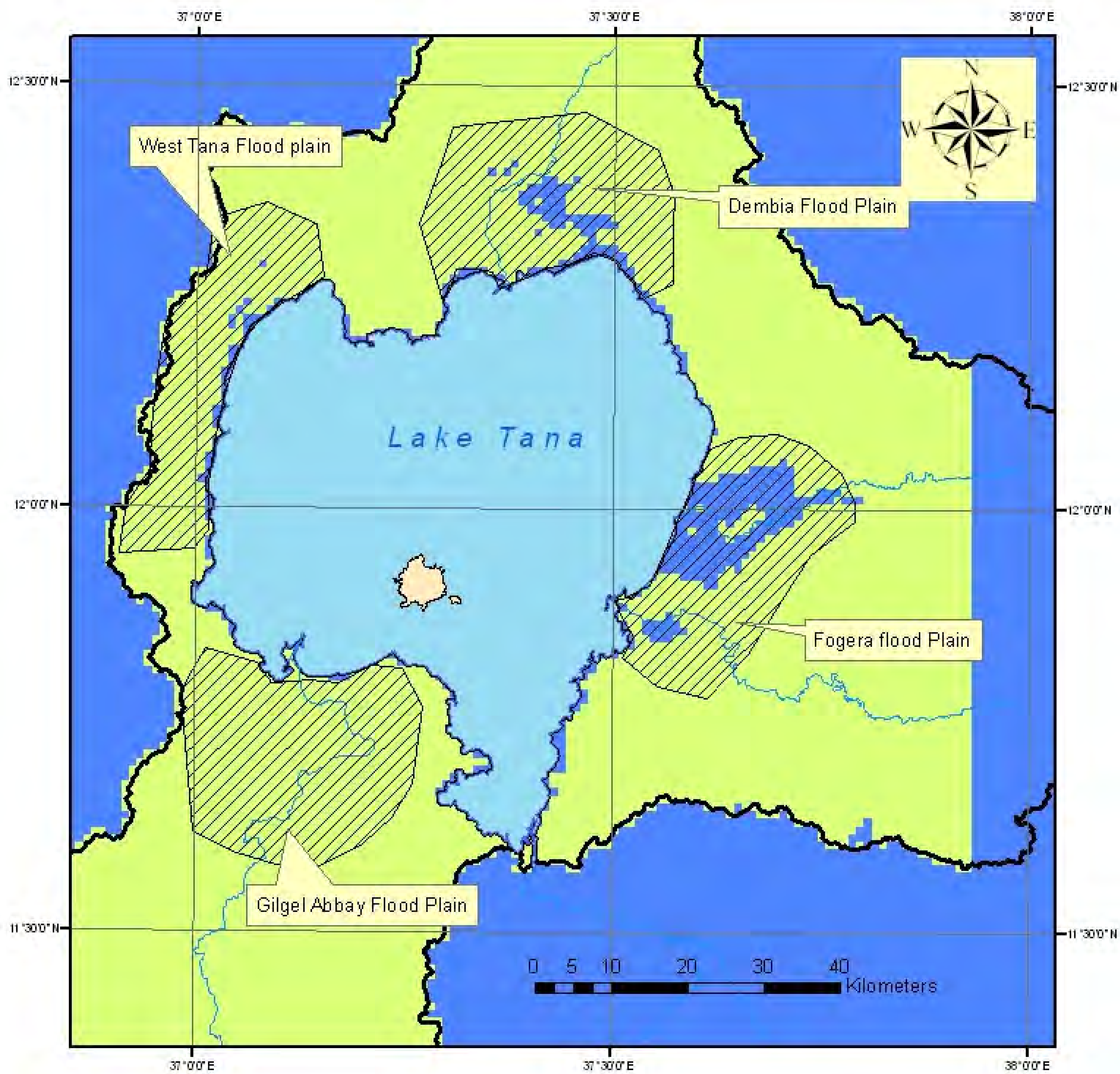

Figure 6-9 Flood map around Lake Tana for 21-aug-2003

6.6. Soil data analysis

Among the inputs to any catchments water yield estimation models, soil data is one of the essential input parameters for the hydrologic model. Soil properties influence the process of generation of runoff from rainfall and they must be considered, even if only indirectly, in methods of runoff estimation [8].

Here in this thesis soil data that is obtained from the Ministry of agriculture was used. The soil data basically contains information of general soil group as per FAO classification, Fig (5-7) .

Table(5-3) lists the soil group in the basin along with the percentage of spatial coverage. The Dominant soil groups in Lake Tana basin that contribute to about 60% of the catchment are the four soil types i.e. Eutric Vertisols , Eutric Leptosols , Chromic Luvisols, Haplic Luvisols.

Table 5-3 Major Soil Group in Tana Basin

Major Soil Group	Area In Sqr.Km	Percentage
Chromic Luvisols	2337.38	15.55%
Eutric Cambisols	1.63	0.01%
Eutric Fluvisols	1477.94	9.83%
Eutric Leptosols	1842.84	12.26%
Eutric Regosols	38.27	0.25%
Eutric Vertisols	1779.92	11.84%
Haplic Alisols	747.88	4.98%
Haplic Luvisols	3115.36	20.72%
Haplic Nitisols	185.73	1.24%
Lithic Leptosols	452.27	3.01%
Urban	10.49	0.07%
Water	3042.39	20.24%
Total Area	**15032.12**	**100.00%**

Luvisols -these soils are derived from various volcanic and undifferentiated lower complex rocks. They are common on flat and gently sloping topography in cooler climates of west Gojam and North Gonder. They are identified in color as Brown /reddish brown with clay to silty clay texture. These soils are Friable to firm, sticky and slightly plastic.

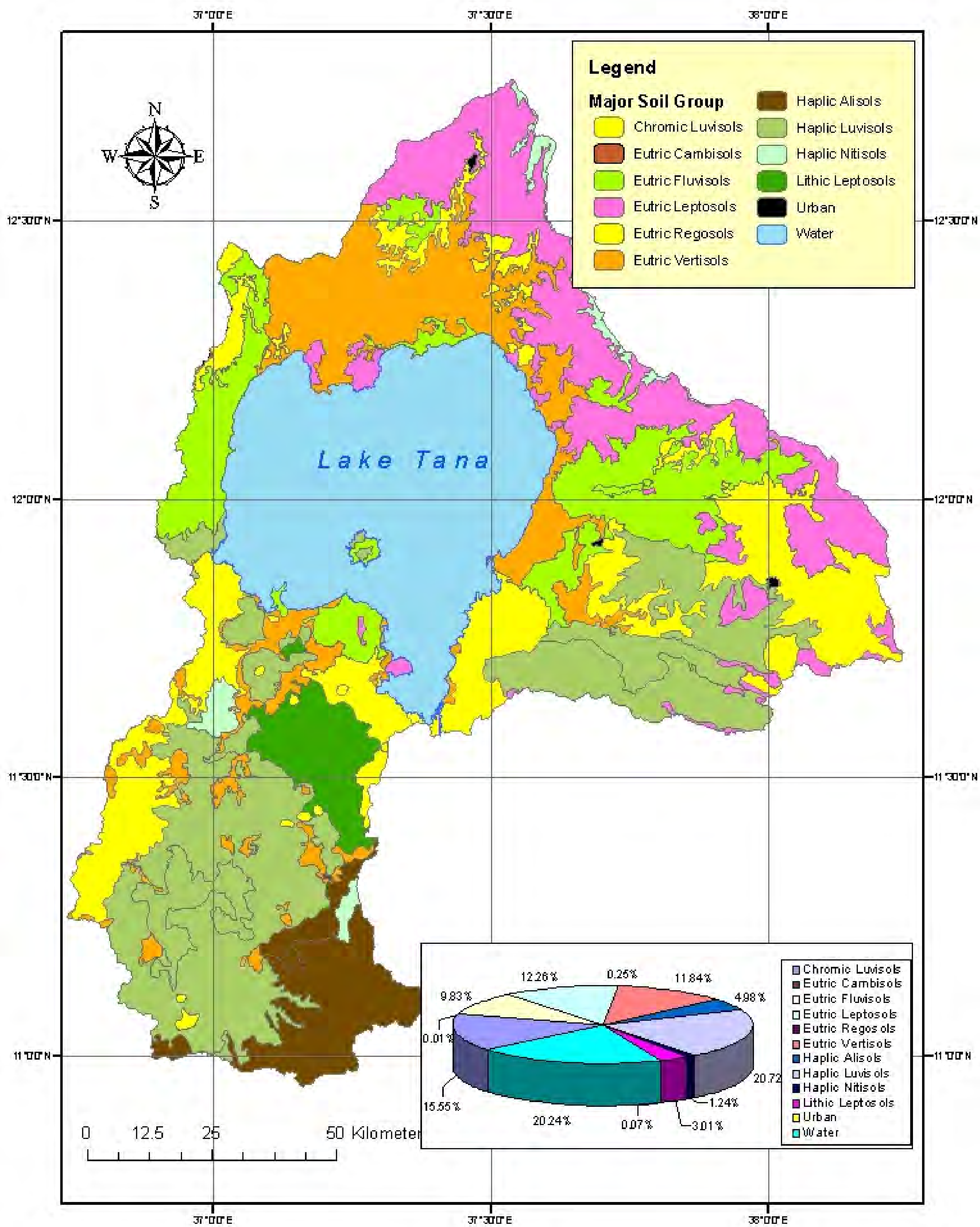

Figure 6-10 Soil map of Lake Tana Basin (Data Source: Ministry of Agriculture)

Leptosols-these soils are developed in relatively younger surface and were probably only moderately deep to deep by origin. The top soil has a thickness ranging from 10 to 30 cm,is mostly brown /yellowish brown in color, and clay loam to clay in texture.

- Litic leptosols:are soils limited in depth by continuous hard rock or continuous cemented layer with in 10 cm of the surface

Vertisols-these soils are mostly imperfectly to poorly drained, dark grayish soils, formed on flat to almost flat plains. The clay fraction of these soils is is dominant by expansible 2:1 lattice clays. Vertisols are very to extremely hard when dry and very sticky and very plastic when wet.

Detail description of each soil unit is found on FAOs digital soil map of the world[34].

Hydrological soil group

Based on this information Hydrological soil group was assigned for each soil type which is later used for computation of Curve Number (CN) to be used in the SCS method of runoff estimation. The hydrologic group designation for any soil type can be either A, B, C, or D, where the runoff potential increases from A to D. The following table summarizes the assigned hydrological soil group based on the soil physical property.

Table 6-9 Major Soil Group, texture and the respective hydrologic soil group.**

Major Soil Group	Soil Texture	Drainage Condition	Hydrological Soil group
Eutric Cambisols	Silty clay	Moderately to deep and well drained	B
Eutric Regosols	Sandy loam to loam	Excessively drained	A
Haplic Nitisols	Silty clay to clay	well drained	B
Lithic Leptosols*	Loam to Clay Loam	moderately deep to deep	D
Haplic Alisols	Clay	favorable drainage	C
Eutric Fluvisols	Silty clay	Moderately well drained	B
Eutric Vertisols	Clay	Imperfectly to poorly drained	D
Eutric Leptosols	Clay loam to clay	Moderately deep to deep	C
Chromic Luvisols	Clay	moderately well to well drained	B
Haplic Luvisols	clay to silty clay	well drained	B
Water	-	-	-

* Lithic Leptosols: Are soils limited in depth by continuous hard rock or continuous cemented layer with in 10 cm of the surface

** Some of the values are assigned are taken from Ministry of agriculture

6.7. LandUse Landcover data

Land use and Land cover information are equally useful as the soil data and hence accurate identification of land use and land cover information has a major impact on the runoff estimation result. In addition to the available land use land cover data, that is obtained from the ministry of agriculture, further validation and correction has been carried out with the help of LandSat ETM images of a spatial resolution approximately 15 meters and USGS land use/ land cover product of spatial resolution of 1000 meter.

Hybrid classification technique (supervised and unsupervised) was applied and the Landsat image (fig 5-10, C) was classified according to the pixel values. This classified image ,along with USGS land use grid(fig 5-10, D), was used to updated the one obtained from the ministry of agriculture. Finally, a modified land use and land cover maps were produced (fig 5-10 A,B)

Estimating CN Values for Each Sub Basin:

The land use land cover data of the basin, along with the soil information obtained has been used while producing the gridded runoff curve number for the entire sub-basin, figure 5-11. The CN value for each hydrologic soil group and land use land cover is calculated based on cell-by-cell computation using map algebra utility of ESRI ArcGIS Software.

Later this gridded CN values were summarized to a single mean value for a sub-catchment using the spatial analysis. In sub-catchments where more than one soil groups are identified, and hence CN, the runoff curve numbers (CN) is determined by linear interpolation as suggested in Engineering Manual SCS method [7]

The final output of CN values corresponding to major sub-basin is presented in the table 5-9 below.

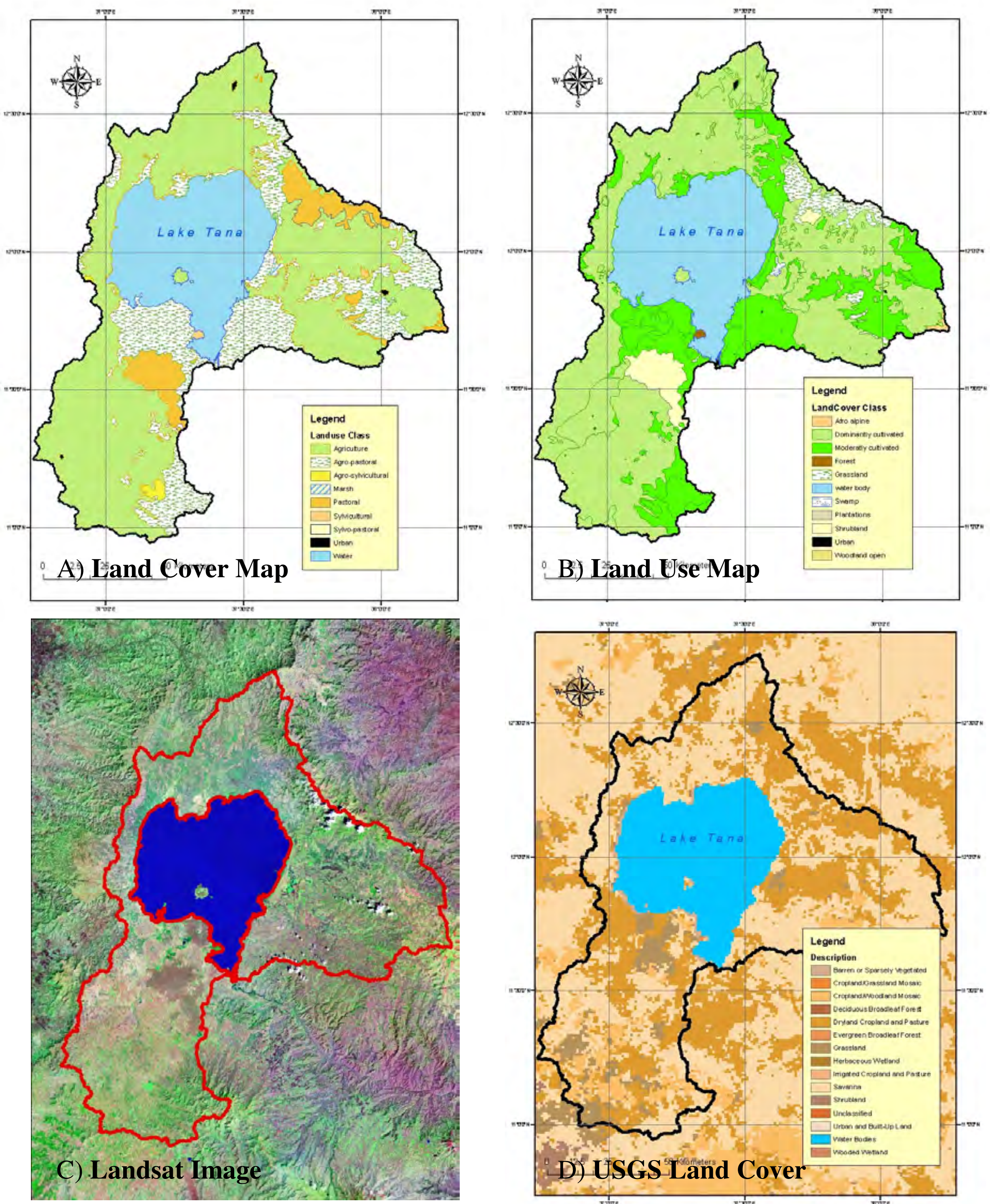

Figure 6-11 Updated land Cover maps and Land Cover maps of Satellite products

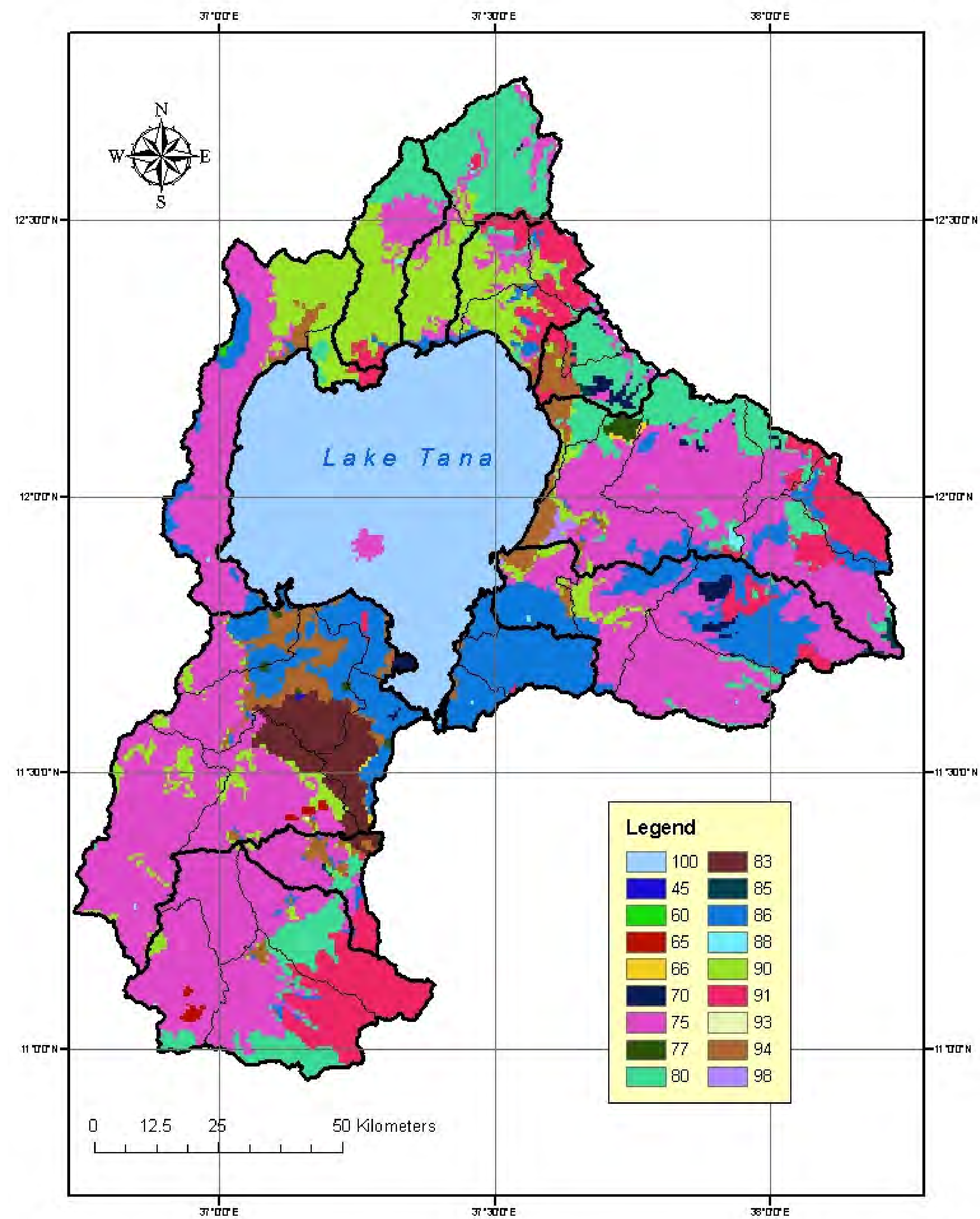

Figure 6-12 Spatial CN map of Lake Tana Basin

Table 6-10 Computed CN for major Sub-Basins

SUB-BASIN NAME	MIN	MAX	RANGE	**MEAN (AMC II)**	MAJORITY	**DRY (AMC I)**	**WET (AMC III)**
Upper Gilgel Abbay	65	94	29	80.02	75	63.71	90.37
Koga	70	94	24	81.33	75	65.64	91.07
Lower Gilgel Abbay	45	94	49	80.79	75	64.84	90.78
Ribb-shine	66	98	32	80.02	75	63.72	90.37
Gumara	70	98	28	80.22	75	64	90.47
Gelda	75	94	19	86.15	86	73.17	93.58
Arno-Garno	70	94	24	82.35	80	67.16	91.61
West Tana	60	94	34	81.02	75	65.17	90.91
Megech	70	93	23	82.26	80	67.02	91.57
Ambagenen	75	94	19	84.74	90	70.88	92.86
Gumaro-Sizele	75	94	19	87.73	90	75.82	94.37

7. Un-gauged watershed Analysis

7.1. General

As it is indicated in chapter 5 of this document, the total gauged area in lake Tana basin is only about 46.7% the remaining 53.3% of the area in un-gauged. Certainly, it is evident that some flow estimation mechanism be established and realized to account the runoff from these catchments. Furthermore, in wet seasons of some years, it has been illustrated that even the gauged catchments did not capture the flow in times when the flood over-tops river banks, such as in the case for Ribb catchment in 1998. Thus, same flow estimation mechanism should also be employed to fill missing information in terms of flow from the gauged catchments with tarnished record of stream flow. Accordingly, SCS Runoff estimation model and Soil water balance model were selected and tested in catchments of Lake Tana basin. This section of this report, therefore, discusses the modeling approach which aimed at determining the amount of water that is contributed from the un-gauged catchment using the selected mathematical Models.

7.2. SCS-CN modeling

To apply the SCS loss model to the un-gauged catchments in Lake Tana basin, the CN values computed, as described in previous chapter of this report, was adopted and determination of direct runoff was carried out by the method outlined in chapter 3 of this report. The runoff estimation was initially carried out on daily time step using HEC-HMS flood hydrograph package using SCS model and SWAT (Soil Water Assessment Tool) which uses Multi-layer Soil water balance Model .Selected catchments for the daily modeling were Ribb, Gilgel Abbay and Gumera catchments within time span for analysis of 1998-1999. Daily average gridded rainfall was provided as an input to the models. Comparison of Simulated and observed after calibration however, showed very little correlation for either of the models with the measured out flow at stations. Consequently, monthly time step was then considered for all the gauged catchments.

(i) Daily time step modeling

Modeling was carried out for three cases wet-season, dry-season and all season. HEC-HMS software has a self- calibrating utility based on optimization techniques that allows the user to select different combinations of objective function .Hence, the selected three catchments were modeled and the results were calibrated using least square techniques of optimization. However, results have indicated that in all the selected three catchments the correlation coefficients were very small indicating little or no correlation between the simulated and the observer stream flow measurement.

Similarly the three selected sub-basins were further tested using Soil water balance model of SWAT hydrologic modeling software. Still the indicating coefficient (R^2) was very small 5%. Figure 6.1 shows time series plot of wet season model for Gummara using HEC-HMS.

It has been observed during the simulation in both cases (HEC-HMS and SWAT) that the result is mainly very sensitive to the rainfall input. Hence, the accuracy of the rainfall input and the rainfall interpolation technique were the two major determinant factors to the accuracy of the daily simulation. Furthermore, the SCS-model employed using HEC-HMS was observed to be also sensitive to the Curve Number used for the catchments. Again during the simulation carried out using SWAT the soil parameters were found to be the determining factors in the results obtained. Generally the Author concludes the accuracy of the data available for Lake Tana basin is not sufficient to carry out rainfall-runoff simulation in daily resolution and hence further data quality validation and refining of input would result in a better result of simulation.

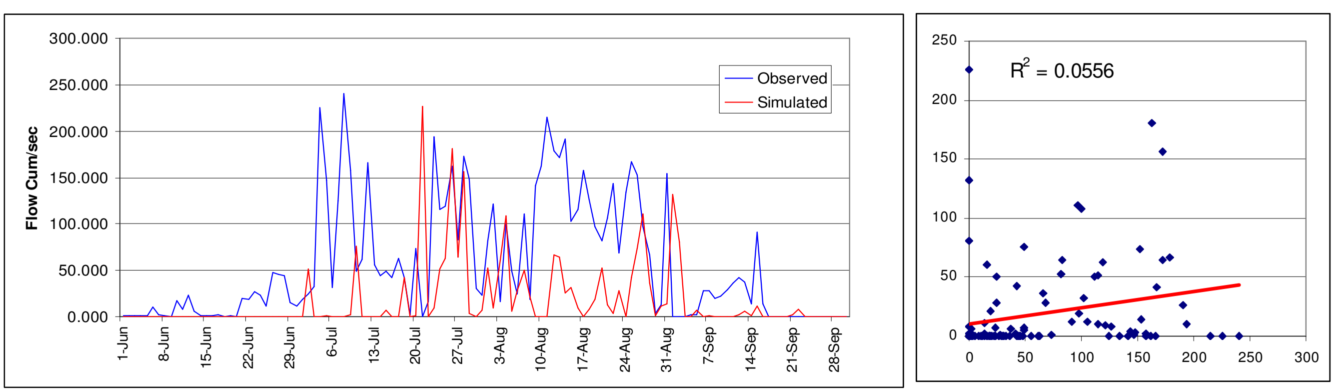

Figure 7-1 Daily Simulation result for Gumara Sub-basin using HEC-HMS

(ii) Monthly time step

A semi-distributed modeling approach was applied for the basins and as discussed in chapter 3 of this report. Major sun-basins were further divided into smaller sub catchments. Although, in the rainfall variation doesn't show exaggerated variability spatially within the major sub-basins, however, the discretization was necessary in order to account the significant spatial variation of the soil property hence, hydrologic curve number of the area. Later the runoff from the smaller catchments were summed and estimation for the major sub-basins were carried out

Simulations on monthly time step was carried out from 1998-2003 using excel application. Runoff modeled results were compared with the recorded runoff at the out let of gauged basins. Runoff estimation for Gigleb abbay sub-basin showed the best correlation of 88.2% unlikely the smallest correlation was observed for Garno catchment, which is 56.4 %. The likely justification for this is because the runoff gauged at this station contains a wide gap ,recording is available for only 21 months with in 1998 up to 2003 and therefore the small correlation coefficient obtained could be results from this the 21 records may not represent the actual catchment water yield.

Table 6-1 summarizes the obtained correlations results for each major sub basin considered detail correlation tables and simulation results are attached in ANNEX III of this report.

Table 7-1 Result of Monthly SCS-CN Model For sub-catchments

Sub-Basin	Model Equation	Correlation Coefficient
Upper Gilgel Abbay	y = 0.681x + 9.1026	R2 = 0.882
Garno	y = 0.2962x + 0.5808	R2 = 0.5639
Gumaro	y = 0.1376x + 0.0282	R2 = 0.6211
Gumera	y = 0.6218x + 10.426	R2 = 0.7362
Koga	y = 0.3636x + 4.2274	R2 = 0.7356
Megech	y = 0.4409x + 4.5206	R2 = 0.6791
Ribb	y = 0.2826x + 5.0688	R2 = 0.7927

Simulation results and correlation graphs for Gilgel Abbay, however, is shown in figure 6-2 (a, b, c) below for the purposed of demonstration. Result for all the sub-basins is given in ANNEX II of this report.

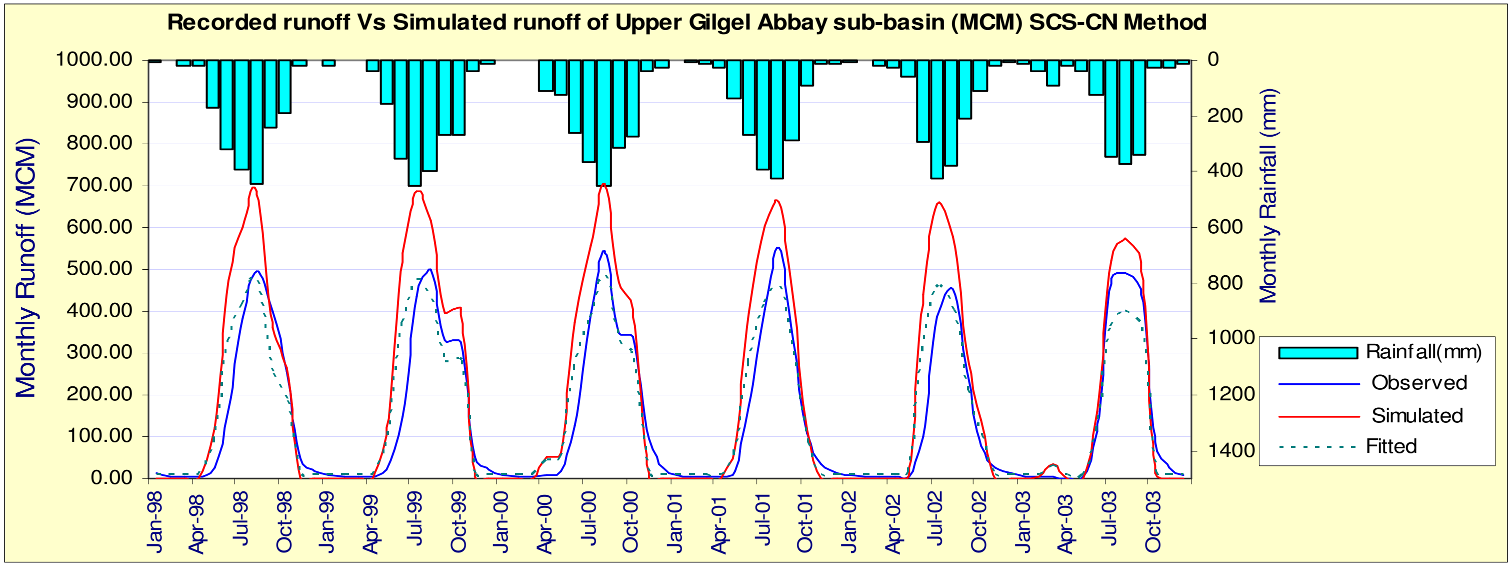

A) Time series plot of observed vs simulated

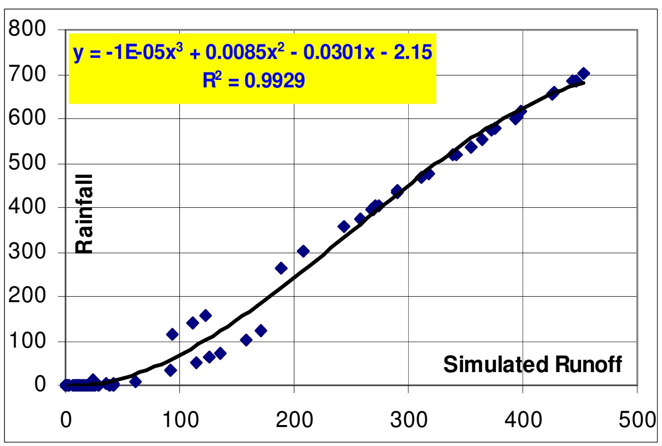

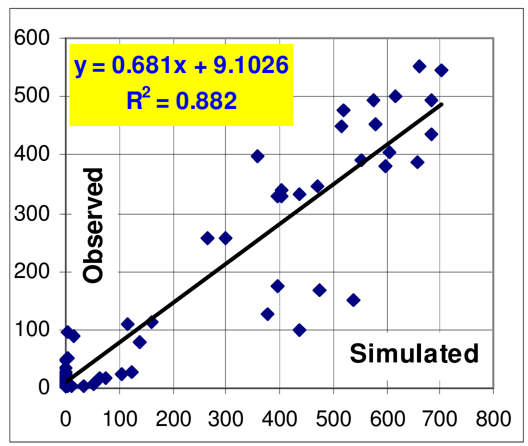

B) correlation results **C) Runoff vs Rainfall Correlation result**

Figure 7-2 SCS–CN Monthly modeling result for Gilgel Abbay

The mean annual error for the fitted and observed runoff is found to be 0.06 MCM which is less than 0.003 %.

Total Mean annual estimated of each sub-basin was found out to be 8.397 BCM. Gilgel Abbay contributes majority (46.3 %) of the total runoff .while, Gumaro giving a runoff 1% of the total. Figure 6.3 and table 6-2 summarized the annual mean runoff estimates from the sub-basins.

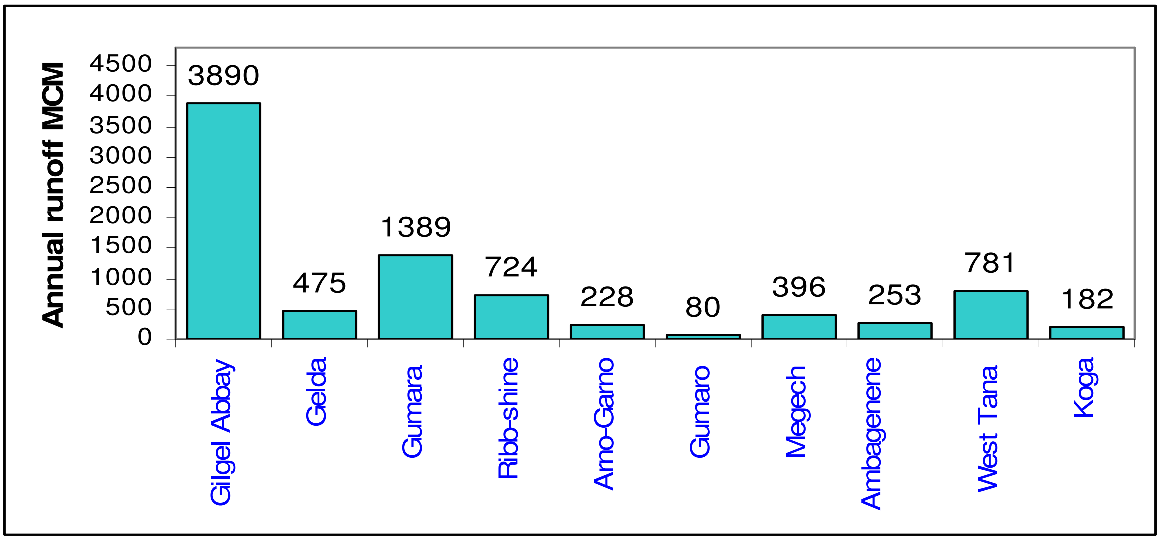

Figure 7-3 Estimation of total runoff from major Sub-basins SCS-CN

Table 7-2 Estimation of total runoff from Sub-Catchments

Sub-Basin	Annual (MCM)
Gilgel Abbay	3890.06
Gelda	474.58
Gumara	1388.84
Ribb-shine	724.04
Arno-Garno	228.08
Gumaro	79.93
Megech	396.30
Ambagenene	252.62
West Tana	781.11
Koga	182.13
Sum	**8397.69**

7.3. Soil water balance modeling using WatBal

David Yates of the Stockholm Environment Institute (SEI) in the USA implemented an excel based software model that simulates changes in soil moisture and runoff, the WATBAL model. It is essentially an accounting scheme based on a conceptualized, one-dimensional bucket that lumps both the root and upper soil layer as it is outlined in the literature review part of this report. The software model comprises two elements.

- The first is a water balance component that describes water movement into and out of a conceptualized basin.
- The second is the calculation of potential evapotranspiration, for which there are three possible alternatives, depending on data availability.

In this thesis work this water balance component of the software model assisted in simulation of gauged catchments in determining core parameters of the soil water balance model. Runoff estimates for the un-gauged catchments was made using an excel based application that was specifically developed for this thesis work that implements the one-dimensional bucket model taking calibrated parameters from the WATBAL model.

On the other hand, evapotranspiration component of the WATBAL model were not used in this thesis work because One, climate input time series i.e. humidity, sunshine hours, hours, are monthly mean values and two, results were found to deviate with the one calculated using radiation based theory .Therefore, evapotranspiration calculated using the radiation balance theory as it is described in chapter 5 of thesis report were used as input.

(i) Gauged sub-basin analysis and parameter estimation

The main input data for the WATBAL software model are the following

- Effective precipitation
- Potential Evapotranspiration
- Runoff
- Coefficient is the power term, γ, in the sub-surface runoff equation (3.8).
- Initial relative storage at the beginning of the calibration, validation, or simulation.
- Epsilon, ε, is the power term on the surface runoff expression (3.8).

- Alpha, α, is the multiplier in the sub-surface runoff expression (3.8).
- S_{max} is the maximum catchment holding capacity.
- Beta, β, is the multiplier in the direct runoff equation (3.9).
- Base flow

Firstly, maximum water holding capacity was estimated from the available soil data similarly base flow were applied using the computed result of SWAT base flow program as discussed in chapter 3 of this report.

Initial values S_{max} were assigned for each gauged sub basin. Following, starting values of other parameters were assumed and simulation was carried out. Considering the identifying variable (R^2) and the average error (which is calculated as the difference of the simulated and observed runoff) as criteria for best fit simulation and the models were calibrated by trial and error procedure. Detailed result of the simulation are attached in ANNEX-IV of this report. Table 6.3 summarizes the obtained correlation coefficient for each sub basin.

Table 7-3 Correlation results of soil water balace Model

sub basin	R^2
GilgelAbbay	0.95
Megech	0.86
Gumera	0.86
Gumaro	0.70
Ribb	0.93

We can observe that except for Gumaro catchment the rest show a good correlation with the observed runoff. When these values are compared with the once obtained using SCS method in all of the catchments, soil water balance modeling seems to be a good un-gauged runoff estimation mechanism for Lake Tana basin sub-basins. For demonstration purpose figure 6-4 below shows result of runoff estimation using soil water balance model for gauged Gilgel Abbay sub-basin.

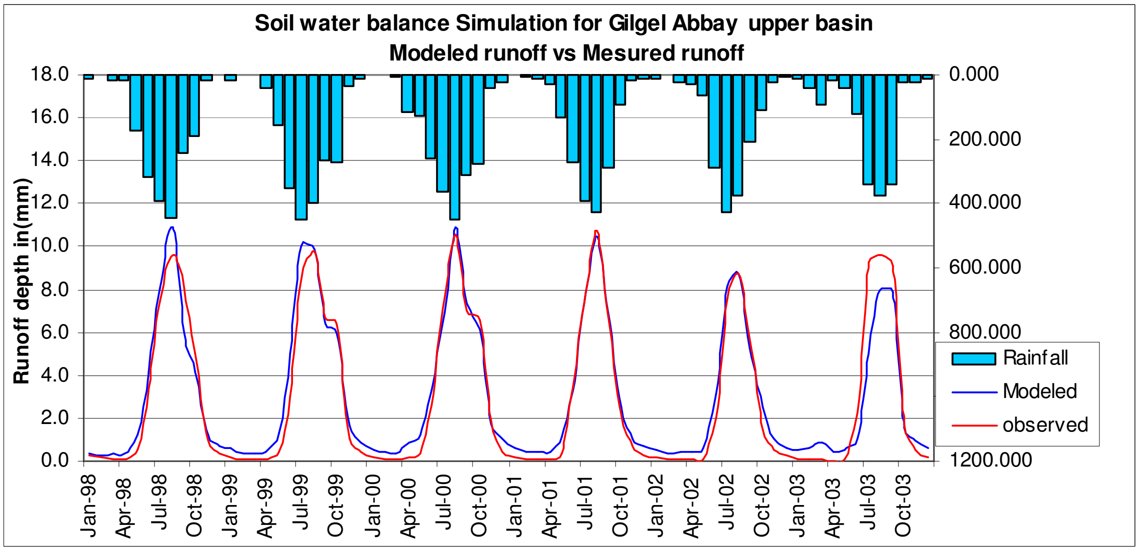

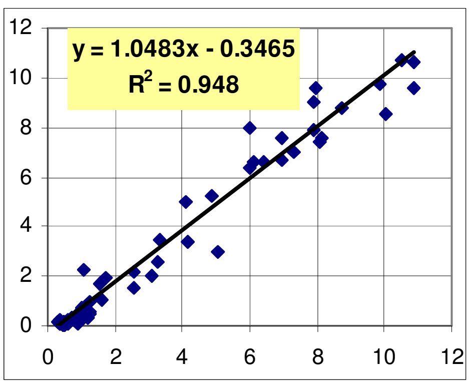

Smax	688.6289
epsilon	1.980566
base flow	0.3
alpha	6.298413
DRC	0.1
SSRC	2
error	51.2668

Figure 7-4 Soil Water Balance result for Gilgel Abbay sub-basin

(ii) un-Gauged sub-basin analysis and runoff estimation

Using the calibrated value parameter for the gauged catchment the un-gauged estimated was chosen based on similar hydrological property and similar climate data. Estimated were carried out for the un-gauged catchments and this values were summed to get the total runoff from the major sub-basins. Results are outlined in the table 6.4.The total estimated runoff from the sub-basins is 7688 MCM. Which is less than the estimate computed using SCS method by 8397.7 MCM.

Table 7-4 Summary of results of SCS-CN and Soil Water balance Models for sub-basins

Sub-basin	Watbal(MCM)	SCS(MCM)
Gilgel Abbay	3729.43	3890.06
Gelda	401.30	474.58
Gumara	1273.26	1388.84
Ribb-shine	686.80	724.04
Arno-Garno	126.01	228.08
Gumaro	191.07	79.93
Megech	360.43	396.30
Ambagenene	232.45	252.62
West Tana	505.11	781.11
Koga	182.13	182.13
Sum	**7688.00**	**8397.69**

8. Lake Water balance simulation

Results from Runoff estimation together with the evaporation loss from flood plain water inundation were simulated using mass balance equation. The main components for the lake water balance simulation are inflows from each major sub-basin, rainfall over lake area, evaporation from Lake Surface and from surrounding flood plains and Lake Tana outflow.

The basic equation implemented is .

Change in storage = Total inflow – total outflow + losses (7.1)

Total inflow comprises of the effective rainfall over lake area, net runoff from the surrounding major sub-basins (deducting the evaporation losses from the flood plain inundations).Out flow consists of evaporation from the lake surface and out flow at Lake Outlet.

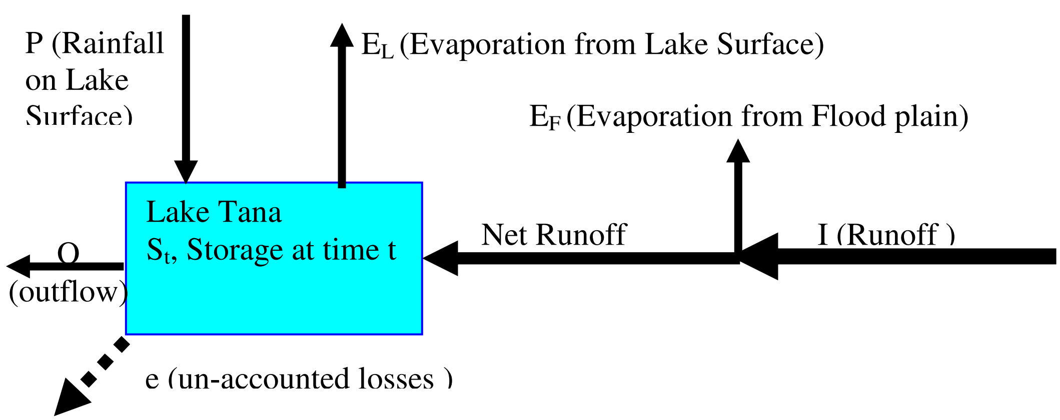

Figure 8-1 schematic representation of model used to simulate lake Tana system

Equation 7.1 can expanded based on the components discussed above and simulation was carried out using the following recursive formula.

$$S_2 = S_1 + (P + I) - (E_L + E_F + O) + \varepsilon \qquad (7.2)$$

Where S_2 ,Lake storage volume at the end of current month.

S_1 , Lake storage volume at the end of previous month.

P , rainfall volume over the lake surface.

I , Runoff volume from surrounding catchments.

E_L , Evaporation volume from the lake surface.

E_F , Evaporation volume from flood plains.

O, outflow volume at the lake outlet.

ε , Miscellaneous un-accounted losses.

In equation 7.2, both evaporation and rainfall are functions of lake surface area at current time step which again is a function of the current storage volume. Therefore, not all the variables on the right side of the equation are determined entirely. In order to solve the equation iterative techniques and observed lake surface elevation are considered in separate cases. Three different cases were considered while carrying out the water balance simulation

Case 1: Observed lake area and zero Loss

Observed Lake Tana water surface elevation was used to compute the monthly average surface area and storage of the lake using lake Volume-Area-Elevation Curves. Following this, the computed area was used to calculate the evaporation and rainfall volumes on the lake surface. The input variables described in section 7.1 of this chapter along with the computed rainfall and evaporation was simulated using equation 7.2 storage was computed at each time step assuming the Loss term in the equation is zero.

The average values of the water balance components are therefore tabulates in table 7.1 below.

Table 8-1 Summary of Out put water balance result for Case 1 simulation

	Average Water Balance Component (1998-2003)	Result (MCM)
Inflows	Total Inflow	7687.99
	Rainfall over the lake area	3839.69
Outflow	Total Evaporation from Surrounding flood Plains	276.30
	Evaporation from Lake Surface	5155.56
	Out flow from Lake	5012.05
	Net deviation	**-1083.77**

Thus, using these calculated variables the lake storage was simulated. Figure7-1 shows simulated Vs Observed plot for this case of simulation.

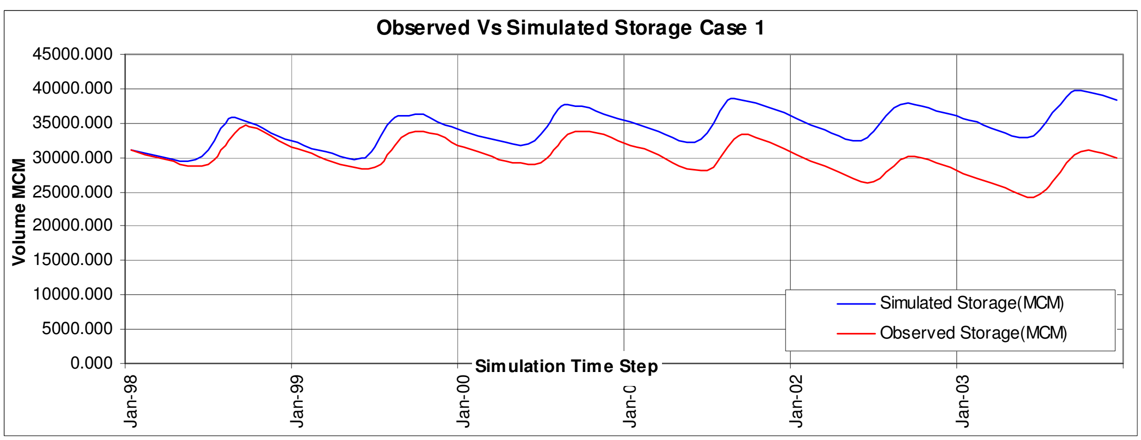

Figure 8-2 Observed Vs Simulated Storage Case 1 simulation

We can note that the simulated and observed values have shown a continuous increasing deviation through out the simulation time span.

Case 2: Zero Loss and Simulated storage.

Area and storage are computed iteratively by solving equation 7.2 taking initial value of area from the previous moth and computing the water balance by trial and error until the computed storage and assumed initial storage value matches. Again in this case the loss term in the equation was assumed to be zero.

The average values of the water balance components are therefore tabulates in table 7.2 below.

Table 8-2 Summary of Out put water balance result for Case 2 simulation

	Average Water Balance Component (1998-2003)	Result (MCM)
Inflows	Total Inflow	7687.99
	Rainfall over the lake area	3879.38
Outflow	Total Evaporation from Surrounding flood Plains	276.30
	Evaporation from Lake Surface	5227.40
	Out flow from Lake	5012.05
	Net deviation	**-1051.62**

Figure 7-2 shows time series plot of simulated Vs Observed reservoir storage volumes

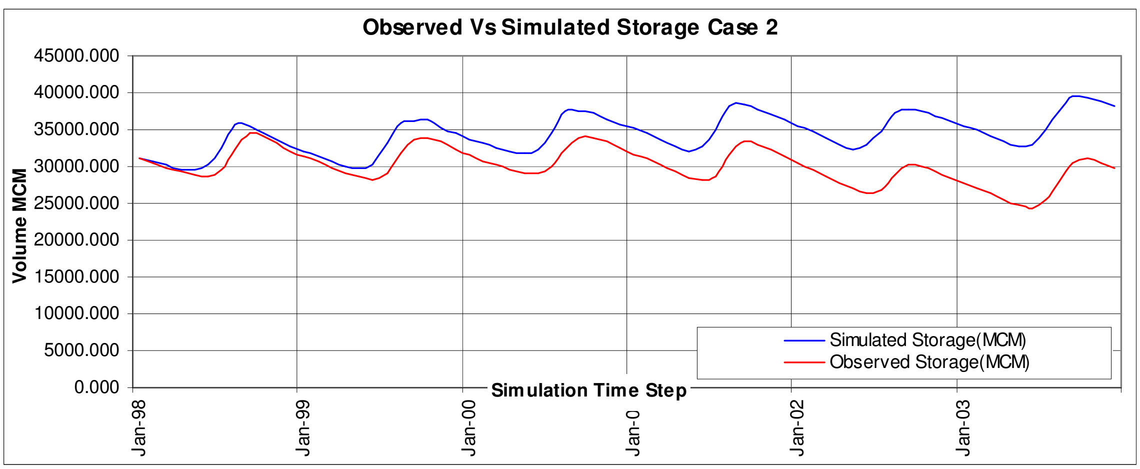

Figure 8-3 Observed Vs Simulated Storage Case 2 simulation

Again, here the same deviation of simulated from the observed can be noted.

Case 3: Observed Storage and 'Un-accounted' Loss Considered

Here in this simulation the observed lake level was first taken and was used to compute observed storage, lake surface area and hence evaporation and rainfall on the lake surface. These computed variables were taken as an input and the equation 7.2 was solved for the un-accounted loss term. After the loss term is computed, again it was taken as input and lake storage was simulated.

Results have showed that average un-accounted loss of 1414.01MCM is in the system. Table 7.3 summarizes the total inflow and outflow terms from the system, difference of storage and average loss for each year. Detail sheet of monthly water balance is attached in Annex VI.

Table 8-3 Annual average inflow and outflow from Lake Tana for case 3 simulation

year	Inflow(MCM)	Outflow(MCM)	Storage Difference	Difference (inflow-outflow)
1998	12548.19	11632.63	-498.45	915.56
1999	12854.71	11162.29	278.41	1692.42
2000	12257.24	11069.35	-226.11	1187.89
2001	11552.29	10745.82	-607.54	806.47
2002	9458.14	9634.09	-1589.95	-175.94
2003	10214.51	8154.24	646.26	2060.27
mean	**11480.85**	**10399.74**	**-332.90**	**1081.11**

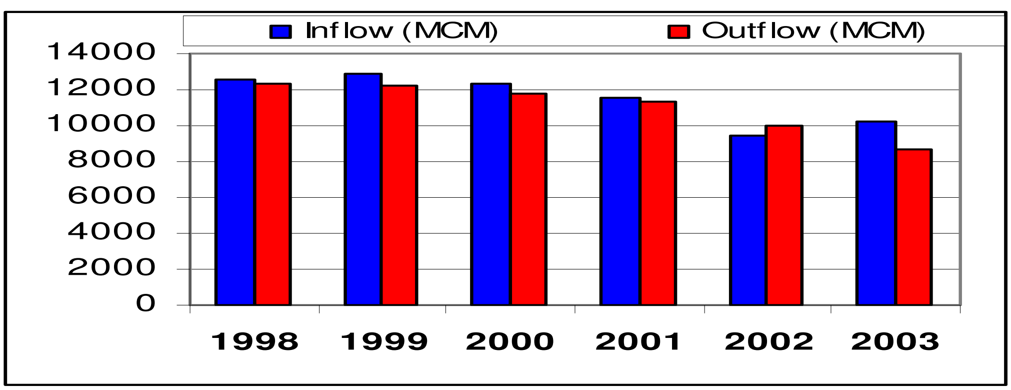

Figure 8-4 Net lake Inflow and outflow from the Lake plots for each year ,Case 3 simulation

The five year annual average result (1998 to 2003) of the water balance components is tabulated in table 7.4

Table 8-4 six year annual average values of the water balance components for case 3

	Water Balance Component	Result (MCM)
Inflows	Total Inflow	7687.99
	Rainfall over the lake area	3792.86
Outflow	Total Evaporation from Surrounding flood Plains	276.30
	Un-accounted loss	1414.01
	Evaporation from Lake Surface	5111.39
	Out flow from Lake	5012.05
Storage	Average Lake storage difference	-332.90

From table 7-3 We can observe that for the years 1998 up to 2000 The fluctuation in reservoir storage (the fourth column in the table) shows comparatively balanced variability from year to year with average value of 150 MCM. On the other hand, for the years 2001 and 2002 the deviation is relatively quite large this is the time where Chara-Chara weir has started operation and the outflow was not naturally regulated. During this time the lake level showed a considerable drawdown, 1589.95 BCM as can be observed from the fourth column in the table .Generally, simulation output shows that there is average unconsidered loss for the 6 year simulation which is 1414 MCM. This loss could be attributed to seepage or underestimation of one of the outflow variable or over-estimation of inflow variables.

Furthermore, a total of 276.30 MCM, which is about 3.56% of the runoff, is lost in the flood plains through evaporation. By volume, this accounts of 25.8 % of the total water that is accumulated in the flood plains during 4 months of the year starting June up to September the remaining water therefore disappears from the flood plains into the lake and to the ground water storage through seepage.

Time series plot of the simulated and observed storage is presented in figure 7.4 below.

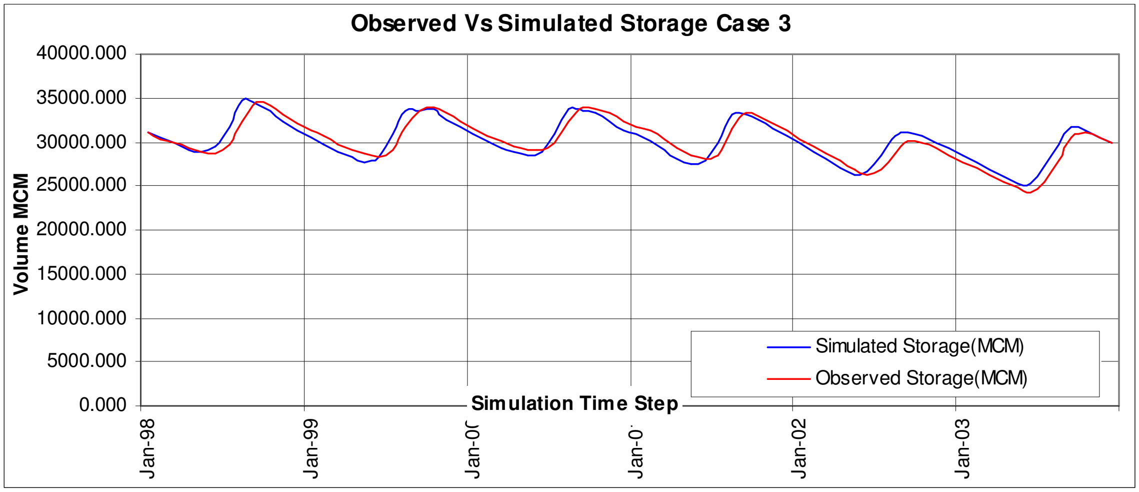

Figure 8-5 Simulated and Observed storage for case 3 simulation

From figure 7.4 above, it can be observed that even though the variation is captured in the simulation process there is an obvious difference of phase between the simulated and observed plots. Since Lake Tana is relatively wide lake this could be attributed to the routing effect of the lake. Cross correlation tests between the two time-series were carried out and a lag of 1 month showed a correlation of 94 %. Therefore, this indicates that the routing effect in delaying the flows could be close to 1 month. Figure7-5 shows result of the cross-correlation analysis.

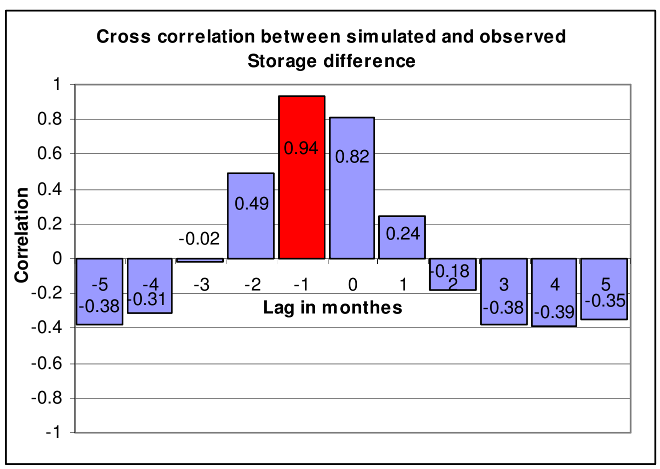

Figure 8-6 Cross correlation between simulated and observed storage case 3

Applying one month of delay in the simulated time series the plot of Simulated Vs Observed flow is shown below for Case 3

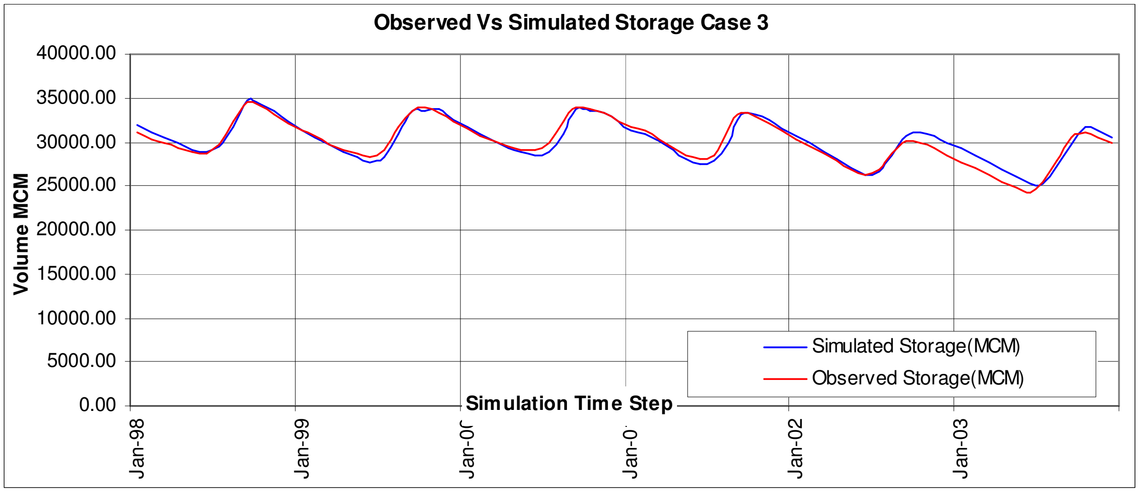

Figure 8-7 Simulated and observed storage after lag difference 1 month is considered for case 3

9. Conclusion and recommendation

Conclusion

This research work has attempted to carry out remote sensing based assessment of water resource potential for Lake Tana basin. Satellite derived products have been employed together with ground based measured information and incorporating ground collected data specific to this study. By means of image analysis techniques along with conventional hydrological analysis, past estimation of hydrological variables have been update .As it is stated in the objective statement evaporation, rainfall, runoff from un-gauged catchments, dynamics of flood plain inundations and water balance of Lake Tana has been assessed in depth.

Despite the little volume of information available regarding the hydrology of the flood plains, this study concludes that remote sensing technique stands to be an option in terms of providing one way of explaining the dynamic of water on the flood plains. Through the analysis of sequential extent of flooded area and their temporal volumes, it has been possible to state the total evaporation loss from the system. This can be a great input to the current integrated water resource management, flood protection and environmental management works and future plans for Lake Tana sub-basin. As results revealed, total of 918 MCM is lost in the flood plains through evaporation, this is considered as loss in the resource, and therefore this can give a preliminary indication on the amount of water resource that can be saved and be used for additional development works.

This study has also demonstrated the use of TRMM Rainfall estimates to fill missing rainfall data. Based on the results obtained, it can be concluded that rainfall estimates from TRMM satellite can be applied, as one option, for rainfall gap filling applications in monthly time scale. In addition to this, it owns additional advantage in capturing the spatial distribution of rainfall within the system as well. In southern part of the basin where rainfall records are relatively scares, when compared to than eastern or northern part of the basin, this rainfall estimate technique can serve the purpose of providing additional way of rainfall data generation mechanism.

The potential evapotranspiration estimates made using the combined equations, which resulted annual mean evaporation of 1666mm from Bahirdar station for example, corresponds to annual piche evaporation at Bahirdar station which is 1624mm per annum. This consistency, therefore, gives reliability to the evaporation estimates conducted in this study work.

According to outputs from un-gauged watershed analysis, semi-distributed approach using Soil Water balance model is found to me more suitable in the estimation of runoff for un-gauged catchments in Lake Tana sub-basins than SCS method. Results have indicated that up to 95% of correlation with the measured flows can be obtained using the model. Furthermore, apart from the runoff, this model also holds an advantage that it also integrates other key hydrologic processes in modeling the system such as the sub-surface flow component and actual evaporation from the catchment area.

The water balance simulation carried out for Lake Tana has showed that 'un-accounted' flow of 1414.01 MCM that is detected in the system. This can be as the result of under estimation of the outflow parameters or over estimation of inflow parameter or variables that is not modeled in the system such as seepage component.

As conclusion, Great effort has been put forward to come up with better description of the hydro-system of the sub-basin with relatively more precise estimation. Furthermore, this study has also proposed mechanism of water yield estimation for un-gauged catchments. As a result, the total available water in the system, hence water resource potential, can be explained based on results from this study work. Therefore, the objectives of this study have been achieved.

Limitations and Recommendations

One of the major challenges faced while conducting this research work is the difficulty to obtaining satellite image products. Some of the digital imageries are very large in size and most of them are acquired through the internet. Consequently, the limitation of band width was a major constraint in obtaining the datasets. Therefore, this thesis work was limited to using dataset which are possible to acquire though the available bandwidth limit. However, superior results can be obtained if imageries with higher resolution and good spatial accuracy can be used.

Furthermore, because this study is carried out with limited true ground-collected information incorporating more ground information can further refine the results better. If, for example, more data can be gathered, regarding the extent and depth of the water the remains on the flood plains during wet season of the month, satellite products can be better calibrated to give refined output. In regards to flood plain analysis it has been indicated that incorporating more SAR images for calibration can give better-quality results over the optical image and incorporating more radar images gives contributes to the accuracy of the out put.

This research has made use of NDVI images to delineate the flooded area. One of the major limitations to using the NDVI images, as observed, was their insufficiency to identify water covered area below a certain depth of inundations and therefore areas covered with thin layer water were not detected by the methodology followed in this research work. This was reflected in the results; as can be observed from the monthly average plots, after December the reported area of flooded zone suddenly drops to zero in January. Consequently, in wide flood plains such as Fogera and Dembia a certain amount of water in the flood plains might have not been detected using this technique. Further research work may incorporate other type of images along with the NDVI images to address this gap.

The simulation studies carried out in this research work are within time span of 1998 up to 2003.This was originally constrained with the available dataset that can be obtained. However, wider time span of analysis can enhance the reliability on the results and accuracy of the results.

As it is stated in the conclusion part, in the lake water balance simulation study the un-accounted flow may be as a result of the seepage component which was not possible to consider in this research. However, incorporating ground flow studies could further validate this hypothesis and could lead to a better understanding of the hydro-system.

Generally it has been demonstrated that remote sensing techniques can provide significant information and analytical capability to water resource assessment of a certain basin. Hence, further studies on this sub-basin could make use of this versatile tool to update the hydrologic description of Lake Tana Sub-basin .

10. Reference

[1] Townsend P.A, Walsh S.J. (1998).Modeling floodplain inundation using an integrated GIS with radar and optical remote sensing. Geomorphology V.21,No 3.

[2] GuamScientific Investigations Report 2004–2005

[3] Kenlo Nishida; Ramakrishna R. Nemani ; Steven W. Running; Joseph M. Glassy (2002) . Remote Sensing of Land Surface Evaporation Theoretical Basis for an Operational Algorithm.

[4] Humphrey & associates. (1996).Feasibility Study of Tis Abbay II-Ethiopia

[5] Rossato, Luciana; Alvala, Regina C. S.; Ferreira, Nelson J.; Tomasella, Javier (2005). Evapotranspiration estimation in the Brazil using NDVI data.

[6] M. Ledwith (2002). Land cover classification using SPOT Vegetation 10-day composite images – Baltic Sea catchment basin.

[7] David R. Maidment (1994). Hand book of Hydrology.

[8] Soil Conservation department. (1985). National engineering handbook. Section 4, Hydrology. Washington, DC.

[9] David N. Yates (1996). WatBal: An Integrated Water Balance Model for Climate Impact Assessment of River Basin Runoff.

[10] Kaczmarek (1993). Water balance model for climate impact analysis, ACTA Geophysical Polonica.

[11] Environmental System Research Institute, ESRI, (2001). ArcGIS Hydro Data Model.

[12] University of Maryland Institute for Advanced Computer Studies, University of Maryland Department of Geography, (year) .Shuttle Radar Topography Mission (SRTM) Technical Guide.

[13] Studio Pietrangeli , (1990). Tana Beles Project studies document.

[14] Melkamu Amare , (2005).Reservoir operation and establishment of reservoir rule for lake Tana.

[15] J.G. Arnold ; P.M. Allen;R. Muttiah, (1995). Automated base flow separation and recursion analysis techniques.Reprented from Ground water, Vol. 33, No. 6, November-December 1995.

[16] U.S. Army Corps of Engineers, (1994). Engineer Manual 1110-2-1417, Washington, DC 20314-1000.

[17] Vijay P. Singh; David A. Woolhiser. (2002). Mathematical Modeling of Watershed Hydrology. The Journal of Hydrologic Engineering, Vol. 7, No. 4,

[18] Wurbs, R. A. (1998). Dissemination of generalized water resources models in the United States.

[19] ASCE. (1996). Handbook of hydrology, ASCE Manual and Rep. on Engineering Practice No. 28, New York.

[20] J.G. Arnold, P..M. Allen. (1999) . Automated methods for estimating baseflow and groundwater recharge from streamflow records. Journal of the Americam Water Resources Association Vol. 35(2).

[21] Japan Association of Remote Sensing. (1996).Remote sensing Notes.

[22] United Nations, (1986). Principles Relating to Remote Sensing of the Earth from Outer Space.

[23] Joy Sanyal and X. X. Lu. (2003). Application of Remote Sensing in Flood Management with Special Reference to Monsoon. J.Natural Hazards 33: 283–301.

[24] Simonett, D. S.; F. T. Ulaby ; J. E. Estes; G. A. Thorley, (1983). Manual of remote sensing, Falls Church, Virginia: American Society of Photogrammetry.

[25] Boone, R. B.; K. A. Galvin et al. (2000). Generalizing El Nino effects upon Maasai livestock using hierarchical clusters of vegetation patterns. Photogrammetric Engineering & Remote Sensing.

[26] Stefan Wunderle; David Oesch.(2003).NOAA/AVHRR RSGB Normalized Difference Vegetation Index (NDVI) Data Set.

[27] David R. Maidment .(2002). GIS for Water Resources.

[28] Gray T. ; Matthew C. (2004). Use of SLC-Off Landsat Image Data for Monitoring Land Use / Land Cover Trends in West Africa.

[29] K. C. Seto ; C. E. Woodcock; C. Song; X. Huang; J. Lu ; R. K. Kaufmann.(2002). Monitoring land-use change in the Pearl River Delta using Landsat TM.

[30] Wim Bastiaanssen; Henk Pelgrum.(2006). Remote Sensing Studies of Tana-Beles Sub Basins.

[31] Shunlin Liang.(1998). Retrieval of Land Surface Albedo from Satellite Observations. Journal of applied meteorology Vol. 38.

[32] Wolfgang Lucht; Crystal Barker Schaaf; Alan H. Strahler.(2000). An Algorithm for the Retrieval of Albedo from Space Using Semi-empirical BRDF Models. IEEE transactions on geosciences and remote sensing, vol. 38, no. 2.

[33] Jonathan G. Salomon; Crystal B. Schaaf; Alan H. Strahler; Feng Gao, Yufang Jin. (2006).Validation of the MODIS Bidirectional Reflectance Distribution Function and Albedo Retrievals Using Combined Observations From the Aqua and Terra Platforms. IEEE transactions on geoscience and remote sensing, vol. 44, no. 6.

[34] FAO ,(1995). The digital soil map of the world, version 3.5.

[35] Walter J. Rawls, William P. Kustas, Thomas J. Schmugge, Jerry C. Ritchie, Thomas J. Jackson,Al Rango, Paul Doraiswamy (2003), Remote Sensing in Watershed Scale Hydrology.

[36] A Canada Centre for Remote Sensing, Fundamentals of remote sensing ,remote sensing turorial.

[37] D.G. Hadjimitsis , I. E. Evangelou , A. Lazakidou , C. R. I.Clayton. (2002). Unsupervised Classification of Remotely Sensed Images Using Self-Organizing Maps for Mapping Land-Cover Changes.

[38] NASDA,National Space Development Agency Japan.(2001), Tropical Rainfall Measuring Mission TRMM data user hand book.

[39] Bastiaanssen, W.G.M., M. Menenti, R.A. Feddes and A.A.M. Holtslag, (1998). A remote sensing surface energy balance algorithm for land (SEBAL).Journal of Hydrology. 212-213: 198-212.

[40] M. A. H. Shamseddin,T. Hata , A. Tada , M. A. Bashir , and T. Tanakamaru. (2006). Estimation of flooded area in the BahrEl-Jebel basin using remote sensing techniques. Hydrol. Earth Syst. Sci. Discuss., 3, 1851–1877.

[41] Dr. Gholan Reza Zehtabian;Dr. Seyed Kazem Alavi Panah; Rahin Hamedpanah (1999) .Determination of an appropriate area for flood –water spreading by remote sensed data and gis in the tagharood catchment (iran).

11. Annex

Annex – I Rainfall statistical analysis out put result

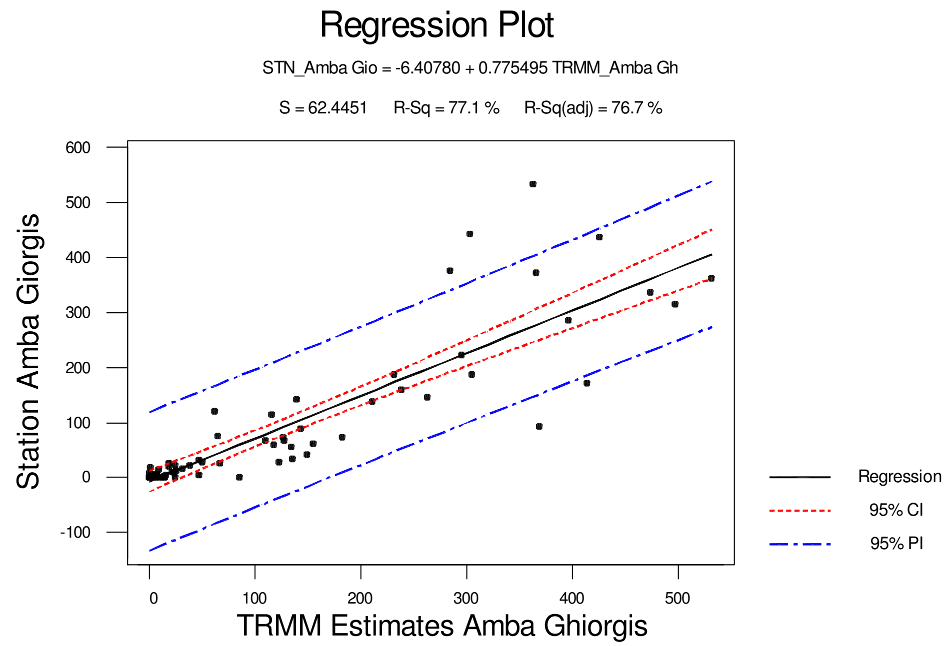

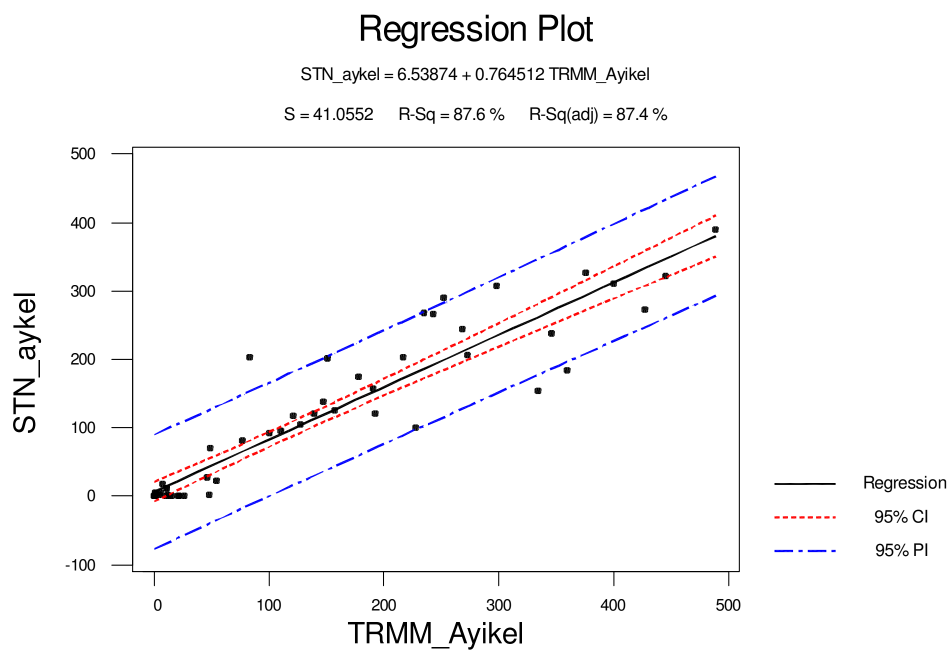

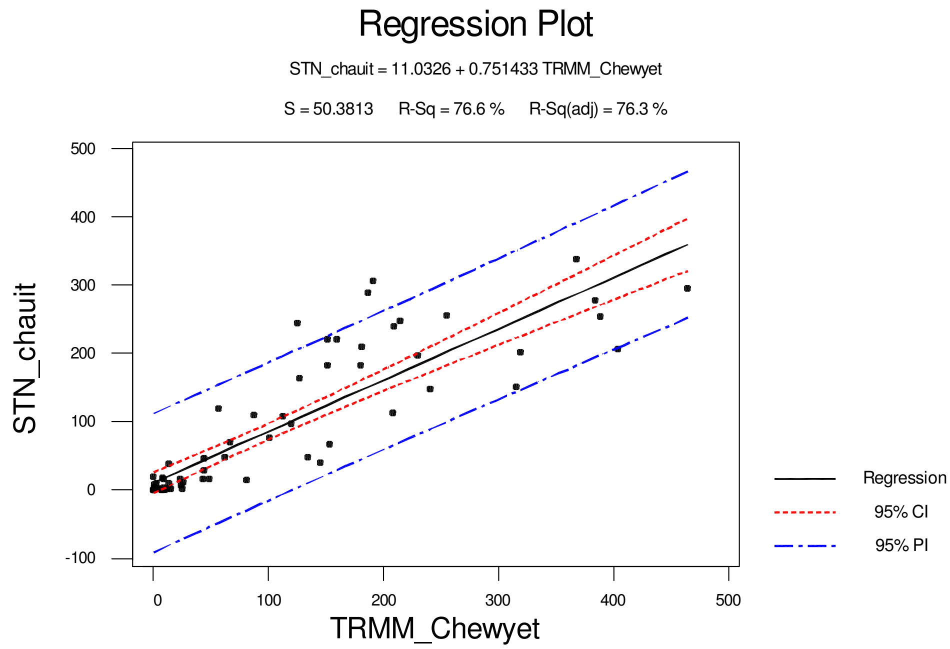
Regression Plot
STN_chauit = 11.0326 + 0.751433 TRMM_Chewyet
S = 50.3813 R-Sq = 76.6 % R-Sq(adj) = 76.3 %
STN_chauit
TRMM_Chewyet
500
400
300
200
100
0
-100
0
100
200
300
400
500
Regression
95% CI
95% PI

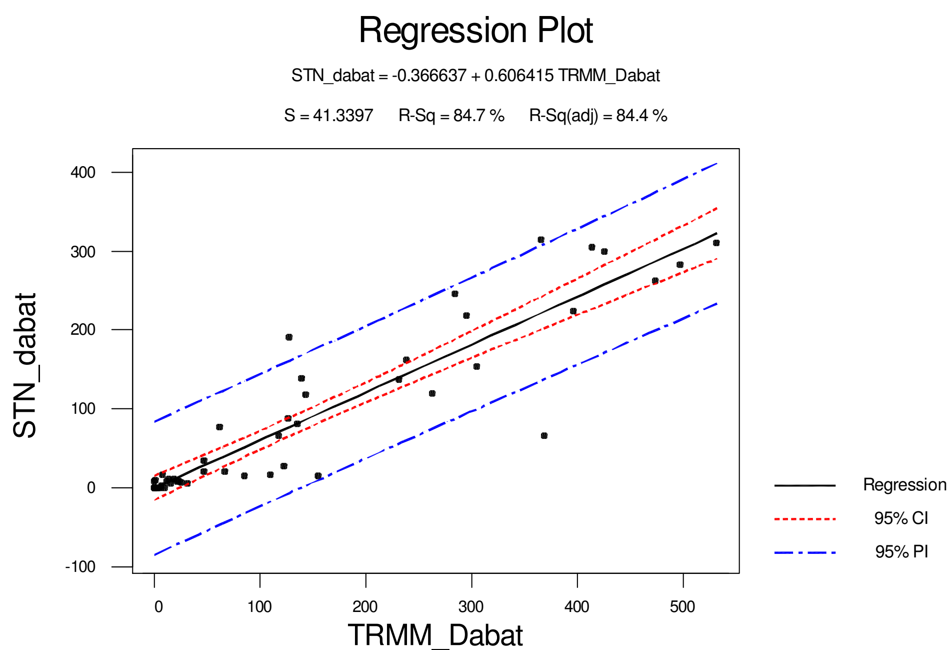
Regression Plot
STN_dabat = -0.366637 + 0.606415 TRMM_Dabat
S = 41.3397 R-Sq = 84.7 % R-Sq(adj) = 84.4 %
STN_dabat
TRMM_Dabat
400
300
200
100
0
-100
0
100
200
300
400
500
Regression
95% CI
95% PI

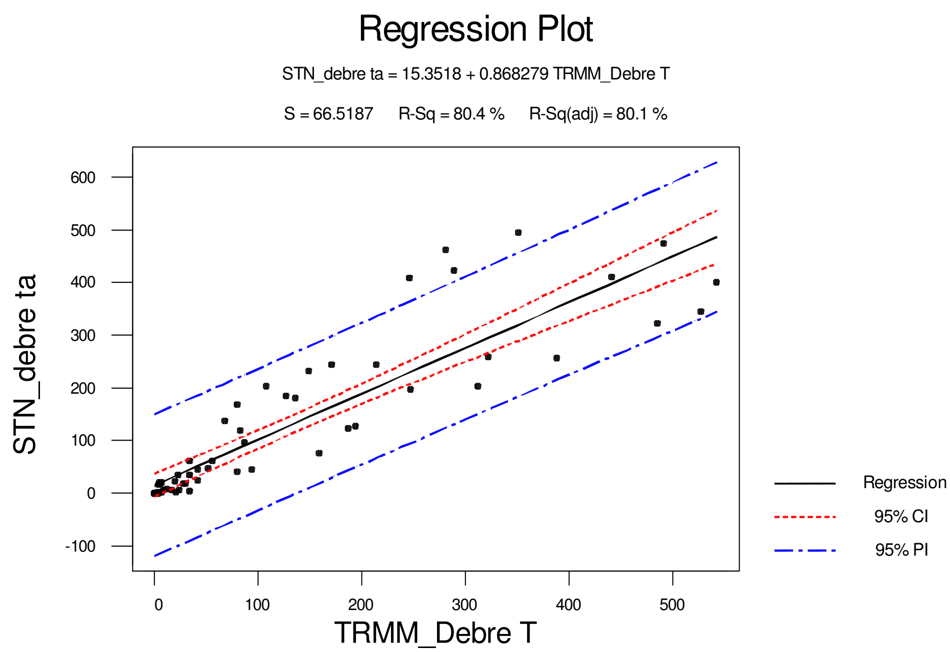
Regression Plot
STN_debre ta = 15.3518 + 0.868279 TRMM_Debre T
S = 66.5187 R-Sq = 80.4 % R-Sq(adj) = 80.1 %
STN_debre ta
TRMM_Debre T
Regression
95% CI
95% PI

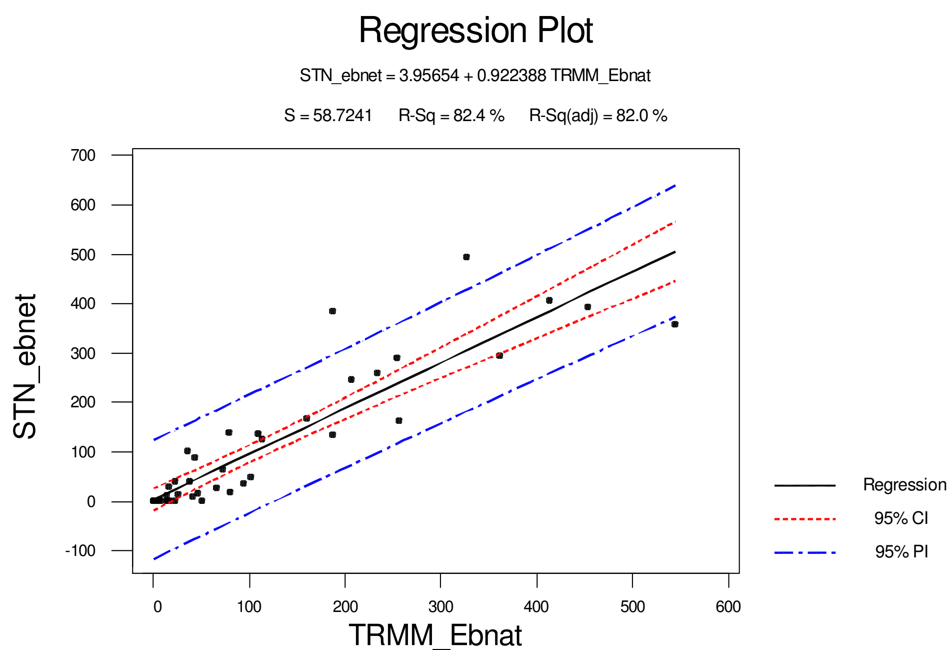
Regression Plot
STN_ebnet = 3.95654 + 0.922388 TRMM_Ebnat
S = 58.7241 R-Sq = 82.4 % R-Sq(adj) = 82.0 %
STN_ebnet
TRMM_Ebnat
Regression
95% CI
95% PI

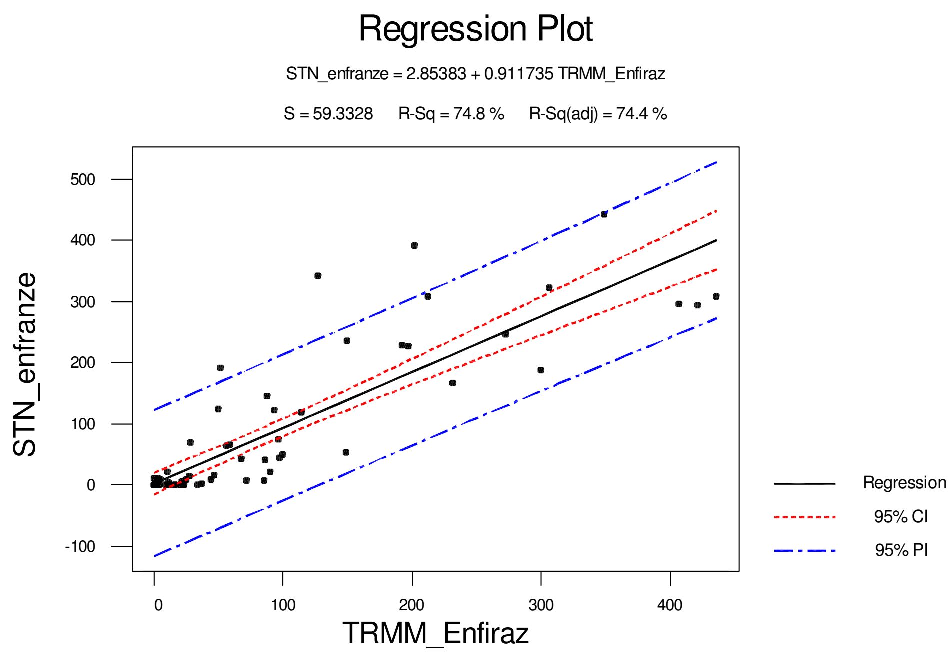
Regression Plot
STN_enfranze = 2.85383 + 0.911735 TRMM_Enfiraz
S = 59.3328 R-Sq = 74.8 % R-Sq(adj) = 74.4 %
STN_enfranze
TRMM_Enfiraz
Regression
95% CI
95% PI

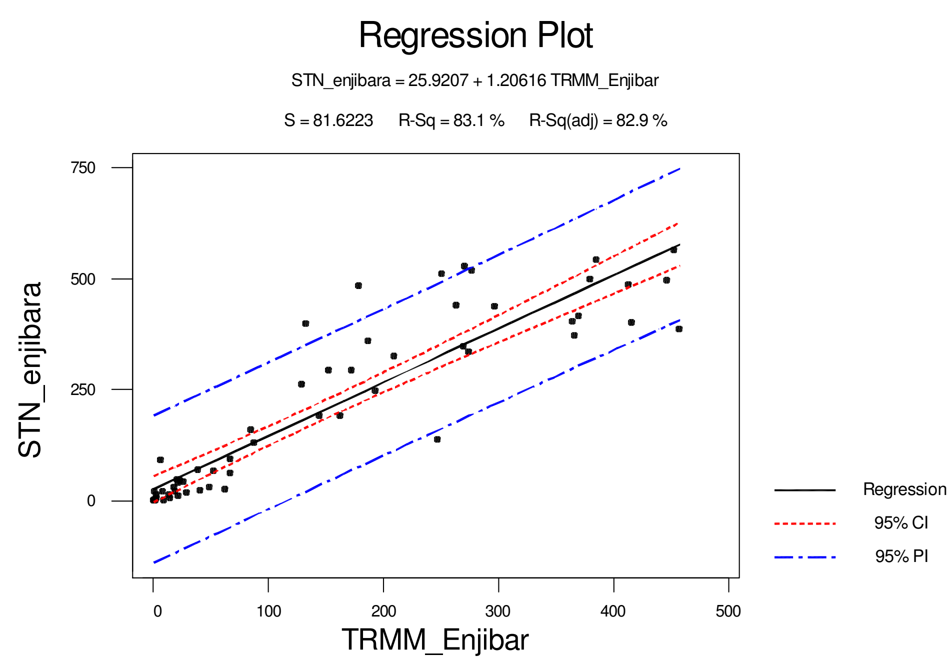
Regression Plot
STN_enjibara = 25.9207 + 1.20616 TRMM_Enjibar
S = 81.6223 R-Sq = 83.1 % R-Sq(adj) = 82.9 %
STN_enjibara
TRMM_Enjibar
Regression
95% CI
95% PI

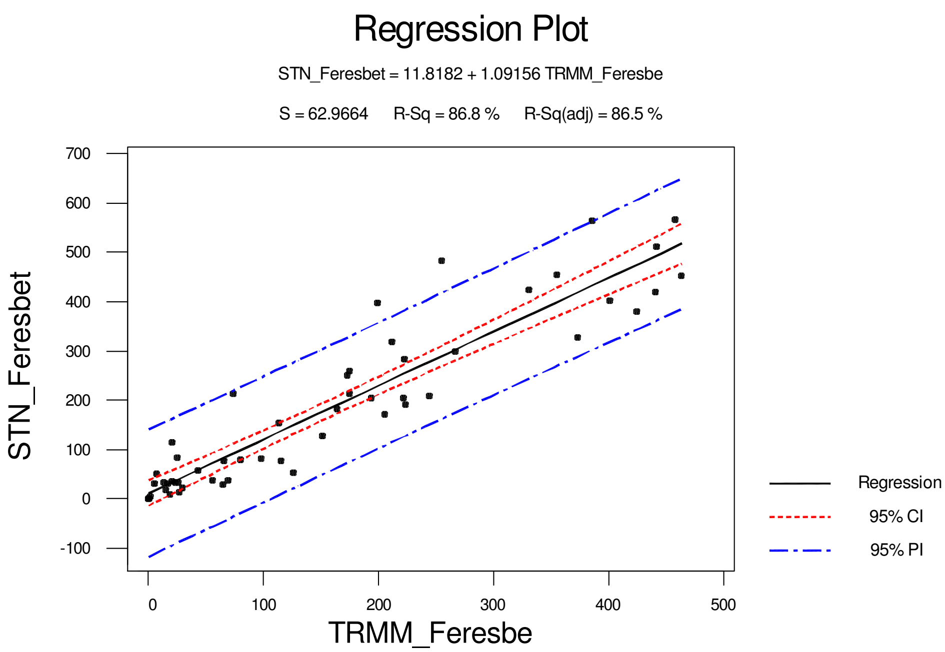
Regression Plot
STN_Feresbet = 11.8182 + 1.09156 TRMM_Feresbe
S = 62.9664 R-Sq = 86.8 % R-Sq(adj) = 86.5 %
STN_Feresbet
TRMM_Feresbe
Regression
95% CI
95% PI

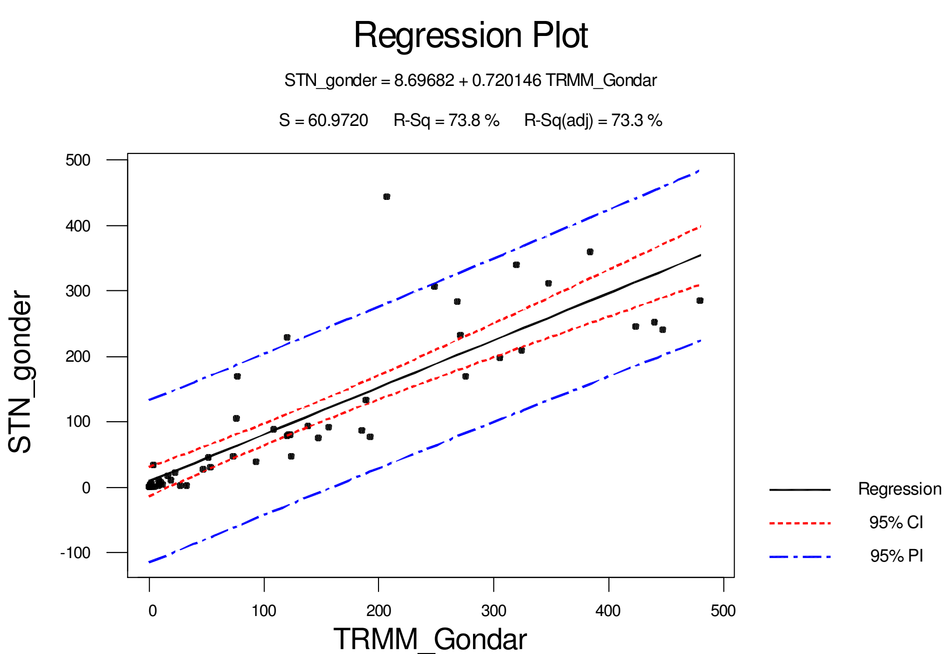
Regression Plot
STN_gonder = 8.69682 + 0.720146 TRMM_Gondar
S = 60.9720 R-Sq = 73.8 % R-Sq(adj) = 73.3 %
STN_gonder
TRMM_Gondar
Regression
95% CI
95% PI

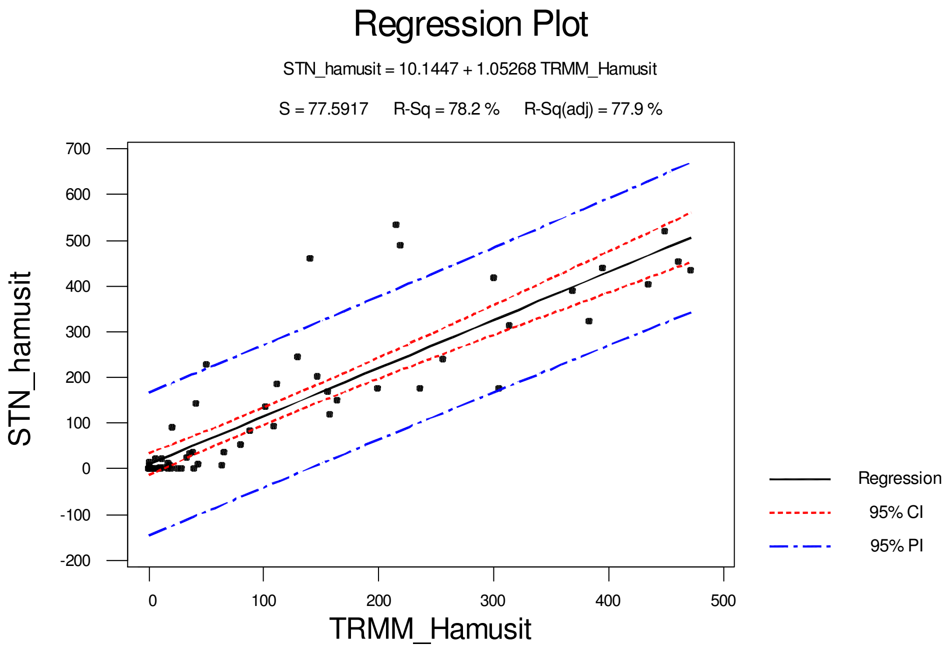
Regression Plot
STN_hamusit = 10.1447 + 1.05268 TRMM_Hamusit
S = 77.5917 R-Sq = 78.2 % R-Sq(adj) = 77.9 %
STN_hamusit
TRMM_Hamusit
Regression
95% CI
95% PI

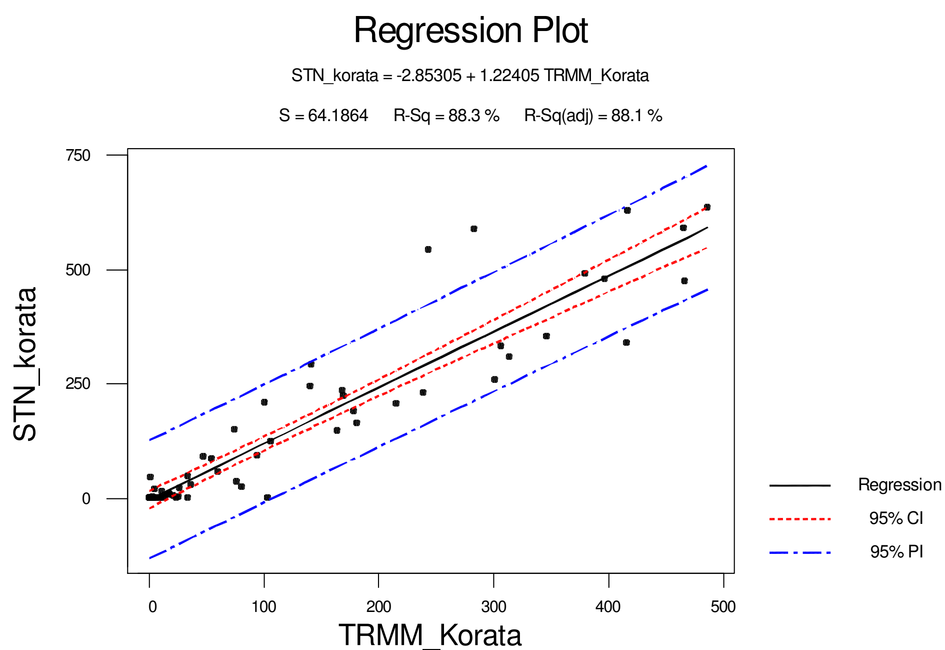
Regression Plot
STN_korata = -2.85305 + 1.22405 TRMM_Korata
S = 64.1864 R-Sq = 88.3 % R-Sq(adj) = 88.1 %
STN_korata
TRMM_Korata
Regression
95% CI
95% PI

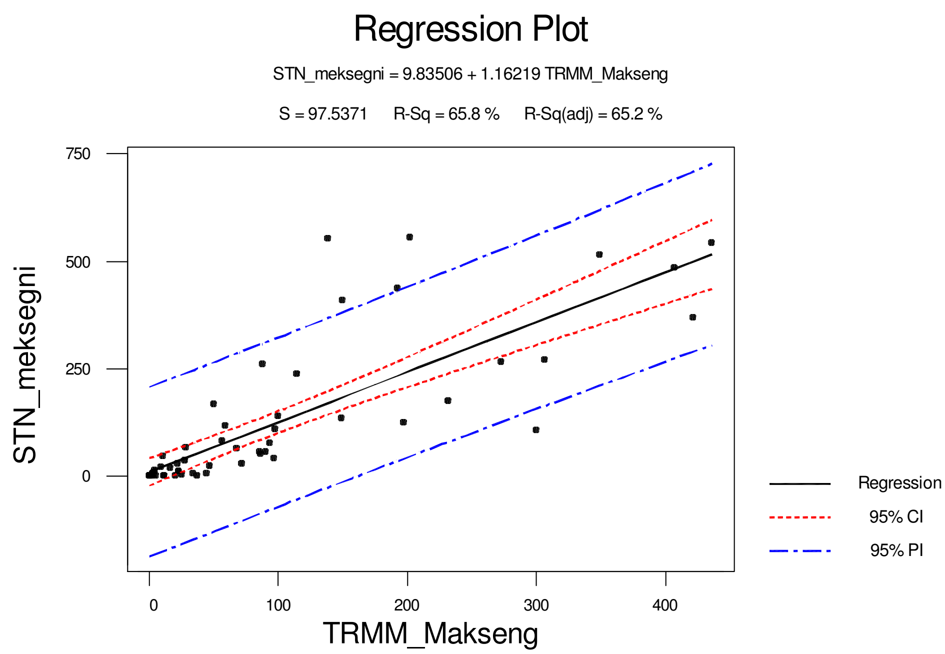
Regression Plot
STN_meksegni = 9.83506 + 1.16219 TRMM_Makseng
S = 97.5371 R-Sq = 65.8 % R-Sq(adj) = 65.2 %
STN_meksegni
TRMM_Makseng
750
500
250
0
0
100
200
300
400
Regression
95% CI
95% PI

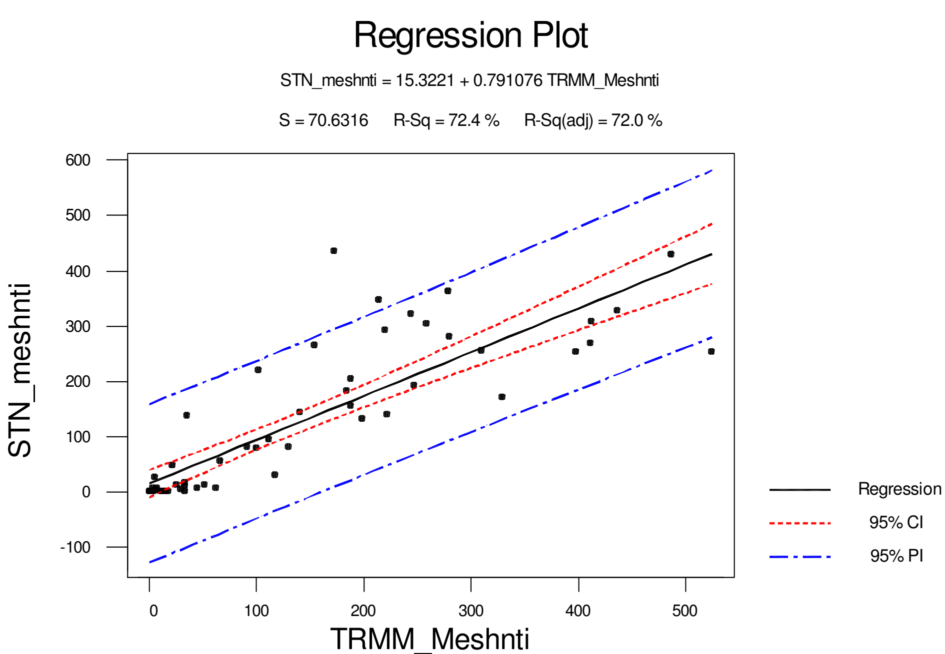
Regression Plot
STN_meshnti = 15.3221 + 0.791076 TRMM_Meshnti
S = 70.6316 R-Sq = 72.4 % R-Sq(adj) = 72.0 %
STN_meshnti
TRMM_Meshnti
600
500
400
300
200
100
0
-100
0
100
200
300
400
500
Regression
95% CI
95% PI

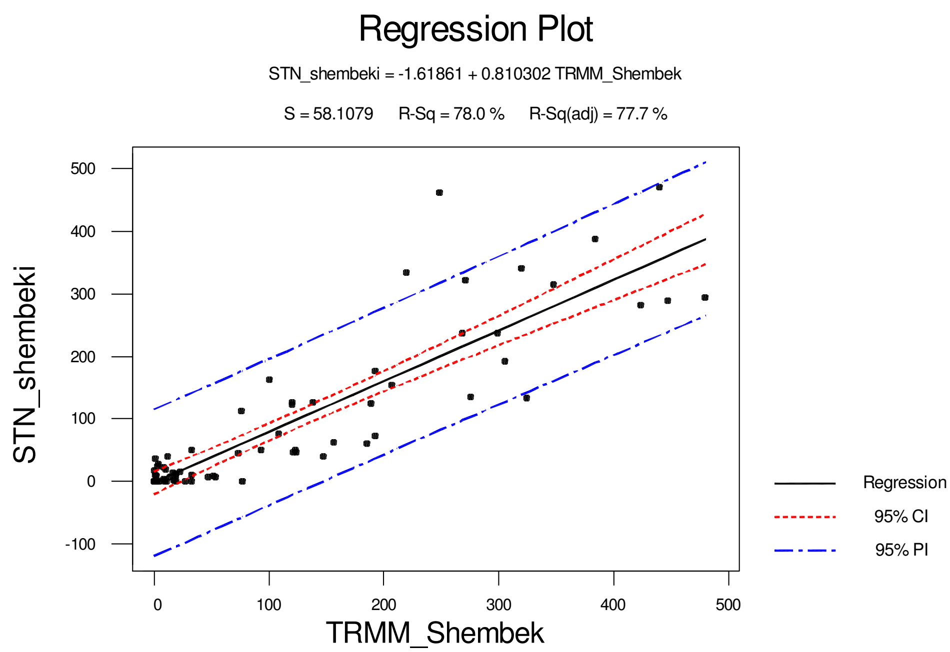
Regression Plot
STN_shembeki = -1.61861 + 0.810302 TRMM_Shembek
S = 58.1079 R-Sq = 78.0 % R-Sq(adj) = 77.7 %
STN_shembeki
TRMM_Shembek
500
400
300
200
100
0
-100
0
100
200
300
400
500
Regression
95% CI
95% PI

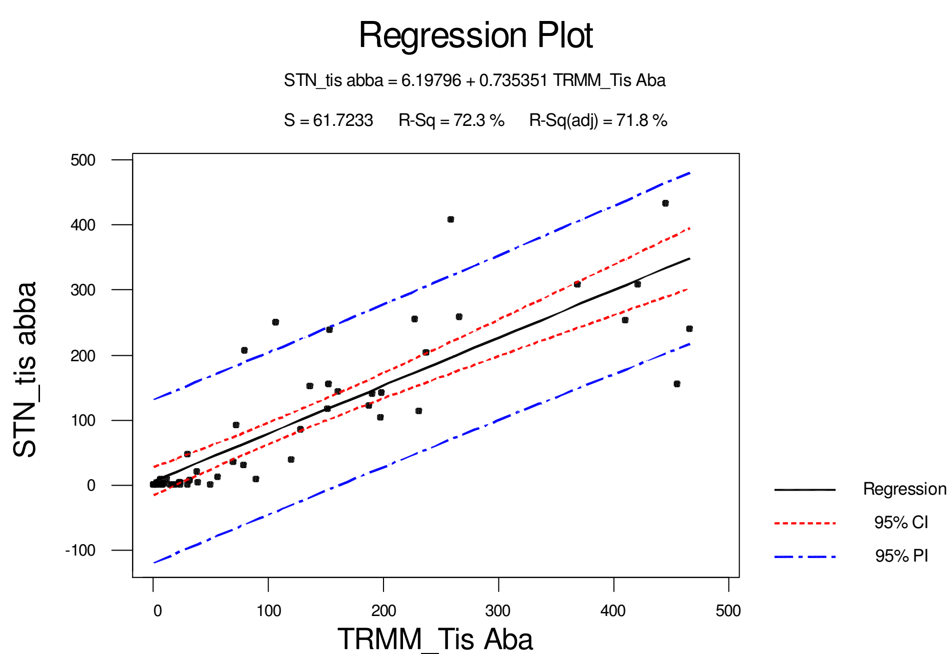
Regression Plot
STN_tis abba = 6.19796 + 0.735351 TRMM_Tis Aba
S = 61.7233 R-Sq = 72.3 % R-Sq(adj) = 71.8 %
STN_tis abba
TRMM_Tis Aba
500
400
300
200
100
0
-100
0
100
200
300
400
500
Regression
95% CI
95% PI

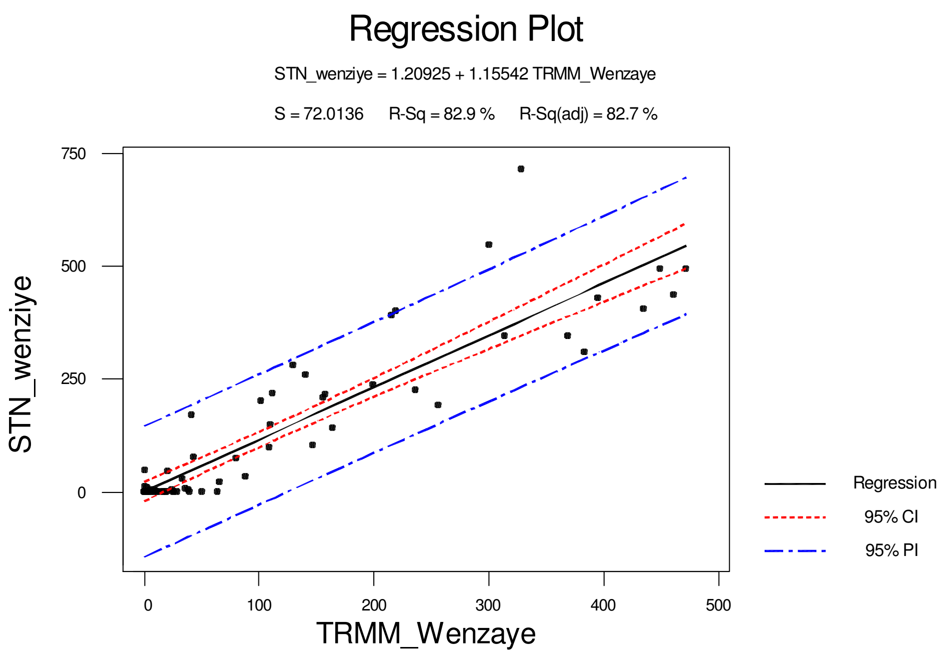

Regression Plot
STN_wenziye = 1.20925 + 1.15542 TRMM_Wenzaye
S = 72.0136 R-Sq = 82.9 % R-Sq(adj) = 82.7 %
STN_wenziye
TRMM_Wenzaye
750
500
250
0
0
100
200
300
400
500
Regression
95% CI
95% PI

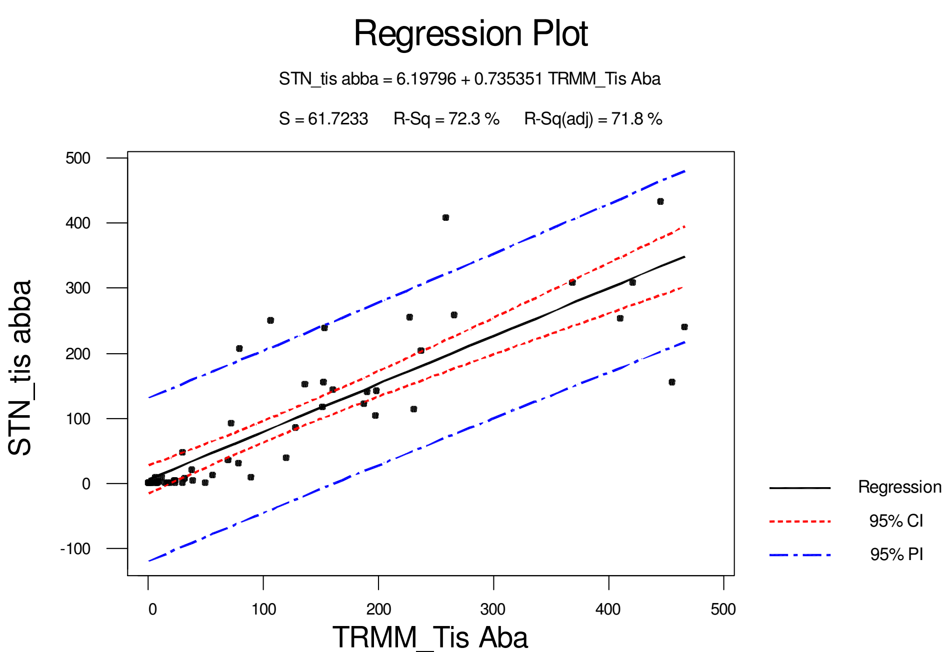

Regression Plot
STN_tis abba = 6.19796 + 0.735351 TRMM_Tis Aba
S = 61.7233 R-Sq = 72.3 % R-Sq(adj) = 71.8 %
STN_tis abba
TRMM_Tis Aba
500
400
300
200
100
0
-100
0
100
200
300
400
500
Regression
95% CI
95% PI

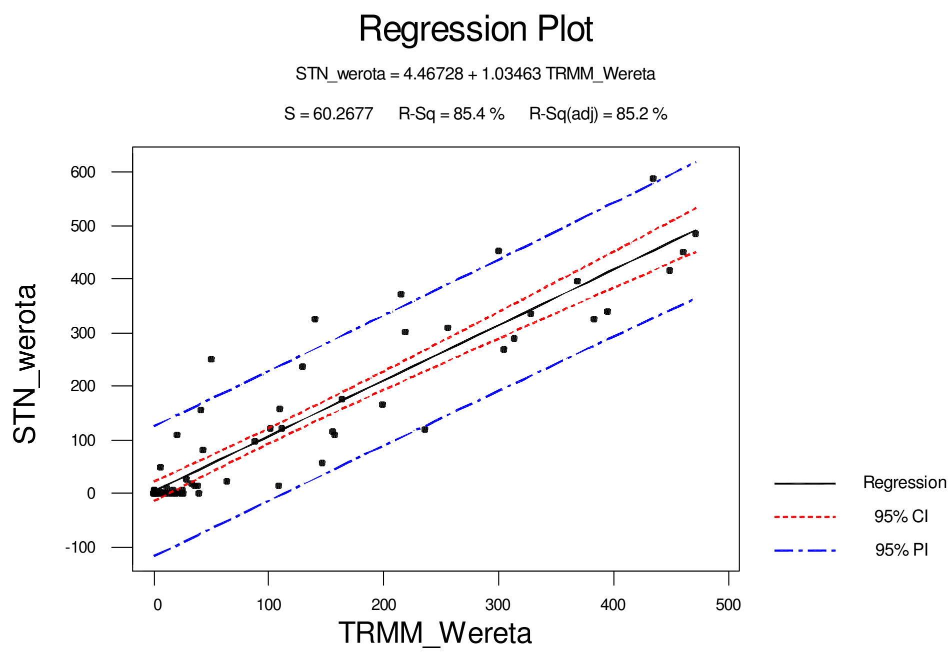
Regression Plot
STN_werota = 4.46728 + 1.03463 TRMM_Wereta
S = 60.2677 R-Sq = 85.4 % R-Sq(adj) = 85.2 %
STN_werota
TRMM_Wereta
Regression
95% CI
95% PI

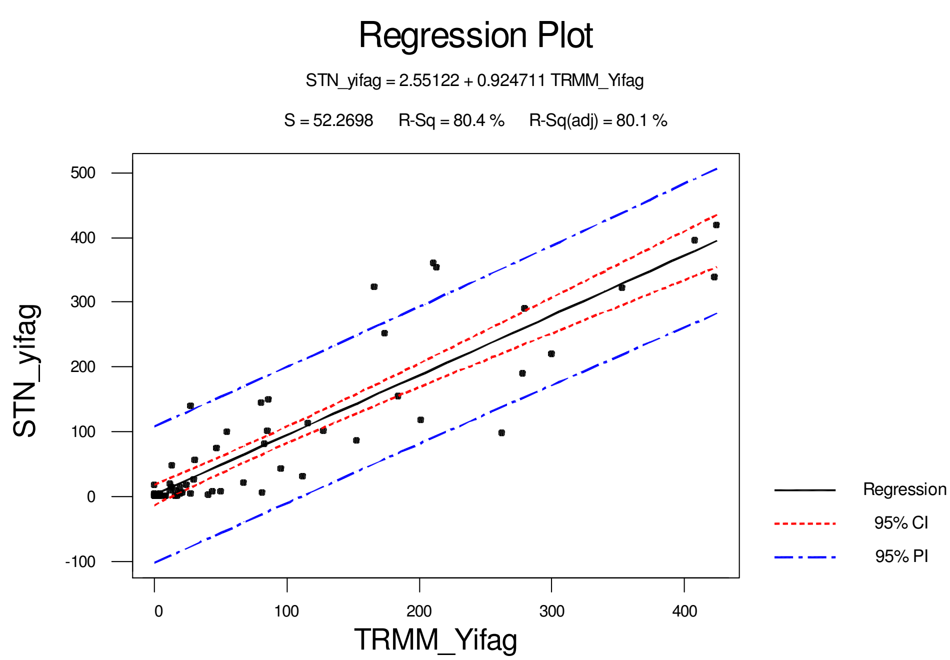
Regression Plot
STN_yifag = 2.55122 + 0.924711 TRMM_Yifag
S = 52.2698 R-Sq = 80.4 % R-Sq(adj) = 80.1 %
STN_yifag
TRMM_Yifag
Regression
95% CI
95% PI

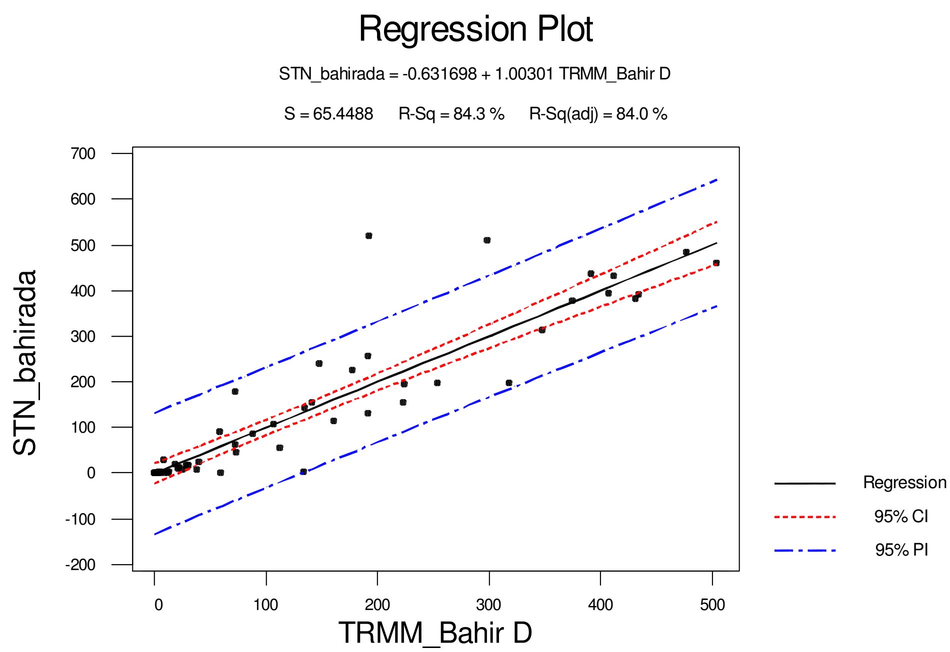

Summary for all stations

West Stations	R2	South Stations		North Stations	R2		East Stations	R2
Aykel	87.6	Enjibar	83.1	Amba Giorgis	77.1		Debre Tabor	80.4
Chandiba	85.4	Feresbet	86.8	chauit	76.6		Ebnet	82.4
Shaura	82.1	Meshnti	72.4	Dabat	84.7		Hamusit	78.2
		Tis ababy	72.3	Enfraz	74.8		Korata	88.3
		Bahirdar	84.3	Gondar	73.8		Wenziye	83.0
				Shembekit	78.6		Werota	85.4
							Yifag	80.4
mean	**85.0**	**mean**	**79.8**	**mean**	**77.6**		**mean**	**82.6**

Annex – II result of Flood plain analysis

Reference Images used

1) Radarsat Image July 27

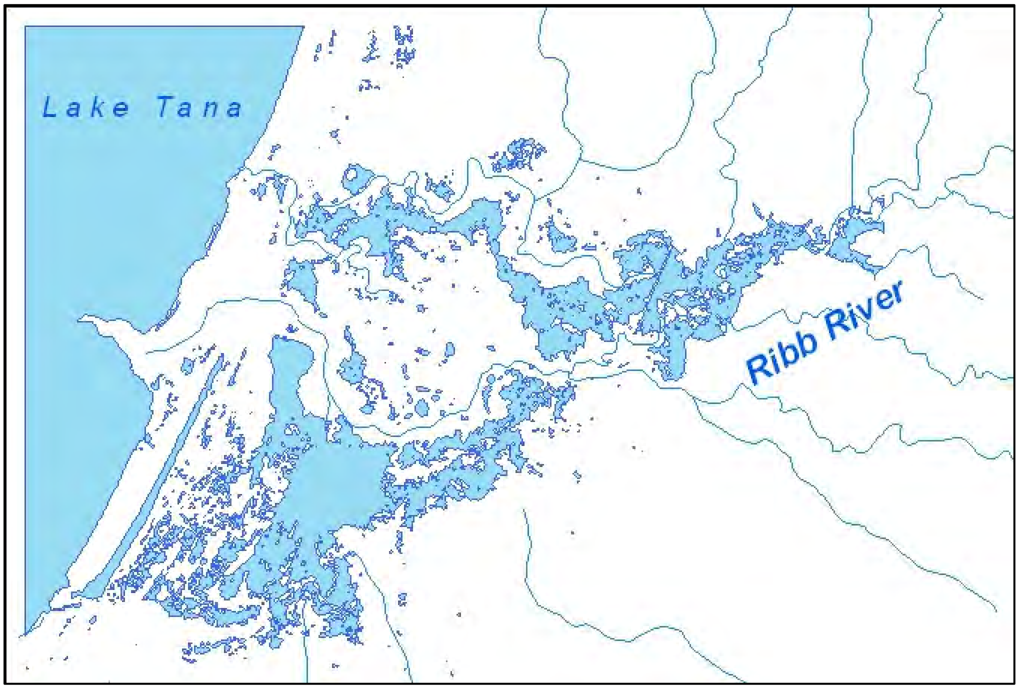

2) Landsat Image Oct 23

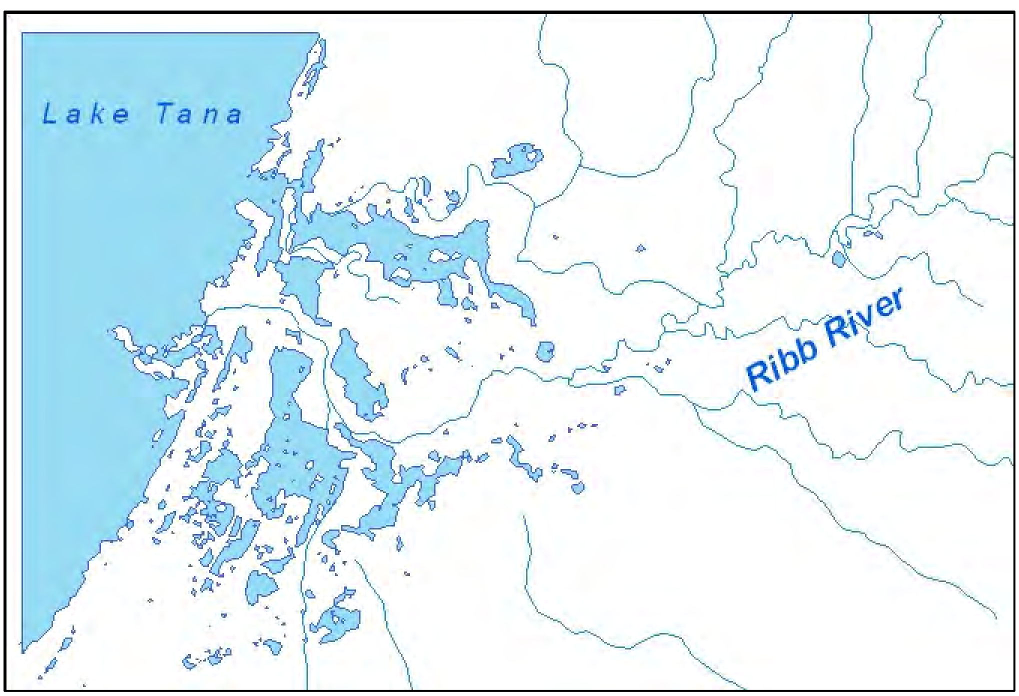

3) ASAR Image Sep 03

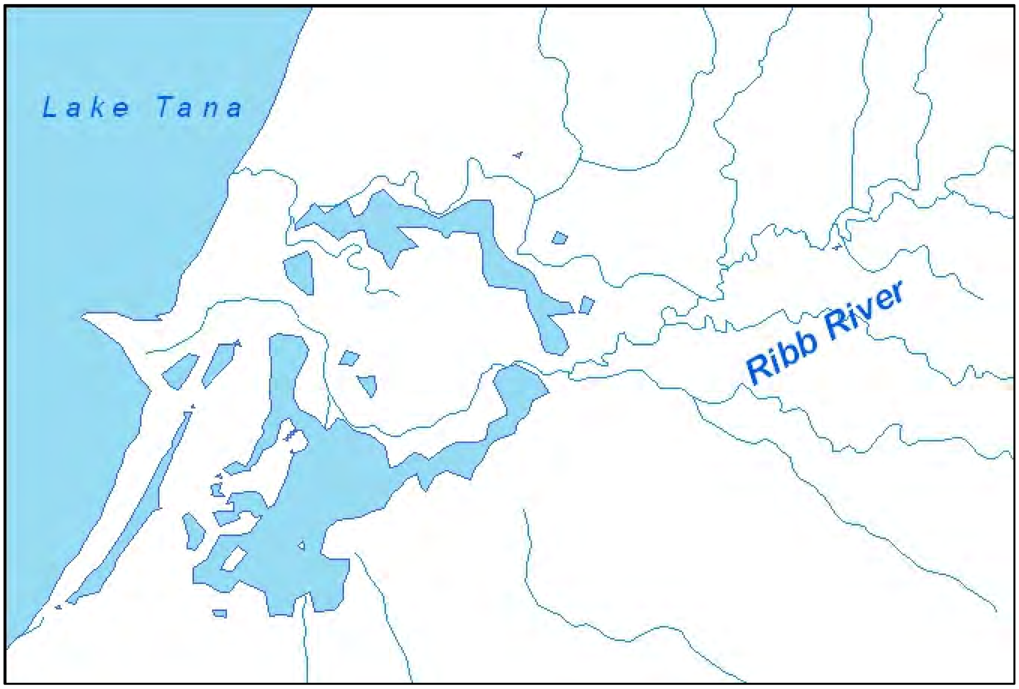

4) Landsat TM Nov 3

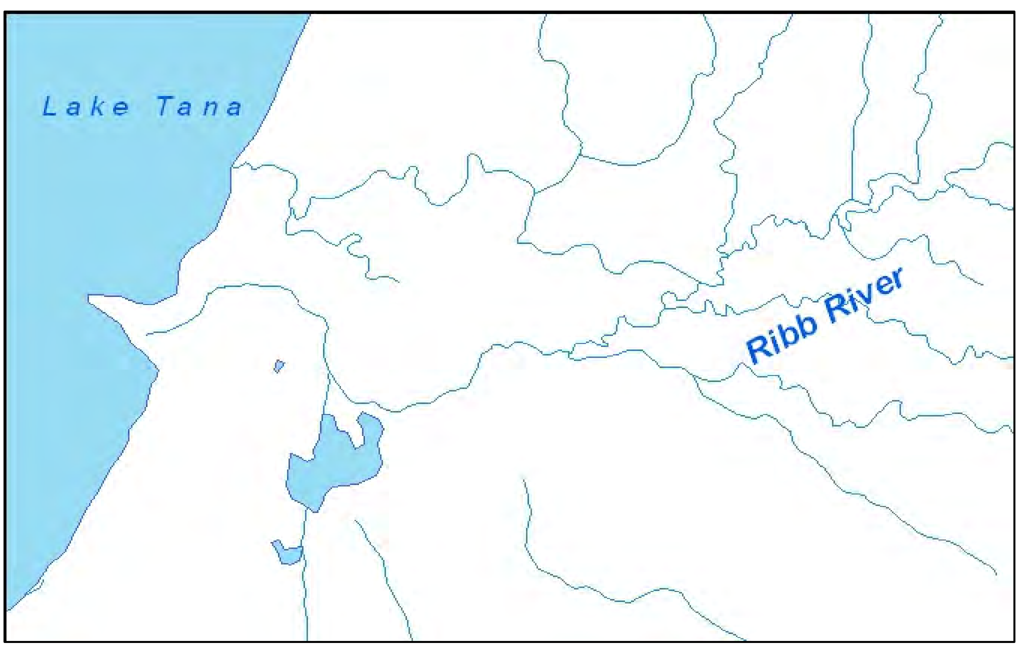

Flooded area extent in sqr.km

Ribb	megech	WestTana	Gumara	Gabbay	Total
0.00	0.00	0.00	0.00	0.00	0.00
0.00	0.00	0.00	0.00	0.00	0.00
0.00	0.00	0.00	0.00	0.00	0.00
0.00	0.00	0.00	0.00	0.00	0.00
0.00	0.00	0.00	0.00	0.00	0.00
17.37	11.43	22.70	7.28	48.03	106.81
113.73	156.48	77.04	10.61	27.55	385.41
205.11	221.65	172.80	29.42	51.81	680.78
172.45	178.55	93.40	22.65	34.69	501.74
173.83	44.59	134.95	23.30	129.49	506.15
44.83	15.40	43.17	24.19	55.41	183.00
18.27	20.36	44.53	28.17	46.05	157.38
0.00	0.00	0.00	0.00	0.00	0.00
0.00	0.00	0.00	0.00	0.00	0.00
0.00	0.00	0.00	0.00	0.00	0.00
0.00	0.00	0.00	0.00	0.00	0.00
0.00	0.00	0.00	0.00	0.00	0.00
16.79	13.39	21.57	3.89	45.50	101.13
115.44	102.86	82.88	11.26	34.56	347.00
227.53	151.97	141.15	22.05	49.17	591.86
159.87	190.65	93.57	13.30	29.43	486.82
646.62	78.48	243.71	48.18	184.19	447.34
145.28	44.60	63.68	35.87	65.19	354.62
182.82	41.38	79.64	30.71	59.09	393.64
0.00	0.00	0.00	0.00	0.00	0.00
0.00	0.00	0.00	0.00	0.00	0.00
0.00	0.00	0.00	0.00	0.00	0.00
0.00	0.00	0.00	0.00	0.00	0.00
0.00	0.00	0.00	0.00	0.00	0.00
15.68	19.50	27.29	8.21	36.70	107.39
114.55	102.21	75.81	15.37	25.19	333.14
235.56	120.18	110.98	34.85	51.14	552.70
146.75	148.62	87.12	13.05	31.66	427.20
294.02	61.69	164.39	36.79	167.11	724.00
81.12	36.03	51.58	36.82	93.32	298.87
29.59	32.66	52.72	18.22	63.95	197.15
0.00	0.00	0.00	0.00	0.00	0.00
0.00	0.00	0.00	0.00	0.00	0.00
0.00	0.00	0.00	0.00	0.00	0.00
0.00	0.00	0.00	0.00	0.00	0.00
0.00	0.00	0.00	0.00	0.00	0.00
50.96	14.74	38.85	8.36	48.57	161.48
133.08	161.51	123.77	13.64	27.19	459.19
205.03	184.84	177.48	37.77	53.35	658.46
101.16	123.11	83.12	14.81	29.03	351.23
74.99	26.32	120.69	11.77	64.22	297.98
22.47	15.70	41.98	16.75	40.84	137.75
16.03	10.07	50.88	12.40	38.76	128.13

0.00	0.00	0.00	0.00	0.00	0.00
0.00	0.00	0.00	0.00	0.00	0.00
0.00	0.00	0.00	0.00	0.00	0.00
0.00	0.00	0.00	0.00	0.00	0.00
0.00	0.00	0.00	0.00	0.00	0.00
32.33	9.12	24.93	13.62	37.50	117.50
65.18	110.98	71.56	13.52	26.04	287.29
155.84	85.23	95.65	29.61	40.98	407.31
100.17	99.00	71.95	20.11	23.43	314.67
42.46	21.56	79.65	9.62	51.52	204.81
16.49	16.95	32.78	18.73	34.88	119.82
17.75	15.92	42.27	16.99	33.04	125.98
0.00	0.00	0.00	0.00	0.00	0.00
0.00	0.00	0.00	0.00	0.00	0.00
0.00	0.00	0.00	0.00	0.00	0.00
0.00	0.00	0.00	0.00	0.00	0.00
0.00	0.00	0.00	0.00	0.00	0.00
19.50	18.00	15.00	7.50	20.50	80.50
101.33	98.00	45.33	13.33	24.07	282.07
196.67	138.67	75.67	33.47	39.90	484.37
191.67	141.33	91.67	39.67	44.13	508.47
100.67	30.33	76.67	32.33	43.70	283.70
45.67	21.33	34.67	21.80	36.60	160.07
43.67	21.33	40.33	17.00	31.50	153.83

Six year average flooded area extent in sqr.km

	Ribb	Megech	West Tana	Gumara	Gilgel abbay	Total
January	0.00	0.00	0.00	0.00	0.00	0.00
February	0.00	0.00	0.00	0.00	0.00	0.00
March	0.00	0.00	0.00	0.00	0.00	0.00
April	0.00	0.00	0.00	0.00	0.00	0.00
May	0.00	0.00	0.00	0.00	0.00	0.00
June	25.44	14.36	25.06	8.14	39.47	112.47
July	107.22	122.01	79.40	12.96	27.43	349.01
August	204.29	150.42	128.95	31.19	47.72	562.58
September	145.35	146.88	86.80	20.60	32.06	431.69
October	222.10	43.83	136.68	27.00	106.70	410.66
November	59.31	25.00	44.64	25.69	54.38	209.02
December	51.36	23.62	51.73	20.58	45.40	192.69

Annex – III Rainfall-Runoff SCS-Method For Sub-basin

1) Regression Analysis of Upper Gilgel Abbay sub-basin SCS-CN Runoff estimation versus measured runoff

```
The regression equation is
Simulated = 0.681*Observed + 9.1026

S = 86.5169      R-Sq = 88.2 %      R-Sq(adj) = 88.0 %

Analysis of Variance

Source           DF        SS        MS        F       P
Regression        1   3916496   3916496  523.234   0.000
Error            70    523962      7485
Total            71   4440458
```

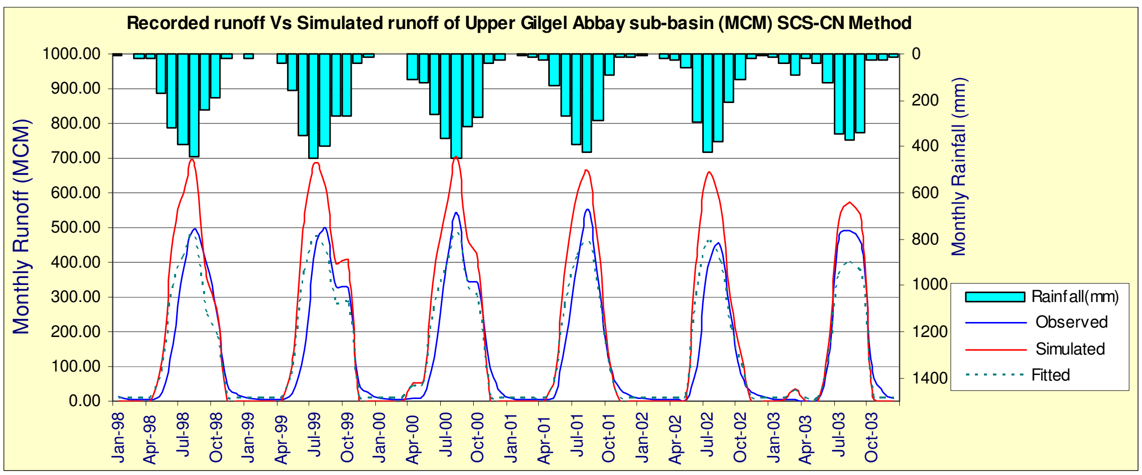

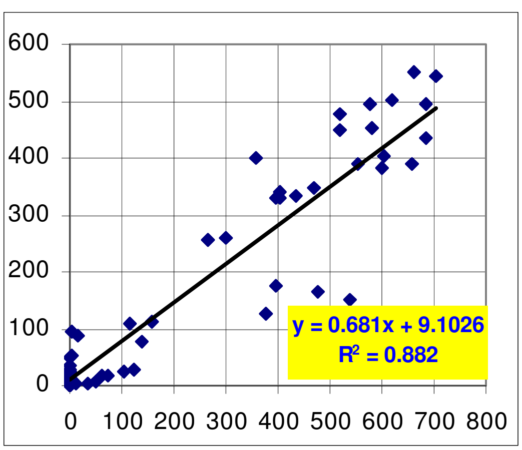

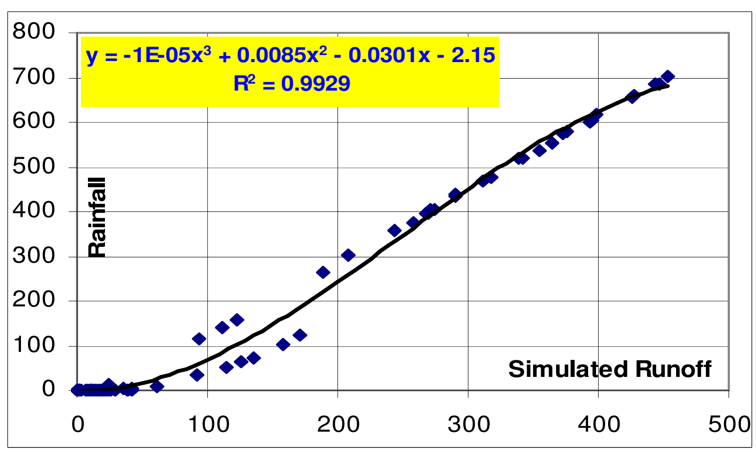

2) Regression Analysis of Gauged Garon sub-basin SCS-CN Runoff estimation versus measured runoff

```
The regression equation is
Observed = 0.581888 + 0.296191*Simulated

S = 3.00050      R-Sq = 56.4 %      R-Sq(adj) = 54.1 %

Analysis of Variance

Source           DF        SS        MS         F      P
Regression        1     221.338   221.338   24.5850  0.000
Error            19     171.057     9.003
Total            20     392.395
```

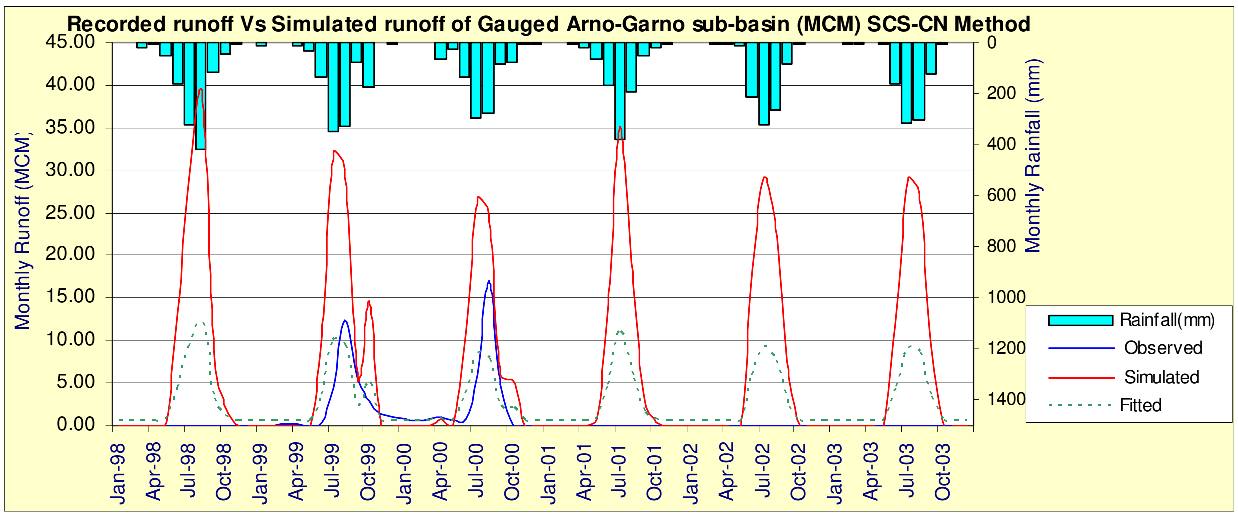

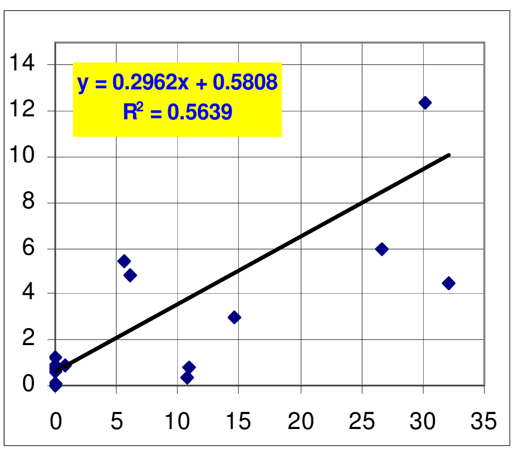

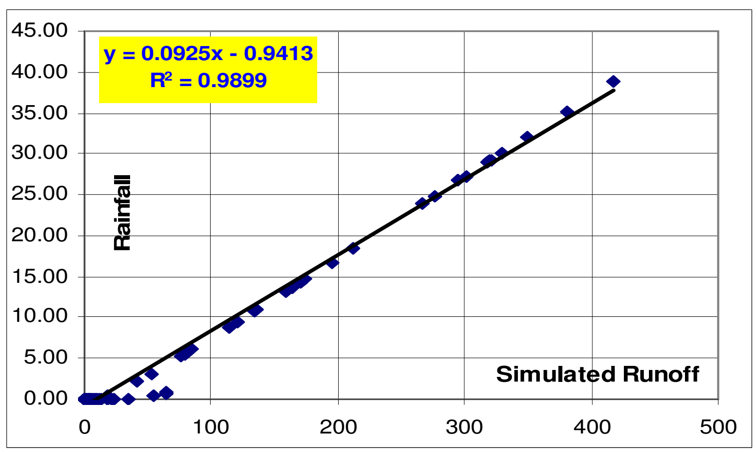

3) Regression Analysis of Gauged Gumaro sub-basin SCS-CN Runoff estimation versus measured runoff

```
The regression equation is
Observed = 31.3331 + 6.94190*Simulated

S = 97.8998      R-Sq = 67.5 %      R-Sq(adj) = 67.1 %

Analysis of Variance

Source          DF        SS        MS         F      P
Regression       1   1396270   1396270   145.682  0.000
Error           70    670906      9584
Total           71   2067176
```

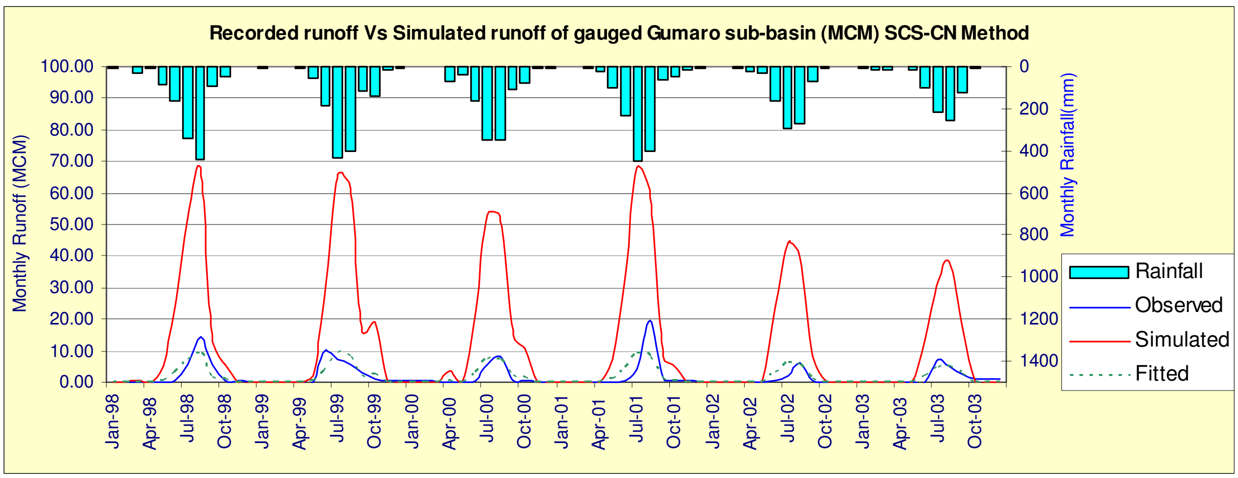

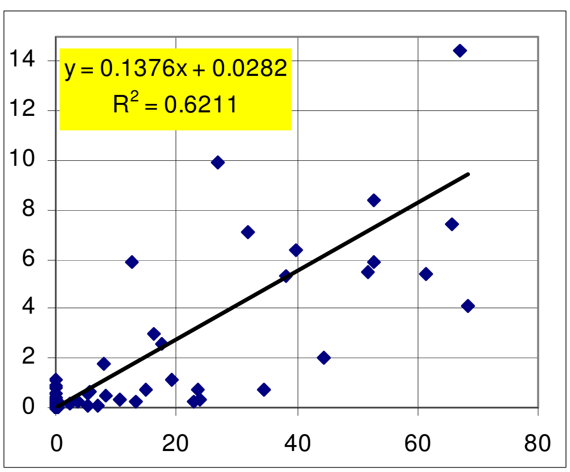

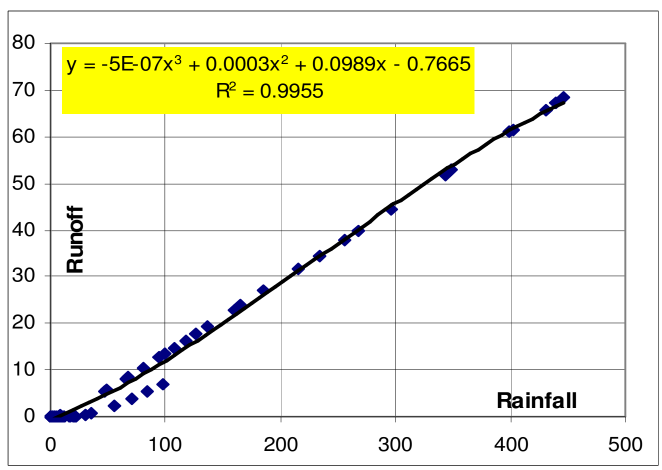

4) Regression Analysis of Gauged Gumera sub-basin SCS-CN Runoff estimation versus measured runoff

```
The regression equation is
observed =  0.6218* Simulated + 10.426

S = 72.5660       R-Sq = 73.62 %       R-Sq(adj) = 73.4 %

Analysis of Variance

Source            DF          SS          MS          F       P
Regression         1      915314      915314    173.822   0.000
Error             65      342279        5266
Total             66     1257593
```

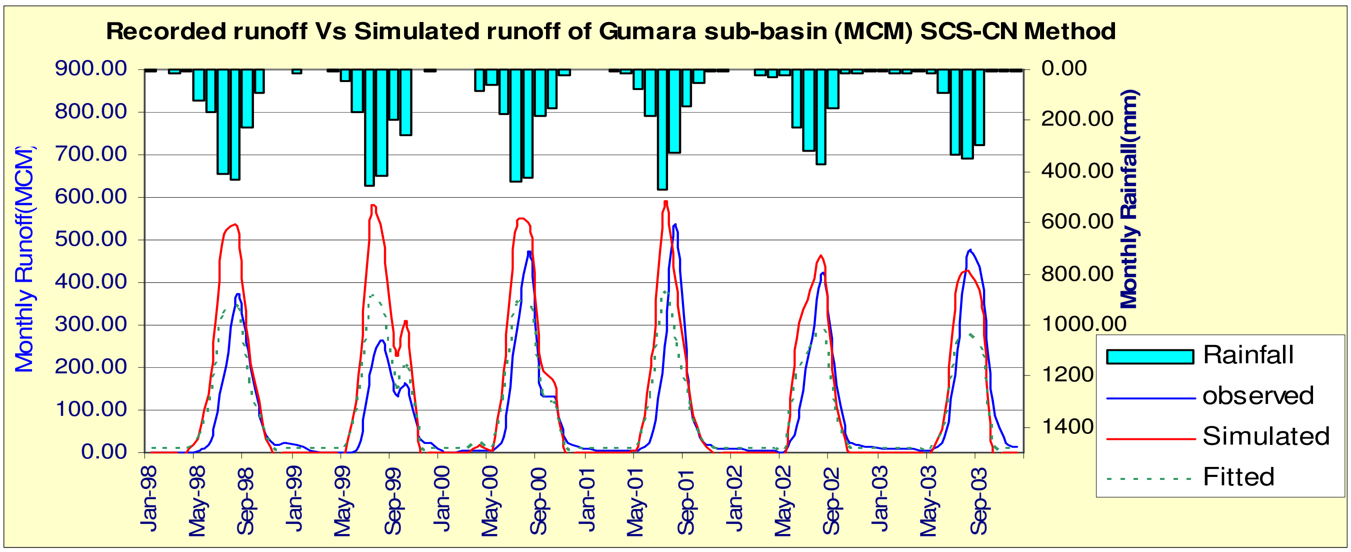

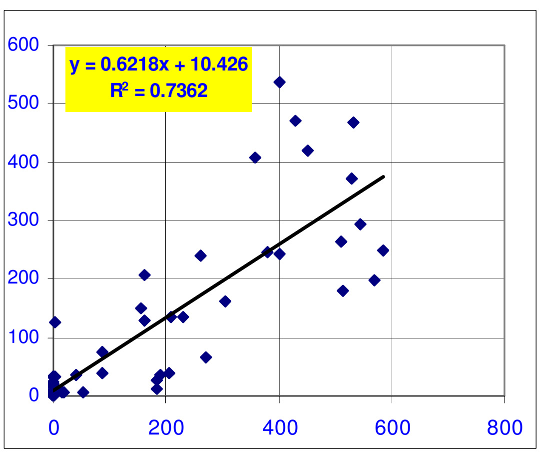

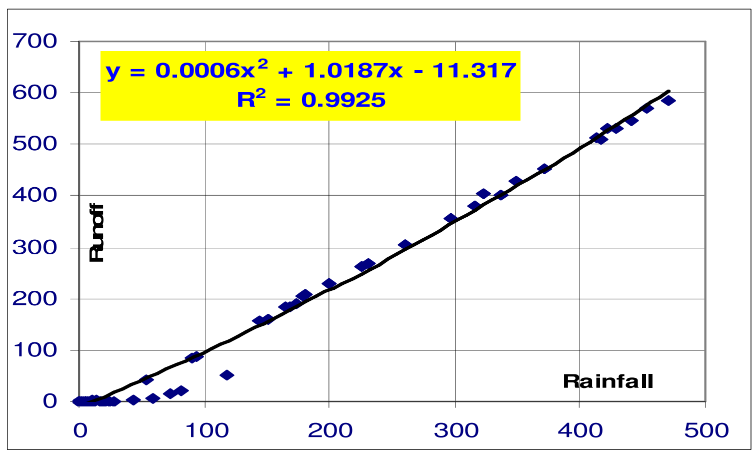

5) Regression Analysis of Koga sub-basin SCS-CN Runoff estimation versus measured runoff

```
The regression equation is
observed = 4.22720 + 0.363616*Simulated

S = 8.84561      R-Sq = 73.6 %      R-Sq(adj) = 73.2 %

Analysis of Variance

Source           DF        SS        MS        F      P
Regression        1   15236.0   15236.0  194.722  0.000
Error            70    5477.1      78.2
Total            71   20713.1
```

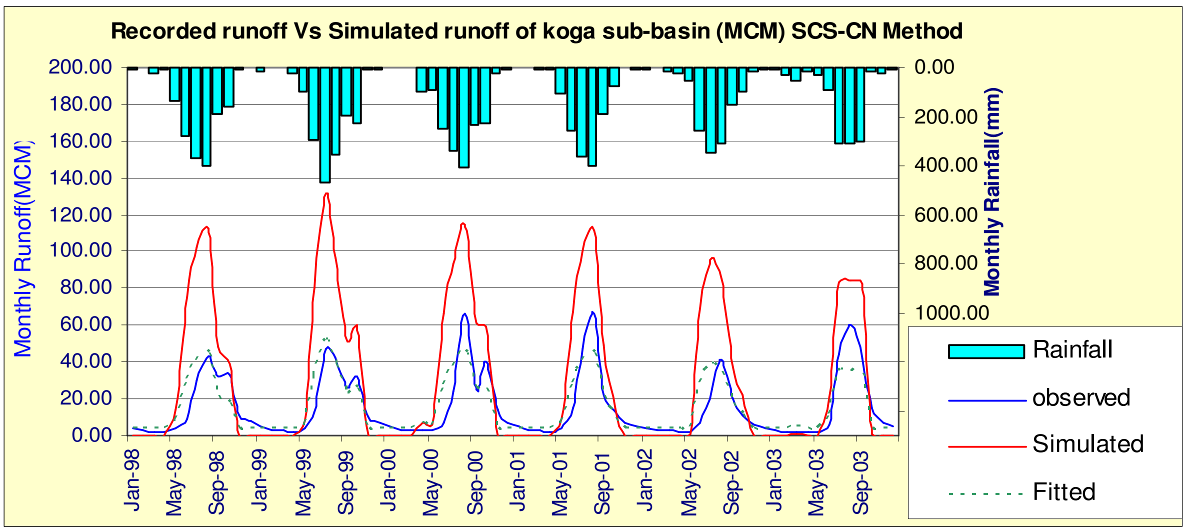

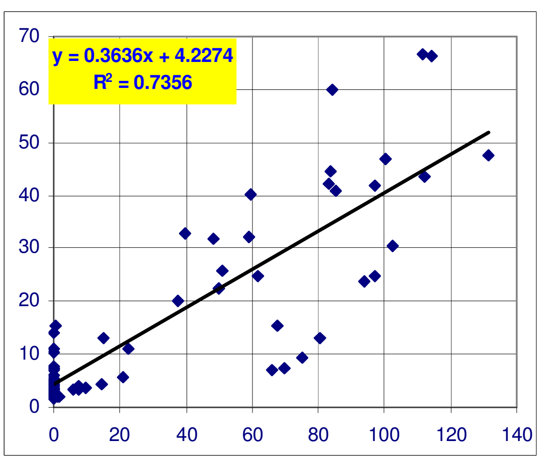

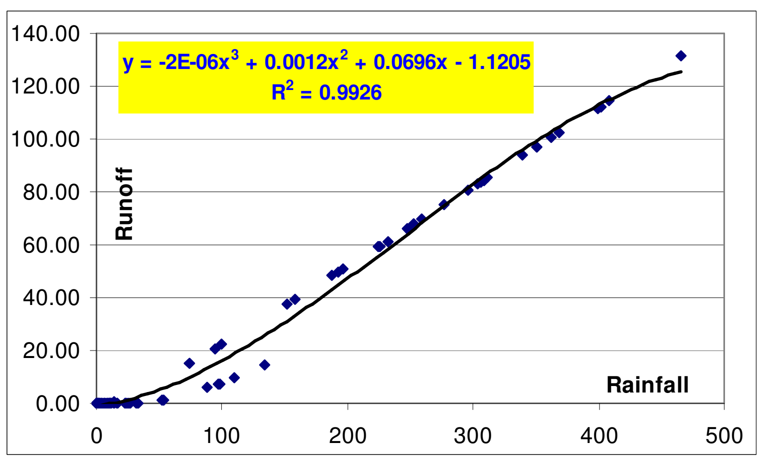

6) Regression Analysis of Megech sub-basin SCS-CN Runoff estimation versus measured runoff

```
The regression equation is
observed = 4.52152 + 0.440902 Simulated

S = 16.4071      R-Sq = 67.9 %      R-Sq(adj) = 67.5 %

Analysis of Variance

Source             DF         SS          MS          F       P
Regression          1    39874.7     39874.7    148.127   0.000
Error              70    18843.5       269.2
Total              71    58718.1
```

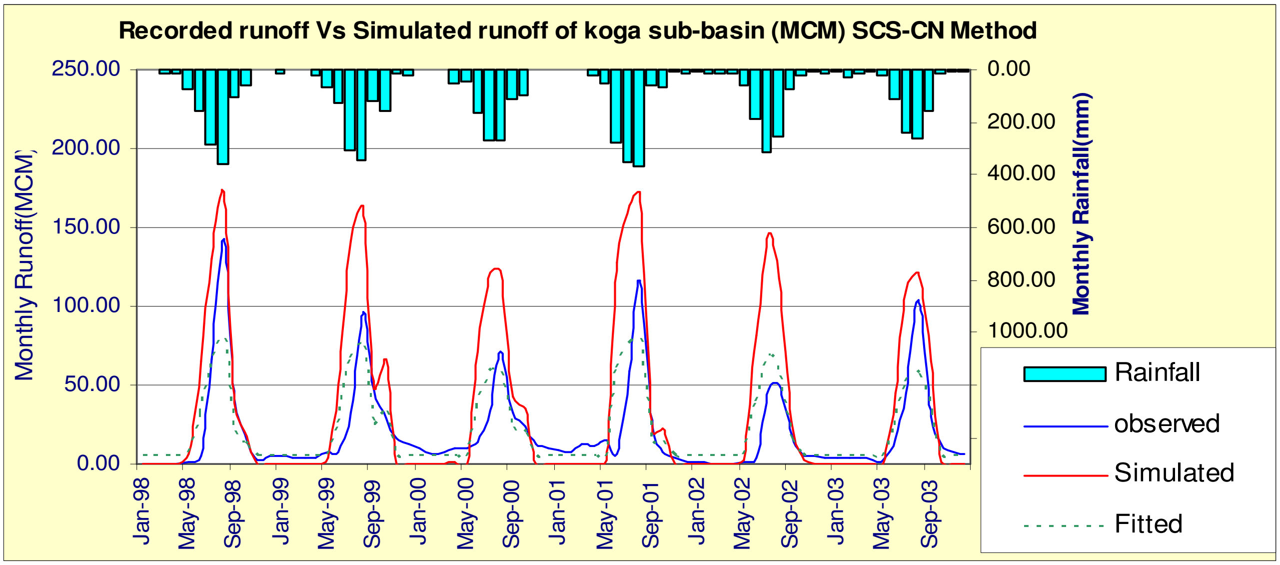

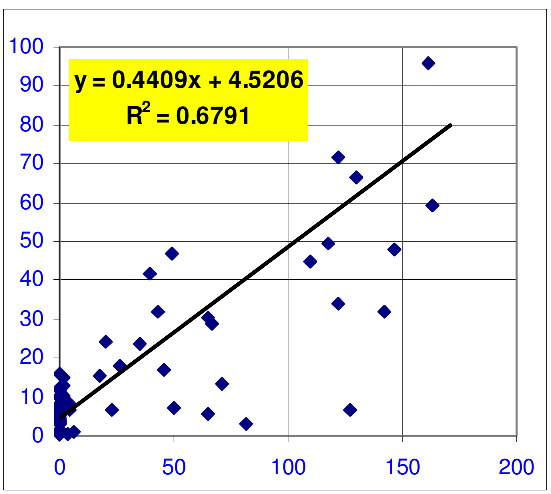

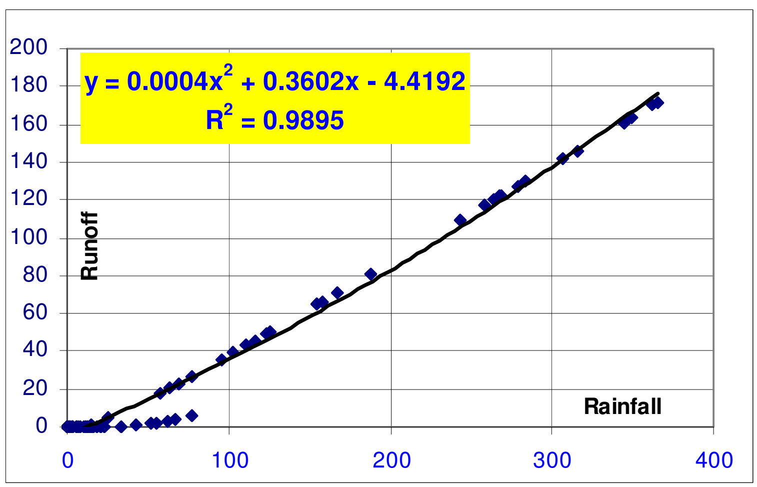

7) Regression Analysis of Ribb gauged sub-basin SCS-CN Runoff estimation versus measured runoff

```
The regression equation is
observed = 5.06837 + 0.282577 Simulated

S = 27.6874      R-Sq = 79.3 %      R-Sq(adj) = 79.0 %

Analysis of Variance

Source          DF        SS        MS        F       P
Regression       1    205139    205139  267.599   0.000
Error           70     53661       767
Total           71    258800
```

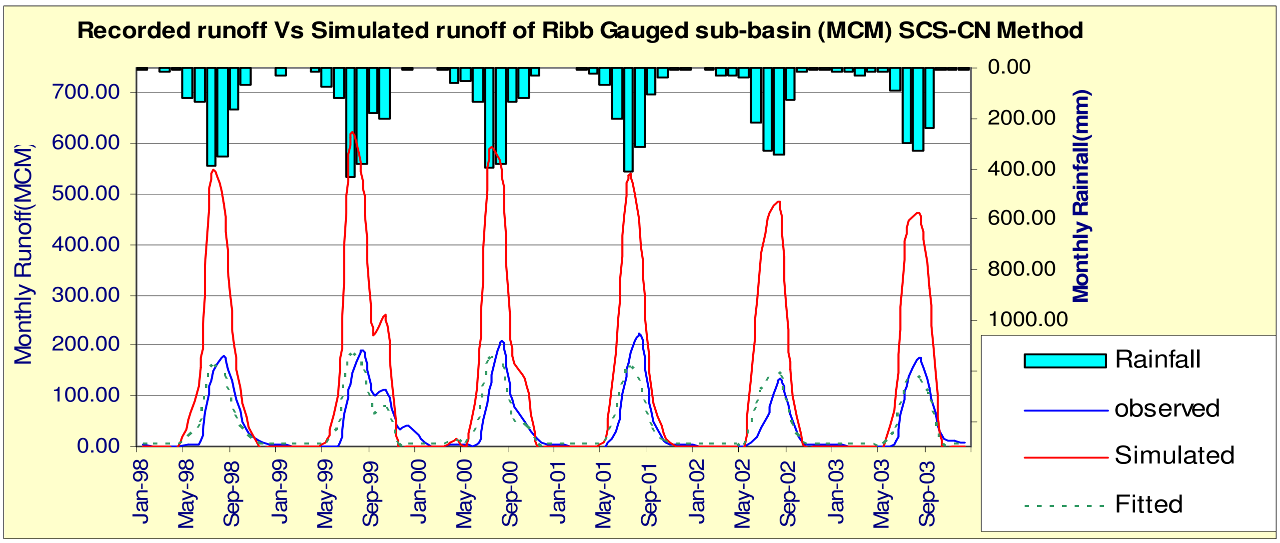

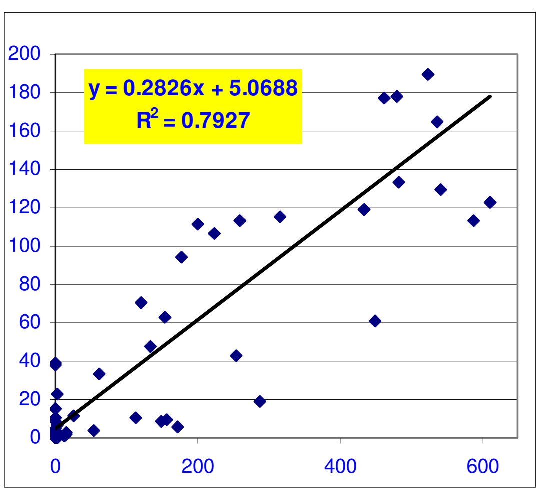

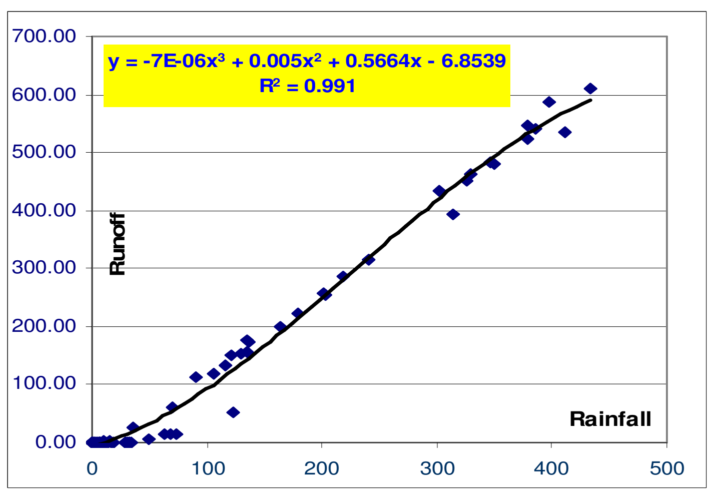

Annex – IV Result of Soil water accounting Model for Sub-basin

1) Result for Upper Gilgel Abbay sub-basin estimation versus measured runoff

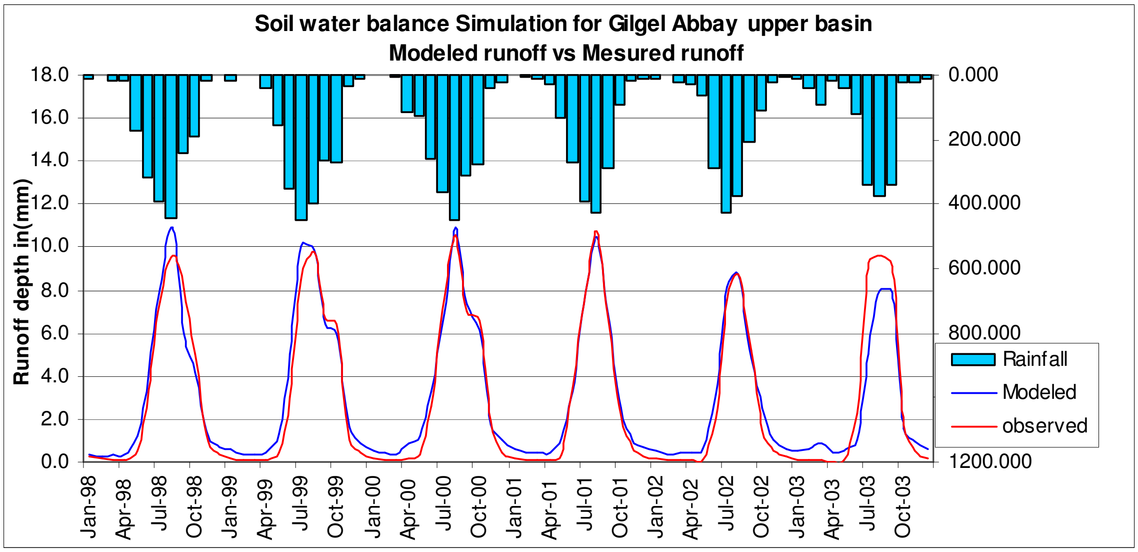

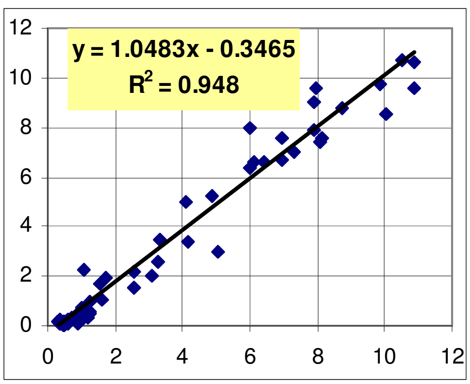

Soil water balance Simulation for upper Gilgel Abbay basin Parameters							
	Gummara ungauged			base flow	0.3		
		error	51.266796	Smax	688.6289063	SSRC	2
		epsilon	1.9805664	alpha	6.298413086		
		Zi	0	DRC	0.1		

2) Result for Gummara sub-basin estimation versus measured runoff

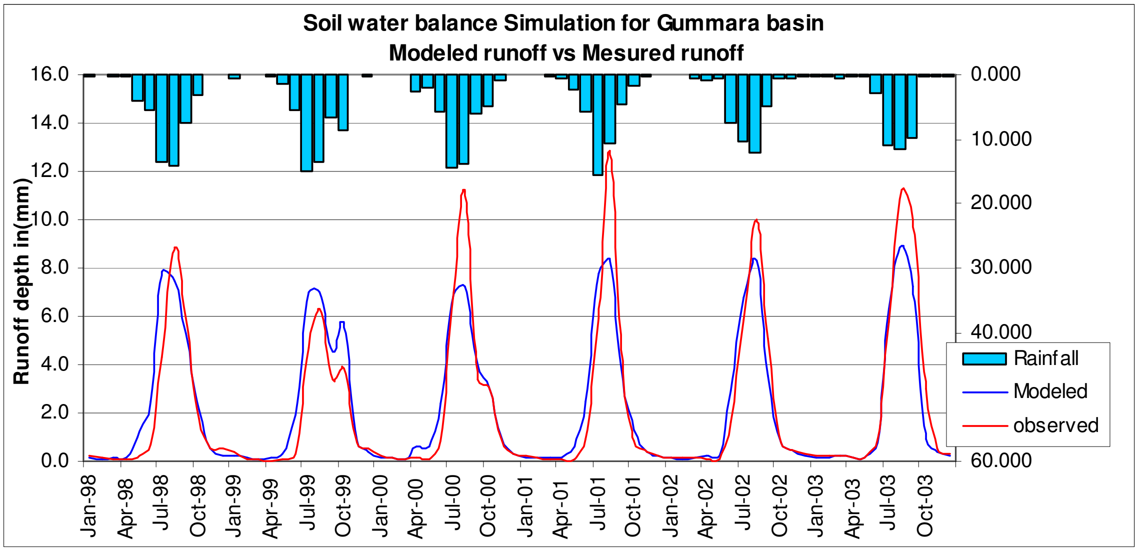

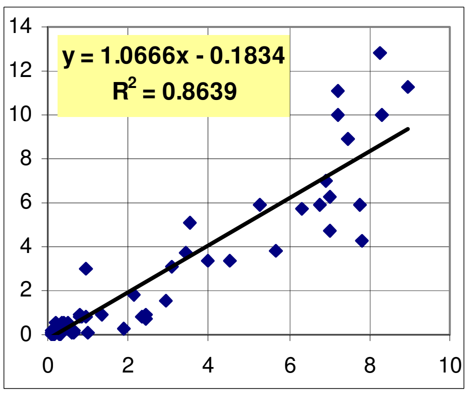

Soil water balance Simulation for Gummara basin estimated Parameters							
	Gummara ungauged			base flow	0.1		
		error	103.31721	Smax	526.9375	SSRC	2
		epsilon	3.953125	alpha	21.81171875		
		Zi	0	DRC	0.1		

3) Result for Gumaro sub-basin estimation versus measured runoff

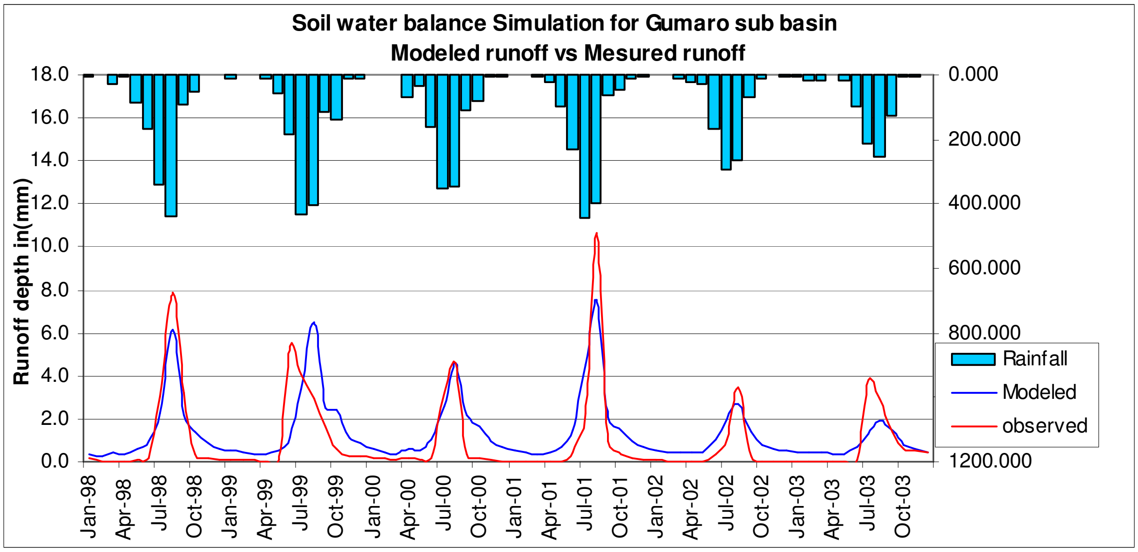

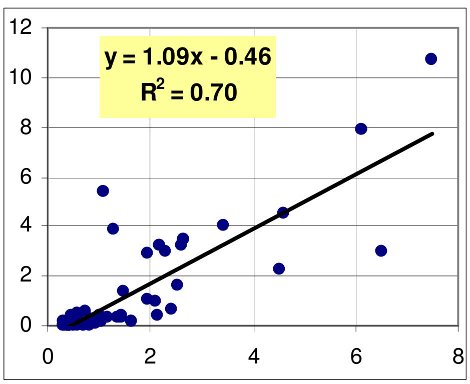

Soil water balance Simulation for Gumaro sub basin estimated parameters							
	Gummara ungauged			base flow	0.3		
		error	87.702063	Smax	863.875	SSRC	2
		epsilon	5.66875	alpha	2.991015625		
		Zi	0	DRC	0.1		

4) Result for Ribb sub-basin estimation versus measured runoff

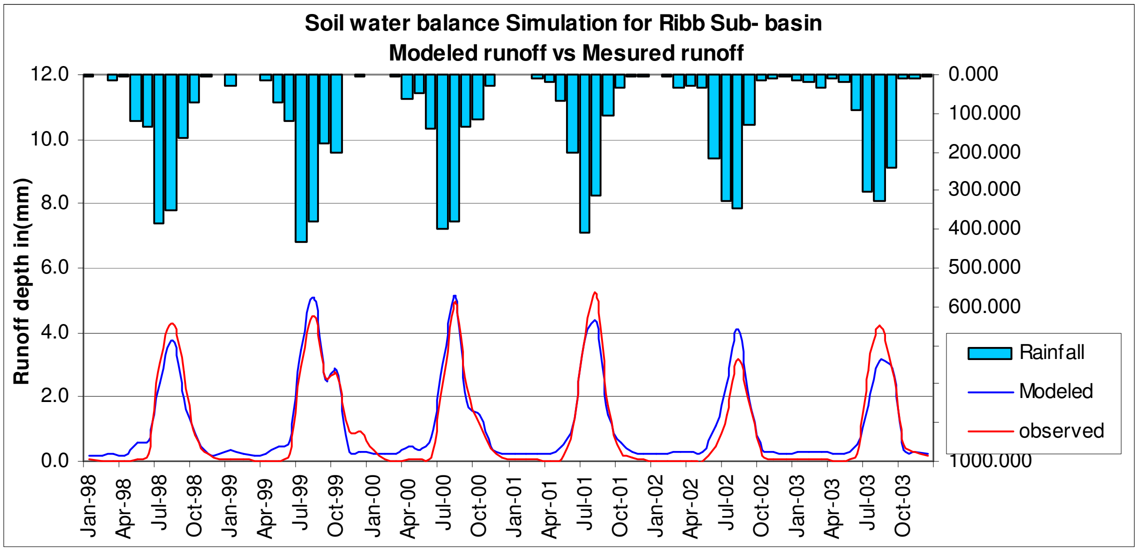

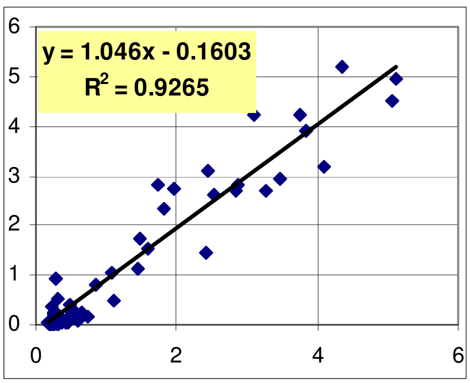

Soil water balance Simulation for Ribb Subbasin Estimated Parameters							
	Ribb gauged			base flow	0.18		
		error	12.006829	Smax	1058.375	SSRC	2
		epsilon	2.996875	alpha	0.362207031		
		Zi	0	DRC	0.1		

5) Result for Ribb sub-basin estimation versus measured runoff

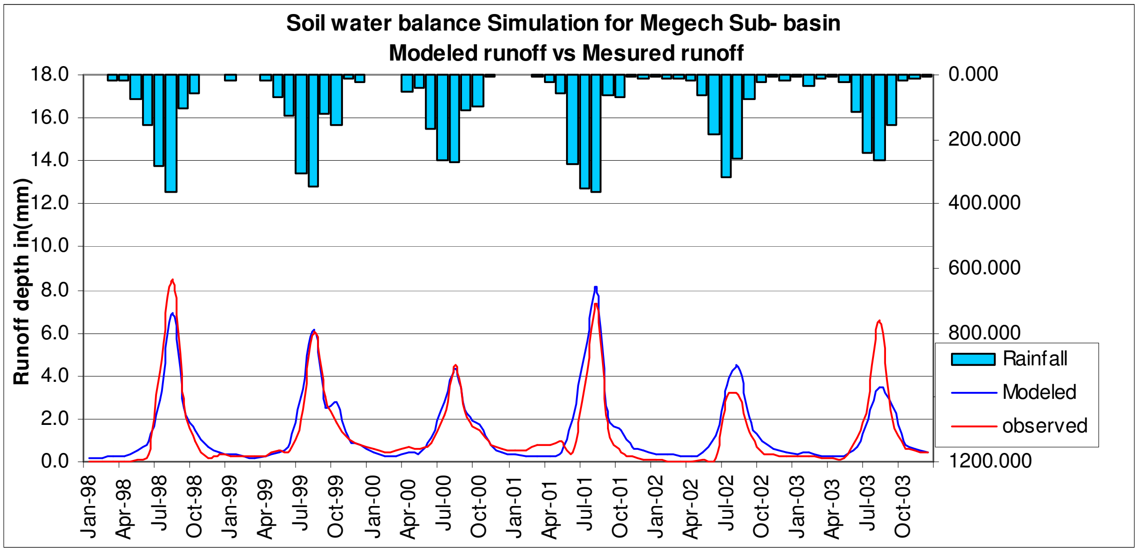

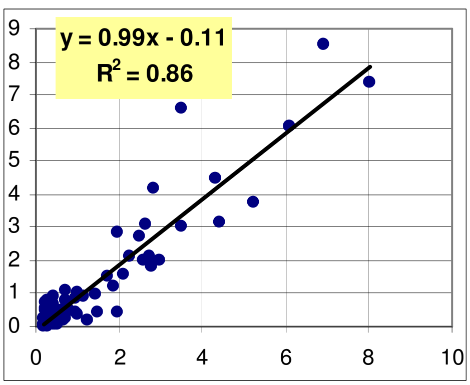

Soil water balance Simulation for Megech Sub- basin Estimated Parametrs							
	Gummara ungauged			base flow	0.2		
		error	31.2845	Smax	634.9980469	SSRC	2
		epsilon	4.175	alpha	4.275		
		Zi	0	DRC	0.1		

Annex – V Monthly rainfall Gap filling multiple regression techniques

1. Regression Analysis: Addis Zemen versus ebnet, enfranze, yifag

```
The regression equation is
Addis Zemen = - 7.6 + 0.451 ebnet - 0.551 enfranze + 1.13 yifag

31 cases used 41 cases contain missing values

Predictor        Coef     SE Coef          T        P
Constant        -7.55       18.46      -0.41    0.686
ebnet          0.4511      0.3843       1.17    0.251
enfranze      -0.5508      0.3548      -1.55    0.132
yifag          1.1345      0.3984       2.85    0.008

S = 80.18       R-Sq = 75.5%     R-Sq(adj) = 72.7%

Analysis of Variance

Source            DF          SS          MS         F        P
Regression         3      533532      177844     27.66    0.000
Residual Error    27      173598        6430
Total             30      707131

Source       DF      Seq SS
ebnet         1      481112
enfranze      1         297
yifag         1       52124
```

2. Regression Analysis: tis abbay versus Bahir dar, meshnti

```
The regression equation is
tis abbay = 0.83 + 0.258 Bahir dar + 0.506 meshnti

57 cases used 15 cases contain missing values

Predictor        Coef     SE Coef          T        P
Constant        0.827       7.940       0.10    0.917
Bahir da      0.25795     0.08485       3.04    0.004
meshnti        0.5061      0.1056       4.79    0.000

S = 45.19       R-Sq = 85.4%     R-Sq(adj) = 84.9%

Analysis of Variance

Source            DF          SS          MS         F        P
Regression         2      646180      323090    158.18    0.000
Residual Error    54      110297        2043
Total             56      756478

Source       DF      Seq SS
Bahir da      1      599262
meshnti       1       46919
```

3. Regression Analysis: Amba Giorgis versus dabat, shembekit

```
The regression equation is
Amba Giorgis = - 2.61 + 0.657 dabat + 0.389 shembekit

50 cases used 22 cases contain missing values

Predictor        Coef     SE Coef          T        P
Constant       -2.613       7.082      -0.37    0.714
dabat          0.6572      0.1356       4.85    0.000
shembeki       0.3886      0.1061       3.66    0.001

S = 39.12       R-Sq = 90.5%     R-Sq(adj) = 90.1%

Analysis of Variance

Source            DF          SS          MS         F        P
Regression         2      686699      343349    224.40    0.000
Residual Error    47       71912        1530
Total             49      758611

Source       DF      Seq SS
dabat         1      666156
shembeki      1       20543
```

4. Regression Analysis: aykel versus chandiba, chwadiba

```
The regression equation is
aykel = 6.01 + 0.926 chandiba

59 cases used 13 cases contain missing values

Predictor        Coef     SE Coef          T        P
Constant        6.013       8.132       0.74    0.463
chandiba      0.92587     0.05301      17.47    0.000

S = 46.20       R-Sq = 84.3%     R-Sq(adj) = 84.0%

Analysis of Variance

Source            DF          SS          MS         F        P
Regression         1      651257      651257    305.11    0.000
Residual Error    57      121668        2135
Total             58      772925
```

5. Regression Analysis: chandiba versus chauit, aykel

```
The regression equation is
chandiba = 9.98 + 0.235 chauit + 0.709 aykel

58 cases used 14 cases contain missing values

Predictor        Coef     SE Coef          T        P
Constant        9.981       7.980       1.25    0.216
chauit         0.2352      0.1786       1.32    0.194
aykel          0.7093      0.1610       4.41    0.000

S = 45.62       R-Sq = 84.9%     R-Sq(adj) = 84.3%

Analysis of Variance

Source            DF          SS          MS         F        P
Regression         2      643536      321768    154.60    0.000
Residual Error    55      114474        2081
```

6. Regression Analysis: chauit versus gorgora, chwadiba

The regression equation is
chauit = 4.31 + 0.533 gorgora + 0.380 chwadiba

59 cases used 13 cases contain missing values

Predictor	Coef	SE Coef	T	P
Constant	4.314	4.919	0.88	0.384
gorgora	0.53312	0.05452	9.78	0.000
chwadiba	0.37950	0.05725	6.63	0.000

S = 28.42 R-Sq = 82.5% R-Sq(adj) = 82.2%

Analysis of Variance

Source	DF	SS	MS	F	P
Regression	2	556569	278285	344.66	0.000
Residual Error	56	45216	807		
Total	58	601785			

Source	DF	Seq SS
gorgora	1	521091
chwadiba	1	35478

7. Regression Analysis: dabat versus Amba Giorgis, shembekit, gonder

The regression equation is
dabat = 6.85 + 0.482 Amba Giorgis + 0.266 shembekit + 0.0447 gonder

47 cases used 25 cases contain missing values

Predictor	Coef	SE Coef	T	P
Constant	6.853	7.068	0.97	0.338
Amba Gio	0.4818	0.1211	3.98	0.000
shembeki	0.2659	0.1048	2.54	0.015
gonder	0.04468	0.09135	0.49	0.627

S = 35.74 R-Sq = 69.4% R-Sq(adj) = 68.7%

Analysis of Variance

Source	DF	SS	MS	F	P
Regression	3	462782	154261	120.77	0.000
Residual Error	43	54922	1277		
Total	46	517704			

Source	DF	Seq SS
Amba Gio	1	452844
shembeki	1	9632
gonder	1	306

8. Regression Analysis: debre tabor versus ebnet, werota

The regression equation is
debre tabor = 23.2 + 0.586 ebnet + 0.457 werota

42 cases used 30 cases contain missing values

Predictor	Coef	SE Coef	T	P
Constant	23.16	10.14	2.29	0.028
ebnet	0.5855	0.1331	4.40	0.000
werota	0.4565	0.1136	4.02	0.000

S = 51.43   R-Sq = 70.6%   R-Sq(adj) = 70.1%

Analysis of Variance

Source	DF	SS	MS	F	P
Regression	2	989521	494761	187.07	0.000
Residual Error	39	103147	2645		
Total	41	1092669			

Source	DF	Seq SS
ebnet	1	946785
werota	1	42736

Unusual Observations

Obs	ebnet	debre ta	Fit	SE Fit	Residual	St Resid
7	360	400.60	502.85	26.90	-102.25	-2.33RX
20	394	345.70	475.62	19.02	-129.92	-2.72R
32	261	462.40	346.50	14.75	115.90	2.35R
33	27	232.30	93.92	12.28	138.38	2.77R
43	496	496.20	466.82	33.53	29.38	0.75 X

9. Regression Analysis: degi versus chwadiba

The regression equation is
degi = 1.96 + 0.704 chwadiba

Predictor	Coef	SE Coef	T	P
Constant	1.961	7.098	0.28	0.783
chwadiba	0.70410	0.04824	14.60	0.000

S = 45.11   R-Sq = 75.3%   R-Sq(adj) = 74.9%

Analysis of Variance

Source	DF	SS	MS	F	P
Regression	1	433610	433610	213.08	0.000
Residual Error	70	142450	2035		
Total	71	576060			

Unusual Observations

Obs	chwadiba	degi	Fit	SE Fit	Residual	St Resid
7	214	243.10	152.64	7.74	90.46	2.04R
8	364	231.70	258.25	13.91	-26.55	-0.62 X
20	191	324.30	136.66	6.98	187.64	4.21R
29	152	14.70	109.13	5.94	-94.43	-2.11R
32	436	257.10	309.16	17.19	-52.06	-1.25 X
42	281	111.50	199.88	10.33	-88.38	-2.01R
44	203	250.10	144.96	7.36	105.14	2.36R
67	215	251.00	152.99	7.75	98.01	2.21R

10. Regression Analysis: ebnet versus debre tabor, Addis Zemen

The regression equation is
ebnet = - 12.8 + 0.807 debre tabor - 0.022 Addis Zemen

35 cases used 37 cases contain missing values

Predictor	Coef	SE Coef	T	P
Constant	-12.75	12.78	-1.00	0.326
debre ta	0.8071	0.1043	7.74	0.000
Addis Ze	-0.0216	0.1105	-0.20	0.847

S = 54.95 R-Sq = 84.2% R-Sq(adj) = 83.2%

Analysis of Variance

Source	DF	SS	MS	F	P
Regression	2	515045	257522	85.28	0.000
Residual Error	32	96627	3020		
Total	34	611671			

Source	DF	Seq SS
debre ta	1	514930
Addis Ze	1	115

Unusual Observations

Obs	debre ta	ebnet	Fit	SE Fit	Residual	St Resid
20	346	393.50	258.75	18.74	134.75	2.61R
31	423	290.20	316.08	37.12	-25.88	-0.64 X
32	462	261.00	349.42	28.53	-88.42	-1.88 X
33	232	26.50	171.51	10.87	-145.01	-2.69R
43	496	495.90	384.57	33.74	111.33	2.57RX
55	257	*	185.21	28.96	*	* X
56	323	*	238.36	28.66	*	* X

R denotes an observation with a large standardized residual
X denotes an observation whose X value gives it large influence.

11. Regression Analysis: enfranze versus meksegnit, yifag, Addis Zemen

The regression equation is
enfranze = - 0.68 + 0.364 meksegnit + 0.524 yifag - 0.0317 Addis Zemen

46 cases used 26 cases contain missing values

Predictor	Coef	SE Coef	T	P
Constant	-0.678	7.166	-0.09	0.925
meksegni	0.3642	0.1132	3.22	0.002
yifag	0.5243	0.1451	3.61	0.001
Addis Ze	-0.03166	0.07826	-0.40	0.688

S = 39.12 R-Sq = 88.5% R-Sq(adj) = 87.7%

Analysis of Variance

Source	DF	SS	MS	F	P
Regression	3	494159	164720	107.66	0.000
Residual Error	42	64262	1530		

12. Regression Analysis: gonder versus shembekit

```
The regression equation is
gonder = 23.7 + 0.797 shembekit

56 cases used 16 cases contain missing values

Predictor        Coef     SE Coef          T        P
Constant        23.68       10.02       2.36    0.022
shembeki      0.79702     0.06291      12.67    0.000

S = 59.75       R-Sq = 74.8%     R-Sq(adj) = 74.4%

Analysis of Variance

Source            DF          SS          MS         F        P
Regression         1      572926      572926    160.50    0.000
Residual Error    54      192756        3570
Total             55      765682

Unusual Observations
Obs   shembeki     gonder         Fit       SE Fit    Residual    St Resid
  8        387     361.00      332.45        19.98       28.55        0.51 X
 20        471     252.50      399.40        24.91     -146.90       -2.71RX
 34          0     169.00       23.68        10.02      145.32        2.47R
 42        154     444.50      146.42         8.77      298.08        5.04R
 44        463     307.20      392.70        24.41      -85.50       -1.57 X
```

13. Regression Analysis: gorgora versus chauit, degi

```
The regression equation is
gorgora = - 5.83 + 0.795 chauit + 0.302 degi

59 cases used 13 cases contain missing values

Predictor        Coef     SE Coef          T        P
Constant       -5.831       7.085      -0.82    0.414
chauit         0.7948      0.1553       5.12    0.000
degi           0.3024      0.1718       1.76    0.084

S = 41.74       R-Sq = 87.3%     R-Sq(adj) = 86.8%

Analysis of Variance

Source            DF          SS          MS         F        P
Regression         2      670457      335229    192.37    0.000
Residual Error    56       97588        1743
Total             58      768045
```

14. Regression Analysis: hamusit versus korata, wenziye

```
The regression equation is
hamusit = 3.58 + 0.535 korata + 0.354 wenziye

65 cases used 7 cases contain missing values

Predictor        Coef     SE Coef          T        P
Constant        3.583       5.816       0.62    0.540
korata        0.53525     0.08098       6.61    0.000
wenziye       0.35371     0.09557       3.70    0.000

S = 38.19       R-Sq = 84.6%     R-Sq(adj) = 84.4%

Analysis of Variance
```

Source	DF	SS	MS	F	P
Regression	2	1585072	792536	543.28	0.000
Residual Error	62	90445	1459		
Total	64	1675517			

15. Regression Analysis: korata versus hamusit, wenziye

The regression equation is
korata = 1.56 + 0.772 hamusit + 0.385 wenziye

65 cases used 7 cases contain missing values

Predictor	Coef	SE Coef	T	P
Constant	1.564	7.005	0.22	0.824
hamusit	0.7723	0.1168	6.61	0.000
wenziye	0.3852	0.1170	3.29	0.002

S = 45.88 R-Sq = 84.4% R-Sq(adj) = 84.2%

Analysis of Variance

Source	DF	SS	MS	F	P
Regression	2	2195661	1097830	521.57	0.000
Residual Error	62	130502	2105		
Total	64	2326163			

Source	DF	Seq SS
hamusit	1	2172856
wenziye	1	22805

Unusual Observations

16. Regression Analysis: meksegnit versus gonder, enfranze

The regression equation is
meksegnit = 2.9 + 0.244 gonder + 1.06 enfranze

54 cases used 18 cases contain missing values

Predictor	Coef	SE Coef	T	P
Constant	2.95	10.49	0.28	0.780
gonder	0.2438	0.1540	1.58	0.120
enfranze	1.0554	0.1523	6.93	0.000

S = 58.32 R-Sq = 87.2% R-Sq(adj) = 86.7%

Analysis of Variance

Source	DF	SS	MS	F	P
Regression	2	1186201	593100	174.37	0.000
Residual Error	51	173471	3401		
Total	53	1359672			

Source	DF	Seq SS
gonder	1	1022818
enfranze	1	163382

Annex – VI Detain simulation result of monthly water balance

	Total Inflow(MCM)	Water Lost in flood Plains (MCM)	Out flow from Lake (MCM)	Lake area	Rainfall over the lake area (MCM)	Evaporation From Lake (MCM)	Un-accounted	Observed Storage(MCM)	Simulated Storage(MCM)
Dec-97								31839.17	31839.17
Jan-98	57.200	0.000	355.98	3101.49	4.962	410.446	117.834	31053.91	31017.070
Feb-98	48.018	0.000	86.08	3087.16	0.617	409.717	117.834	30363.77	30452.070
Mar-98	30.303	0.000	41.60	3077.07	50.464	524.507	117.834	29827.80	29848.899
Apr-98	25.866	0.000	70.97	3066.10	27.901	546.145	117.834	29353.32	29167.713
May-98	141.914	0.000	110.96	3053.44	327.939	468.191	117.834	28879.24	28940.581
Jun-98	553.779	14.713	33.27	3049.15	542.140	420.014	117.834	28700.80	29450.669
Jul-98	1794.474	42.408	226.76	3058.73	1158.647	336.565	117.834	29603.34	31680.224
Aug-98	2943.690	73.621	697.80	3098.75	1304.574	335.104	117.834	32346.64	34704.132
Sep-98	1490.263	59.614	1748.50	3148.26	537.723	374.058	117.834	34558.04	34432.113
Oct-98	830.451	72.810	1510.01	3144.03	362.507	452.265	117.834	34195.53	33472.154
Nov-98	202.836	24.048	870.98	3128.75	7.196	411.150	117.834	33157.50	32258.179
Dec-98	104.410	19.632	496.95	3108.64	0.311	387.770	117.834	32021.32	31340.717
Jan-99	73.129	0.000	355.17	3092.85	23.196	400.884	117.834	31352.17	30563.157
Feb-99	37.883	0.000	294.17	3079.07	1.847	447.218	117.834	30629.62	29743.667
Mar-99	52.507	0.000	169.11	3064.16	0.306	528.502	117.834	29754.93	28981.030
Apr-99	34.296	0.000	155.85	3049.92	22.264	562.414	117.834	29106.39	28201.497
May-99	94.201	0.000	55.92	3035.00	160.248	506.121	117.834	28592.53	27776.073
Jun-99	513.144	13.755	115.00	3026.71	581.431	411.673	117.834	28225.94	28212.387
Jul-99	2133.549	35.683	243.83	3035.21	1265.078	312.115	117.834	29110.15	30901.547
Aug-99	2550.797	66.073	483.65	3085.11	1132.236	344.410	117.834	31712.14	33572.617
Sep-99	1268.013	61.051	1080.56	3130.38	361.246	392.571	117.834	33534.32	33549.862
Oct-99	1395.313	55.583	1287.50	3130.01	659.806	415.216	117.834	33858.79	33728.852
Nov-99	298.210	47.149	932.55	3132.89	6.266	416.538	117.834	33429.88	32519.257
Dec-99	181.967	49.146	534.23	3113.04	7.783	388.663	117.834	32249.66	31619.131
Jan-00	75.239	0.000	352.48	3097.69	2.168	415.460	117.834	31530.49	30810.767
Feb-00	33.312	0.000	213.40	3083.50	0.308	425.723	117.834	30750.11	30087.427

Mar-00	59.781	0.000	84.56	3070.46	0.614	553.674	117.834	30150.84	29391.749
Apr-00	100.562	0.000	205.89	3057.63	234.215	512.241	117.834	29560.03	28890.558
May-00	101.250	0.000	46.08	3048.21	136.255	515.743	117.834	29155.80	28448.404
Jun-00	483.661	14.991	14.85	3039.77	511.593	424.348	117.834	29009.67	28871.636
Jul-00	1781.663	38.517	267.25	3047.85	1074.062	352.389	117.834	29963.70	30951.371
Aug-00	2806.255	60.783	635.15	3085.99	1083.493	339.379	117.834	32336.43	33687.967
Sep-00	1251.430	58.254	1183.00	3132.24	463.571	427.113	117.834	33861.03	33616.766
Oct-00	1100.603	97.894	1205.31	3131.09	453.382	423.364	117.834	33837.07	33326.350
Nov-00	319.974	37.511	875.23	3126.38	57.838	392.392	117.834	33309.57	32281.195
Dec-00	124.150	24.029	493.39	3109.03	1.865	378.943	117.834	32386.48	31393.016
Jan-01	64.409	0.000	128.71	3093.76	0.000	399.243	117.834	31646.15	30811.638
Feb-01	38.280	0.000	184.58	3083.51	1.233	417.678	117.834	31229.27	30131.056
Mar-01	43.073	0.000	442.63	3071.26	2.764	500.891	117.834	30326.25	29115.542
Apr-01	46.207	0.000	477.96	3052.46	57.081	540.573	117.834	29345.10	28082.461
May-01	107.216	0.000	345.91	3032.69	144.963	495.369	117.834	28426.79	27375.523
Jun-01	654.978	20.072	356.61	3018.80	657.797	375.234	117.834	28143.61	27818.545
Jul-01	2033.203	48.556	543.42	3027.54	1098.393	320.143	117.834	28560.94	29920.192
Aug-01	3064.953	64.958	545.93	3067.41	1113.161	302.601	117.834	31600.48	33066.986
Sep-01	1164.159	44.815	903.52	3122.14	354.050	398.365	117.834	33411.77	33120.663
Oct-01	454.970	42.058	727.16	3123.02	198.312	440.783	117.834	32947.71	32446.108
Nov-01	157.302	18.194	467.52	3111.81	7.157	410.996	117.834	32178.60	31596.025
Dec-01	81.505	15.822	383.06	3097.29	7.124	382.461	117.834	31358.24	30785.473
Jan-02	46.555	0.000	496.36	3083.05	0.308	381.946	117.834	30378.43	29836.193
Feb-02	27.489	0.000	405.21	3065.86	3.372	414.604	117.834	29557.90	28929.401
Mar-02	33.484	0.000	348.93	3048.94	12.196	508.624	117.834	28684.39	27999.688
Apr-02	32.120	0.000	348.38	3031.08	44.860	568.620	117.834	27819.00	27041.835
May-02	36.506	0.000	283.13	3012.14	36.748	552.174	117.834	26958.29	26161.955
Jun-02	552.077	16.653	271.15	2994.25	723.412	424.373	117.834	26339.56	26607.432
Jul-02	1641.366	36.138	319.33	3003.37	1040.967	377.800	117.834	26905.80	28438.668
Aug-02	2145.979	46.916	351.26	3039.58	955.340	350.115	117.834	28773.37	30673.865
Sep-02	1066.274	40.764	419.77	3081.06	415.326	399.131	117.834	30142.16	31177.968
Oct-02	336.471	30.154	368.08	3089.99	93.936	454.940	117.834	29992.70	30637.366

Nov-02	131.079	14.966	321.28	3080.40	6.777	384.756	117.834	29281.42	29936.384
Dec-02	72.739	15.725	299.87	3067.70	2.761	382.931	117.834	28522.46	29195.524
Jan-03	47.191	0.000	266.10	3053.96	5.497	424.256	117.834	27731.11	28440.022
Feb-03	47.546	0.000	226.83	3039.61	29.788	410.995	117.834	27049.58	27761.695
Mar-03	49.119	0.000	254.64	3026.43	21.488	524.855	117.834	26318.62	26934.976
Apr-03	30.896	0.000	217.55	3009.99	5.418	564.608	117.834	25506.13	26071.297
May-03	37.884	0.000	184.80	2992.38	35.909	521.407	117.834	24775.76	25321.049
Jun-03	303.726	10.802	167.55	2976.73	387.570	399.443	117.834	24271.67	25316.712
Jul-03	1597.459	29.054	207.19	2976.63	999.256	306.602	117.834	25450.80	27252.747
Aug-03	2270.679	48.780	240.38	3016.36	898.573	303.777	117.834	27871.26	29711.223
Sep-03	1962.720	60.357	263.95	3063.56	773.855	363.656	117.834	30412.59	31642.000
Oct-03	422.951	43.909	238.93	3098.09	37.177	479.503	117.834	31079.15	31221.947
Nov-03	150.331	21.600	252.19	3090.77	9.272	417.087	117.834	30546.49	30572.840
Dec-03	80.969	20.222	278.43	3079.25	9.238	404.773	117.834	29857.77	29841.784

Summary of simulation result Annual water balance

year	Total Inflow(MCM)	Water Lost in flood Plains (MCM)	Out flow from Lake (MCM)	Lake area	Rainfall over the lake area (MCM)	Evaporation (MCM)	Unaccounted component	Observed Storage(MCM)	Simulated Storage(MCM)
1998	8223.206	306.844	6249.855	37121.571	4324.982	5075.934	1414.008	32021.316	31340.717
1999	8633.008	328.440	5707.527	36974.355	4221.707	5126.325	1414.008	32249.663	31619.131
2000	8237.879	331.978	5576.600	37029.839	4019.364	5160.771	1414.008	32386.482	31393.016
2001	7910.255	254.473	5507.015	36901.691	3642.035	4984.337	1414.008	31358.244	30785.473
2002	6122.141	201.317	4232.753	36597.433	3336.004	5200.015	1414.008	28522.455	29195.524
2003	7001.472	234.725	2798.558	36423.753	3213.041	5120.962	1414.008	29857.768	29841.784
mean	**7687.993**	**276.296**	**5012.051**	**36841.440**	**3792.856**	**5111.391**	**1414.008**	**31065.988**	**30695.941**

Annex – VII Remote sensing related Web Resource (as of 2007)

[web-1] **EOS data gateway:**
http://edcimswww.cr.usgs.gov/pub/imswelcome/
[web-2] **Global visualization Viewer**
http://glovis.usgs.gov/
[web-3] **SPOT Vegetation:**
http://www.vgt.vito.be/
[web-4] **NASA – DAAC:**
http://daac.gsfc.nasa.gov
[web-5] **Earth Explorer:**
http://edcsns17.cr.usgs.gov/EarthExplorer/
[web-6] **NASA Global Change Master Directory**
http://gcmd.gsfc.nasa.gov/index.html
[web-7] **UNEP GRID Arendal**
http://www.grida.no/
[web-8] **Tropical Rainfall Measuring Mission (TRMM) sensor**
http://trmm.gsfc.nasa.gov/images_dir/avg_rainrate.html
[web-9] **Moderate Resolution Imaging Spectrometer (MODIS) satellite**
http://modis.gsfc.nasa.gov
[web-10] **SRTM DEM source**
http://edcdaac.usgs.gov
[web-11] **RADARSAT Satellite information**
http://www.radarsat2.info

Addis Ababa University

School of graduate studies

Remote sensing based assessment of water resource Potential for Lake Tana Basin

By Yohannes Daniel Gebretsadik

Approved by board of examiner

Dr.Ing AbulKarim Hussien Seid ________________________________

Research Advisor

Dr.ing Dereje Hailu ________________________________

Internal Examiner

Dr.Ing Yilma Seleshi ________________________________

External Examiner

Ato Abtamu Mihrete ________________________________

Chair-man